Modeling and Simulation of Microbial Enhanced Oil Recovery: A New Approach which Includes the Role of Interfacial Area

MASTER'S THESIS IN APPLIED AND COMPUTATIONAL MATHEMATICS

DAVID LANDA MARBÁN

Department of Mathematics
University of Bergen

May, 2016

Acknowledgments

Foremost, I would like to thank God, for the amazing life I am experiencing.

Dr. habil. Florin Adrian Radu, is by far, one of the best professors and supervisors I have ever had. I am very grateful for all his advice, teaching and time. It is a pleasure working under your guidance and it would be a pleasure if we continue this work to a PhD.

I would also like to thank Dr. Jan Martin Nordbotten, my co-supervisor, for all the advice concerning this work.

I must acknowledge the generous financial support of the Mexican Petroleum Institute (IMP); the work reported in this thesis would not have been possible without the grant they provided me. I would also like to thank the NUPUS group and Department of Mathematics for financing a visit to four excellent universities in USA, where I learnt new concepts and perspectives related to MEOR.

It is not easy to express all the gratefulness I owe to my parents; my mother Julia Marbán Hernández and my father Ing. Daniel Landa Piedra. I will just state that if I were a baby again and I would have to choose the perfect parents that are going to raise me with love and education, you both will be always my choice. Also, a huge thank you to my brother Edgar Landa Marbán.

In the academic work I wish to thank Prof. Radilla, Ing. Bernardo González, Fís. Benito Pantoja, Dr.Wolfgang Bietenholz, and Dr. Jorge Fujioka. These professors are my inspiration for improving myself as a person and teaching to the new generations.

On a more personal note, I would like to thank all my friends in Mexico, specially José Luis Ugalde, Iván Cornejo, José de Jesús Zamora and Brayan Ramírez - thank you for keeping in touch despite the distance and inspiring me to keep going ahead. Also, I was so lucky getting my new family in Norway: Dennis Kontor, Tapash Das and Eirik Eriksen, you guys made me feel at home all this time in Bergen. Finally, thank you Benedicte Bruvold and Blake Collins for your time spent on reading and improving this work.

David Landa Marbán
May, 2016

Abstract

In today's world, oil remains the main source of energy. After discovering a petroleum reservoir, one can extract about 30% of the oil by using and maintaining the initial pressure in the reservoir through water flooding (first and second phase oil recovery). Nevertheless, 60-70% of oil remains in the reservoir after this, so called conventional recovery, so enhanced oil recovery (EOR) is strongly needed. Microbial enhanced oil recovery (MEOR) is an environmentally friendly and very promising EOR technology.

In this thesis we implement a non-standard model for MEOR that includes the interfacial area between the oil and water. We consider the two-phase flow equations and multicomponent reactive transport equations for three components: bacteria, nutrients and biosurfactants. The growth of bacteria affects the properties of the medium (porosity, permeability), up to the extreme case of pore clogging (bioclogging) and generation of new paths. Biosurfactants lower the interfacial tension, which improves the oil recovery. We consider in this thesis, for the first time in context of MEOR, also the role of interfacial area on EOR. The motivation to include the interfacial area in the model is to eliminate the hysteresis in the capillary pressure relationship and model that biosurfactants are mainly living at the oil-water interface.

A typical mathematical model for MEOR consists on nonlinear coupled partial differential equations (PDEs) and ordinary differential equations (ODEs). The spatial discretization is obtained using finite differences (FD) and two-point flux approximation (TPFA), and the time discretization using backward Euler (BE). We make the implementation for 1-D and 2-D domains using cell-centered grids. We present in detail the discretization of the equations, including the treatment of the boundary conditions. After the discretization in space and time, the problems to be solved at each time step are still nonlinear. For solving these equations, we use an implicit scheme that considers a linear approximation of the capillary pressure gradient, which results in an efficient and stable scheme. The code for running the simulations is written in MATLAB. Following this, we test the code with analytic solutions and benchmark simulations.

We consider a 1-D porous medium where we study the spatial distribution and the evolution in time of the average pressure, water saturation, oil-water interfacial area, capillary pressure, porosity, permeability ratio, residual oil water saturation and bacterial, nutrient and biosurfactant concentrations. After, we make a sensitivity analysis in order to examine the effects of the relevant model parameters. Finally, we make simulations considering a porous medium with a thief zone, which is a 2-D problem.

A comprehensive model, including two-phase flow, bacteria, nutrients and biosurfactants was implemented. The model has been tested using analytic and benchmark problems. For the first time, the role of interfacial area in MEOR was studied. We showed that different predictions of oil recovery are obtained by including the availability of interfacial area in the model. Nevertheless, it is necessary to do more experiments in the laboratory in order to compare with the numerical simulations and validate the model assumptions.

Contents

List of Figures

List of Tables

Chapter 1

Introduction

Nowadays, oil is one of the most valuable resources in the world, considering its extensive use in the daily life, such as in the production of gasoline, plastic, etc. After discovering a petroleum reservoir, one can extract about 30% of the oil by using and maintaining the initial pressure in the reservoir through water flooding (first and second phase oil recovery). Nevertheless, 60-70% of oil remains in the reservoir after this, so called conventional recovery. This is the motivation for developing new extraction techniques in order to recover the most oil possible. One of these enhanced oil recovery (EOR) techniques consists of adding bacteria to the reservoirs and using their bioproducts and effects to improve the oil production, which is called microbial enhanced oil recovery (MEOR). It is worth pointing out that MEOR has been already used in some oil reservoirs (Lazar et al. 2007, Patel et al. 2015). Nevertheless, the MEOR technology is not yet completely understood and there is a strong need for reliable mathematical models and numerical tools to be used for optimizing MEOR.

The current MEOR models are based on (non-realistic) simplifications, e.g. only one transport equation for the bacterial concentration is considered, changes in the porosity and permeability due to bioclogging are ignored, numerical simulations are just made in one dimension or the oil-water interfacial area is not included in the model (Kim 2006, Niessner and Hassanizadeh 2008b, Nielsen et al. 2010, Li et al. 2011, Babatunde 2014, Skiftestad 2015). In order to make more accurate simulations of petroleum reservoirs, we need better models where we contemplate most of the phenomena involved.

In the present work we implement a nonstandard model for two-phase flow with transport equations including bioclogging and the oil-water interfacial area in 1D and 2D. The motivation to include the interfacial area in the models is to eliminate the hysteresis in the capillary pressure relationship (Hassanizadeh and Gray 1993) and model that biosurfactants are mainly living at the oil-water interface (Kosaric and Varder-Sukan 2015). To our knowledge, this is the first time that the effects of MEOR including the oil-water interfacial area are studied. We can describe briefly the model presented as follows: we inject water, bacteria and nutrients to a reservoir. The bacteria consume nutrients and produce more bacteria and biosurfactants, which have a tendency to live at the interface between oil and water. As time passes, some bacteria die or attaches to the rock, affecting the porosity and permeability of the medium (bioclogging). The biosurfactants reduce the water-oil interfacial tension, allowing the recovery of more oil. The consideration of interfacial area in the model enables to include that biosurfactants are mainly living at the oil-water interface, which is belived to be a very important feature for MEOR.

Math models for MEOR are based on coupled nonlinear partial differential equations (PDEs) and ordinary differential equations (ODEs), which are very difficult to be solved. Therefore, it is necessary to use advanced numerical methods and simulations to predict the behavior on time of the unknowns in this complex system. Even though it is possible to buy commercial software in the petroleum industry for simulation, it is preferable to do the discretization of the equations and write an own code to perform numerical simulations, in order to implement new relations that are not included in the commercial ones.

For numerically solving the model, we consider 1-D and 2-D rectangular domains with a regular partition consisting of rectangular elements, involving cell-centered grill points. The spatial discretization is obtained using finite differences (FD) and two-point flux approximation (TPFA), and the time discretization using backward Euler (BE). There are different algorithms for solving coupled nonlinear PDEs. For example, for solving the pressure and saturation equations, the implicit pressure explicit saturation (IMPES) is a popular scheme that eliminates the nonlinearities using the structure of the equations but it has a restriction in the time step due to stability problems (Thomas 1995). In order to have a more efficient and stable scheme, we use an implicit scheme that considers a linear approximation of the capillary pressure gradient (Pop et al. 2004, Radu et al. 2010, Kumar et al. 2013). The general algorithm that we use for solving the system of equations is a generalization of the work done by Skiftestad 2015. First we solve the pressure, saturation and interfacial area equations iteratively. Subsequently we solve iteratively the three transport equations. Afterwards, we solve for the change in porosity and then we update the permeability. Finally, we compute the new interfacial tension, capillary number and the residual oil saturation and proceed to the next time step.

The overarching goal of this work is then to develop and implement an accurate numerical simulator for two-phase flow in porous media including the transport equations for bacteria, nutrients and biosurfactants, the oil-water interfacial area and the bioclogging in 1D and 2D using appropriate numerical methods. Overall, we achieved to implement the model. However, it is necessary to do experiments in the laboratory in order to compare with the numerical simulations and validate all the model assumptions.

In the following, we summarize each chapter

- ◇ **Chapter 2** Firstly, we introduce the basic concepts, ideas and equations for modeling an oil reservoir. In addition, we mention all the assumptions, considerations and simplifications in order to propose a model for two-phase flow and multicomponent transport in porous media, including bioclogging and interfacial area.
- ◇ **Chapter 3** Secondly, we give the theory and techniques for discretizing and solving numerically the mathematical model. We use finite differences and TPFA for the spatial discretization and BE for the time discretization. A flux diagram representing the algorithm for solving the model is shown at the end of the chapter, contributing to a better understanding of our approach.
- ◇ **Chapter 4** After having established the model and the numerical algorithm, we proceed with the implementation. We consider 1-D and 2-D domains, the 2D being numerical rectangular with regular rectangular gridding using cell-centered cells with half-cells on the boundaries. We test our code against benchmark results and analytic solutions, and analyze the rate convergence of the L^2-errors.

- **Chapter 5** In this chapter we perform numerical experiments for testing the MEOR model. We consider a 1-D porous medium where we study the spatial distribution and the evolution in time of the average pressure, water saturation, oil-water interfacial area, capillary pressure, porosity, permeability ratio, residual oil water saturation and bacterial, nutrient and biosurfactant concentrations. After, we make a sensitivity analysis of the model in order to examine the effects of the relevant model parameters. We found qualitative differences in the shapes of the curves, thus we gave an explanation for these results. For making use of our 2-D simulator, we study the bioclogging in a porous medium with a thief zone, which is a problem we cannot simulate in 1D.
- **Chapter 6** Finally, we present our conclusions and propose further work inspired by this study.

Chapter 2

Reservoir modeling

In this chapter we explain the phases of oil recovery, we mention some EOR methods and we develop the MEOR technique, giving some definitions and explaining the general process of implementation, the different types of MEOR, advantages and problems for implementing MEOR. In addition, we introduce the definitions and equations for modeling of the oil reservoir, including the interfacial area in the capillary pressure relation.

2.1 Oil recovery

In general, we classify the oil recovery in three stages. Primary recovery produces oil and gas due to the natural pressure of the reservoir, recovering between 10-20% of the total resources (Sen 2008). Once the pressure in the reservoir is in equilibrium, the oil production stops and in order to continue with the oil extraction we need to add energy to the reservoir. Secondary recovery consists in stimulating the oil wells by the injection of fluids, improving the flow of oil and gas to the wellhead, obtaining from 10-40% of the oil in place (Sen 2008). For obtaining the oil remained, we use EOR as a third recovery. In Fig. 2.1.1 we show the types of EOR processses employed in the oil industry. However, some of these methods apart from being expensive, involve the use of toxic chemicals, being harmful to the environment (Patel et al. 2015). Regarding the MEOR technique, it is economically feasible and enviromentally friendly.

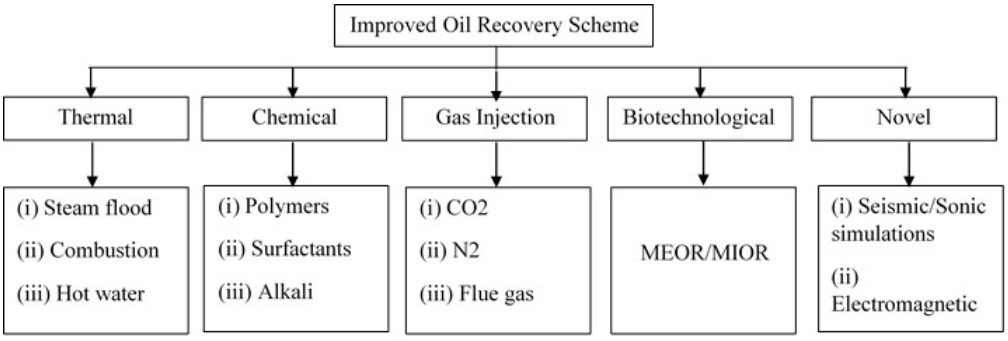

Figure 2.1.1 Flow sheet diagram showing some EOR techiques (borrowed from Sen 2008).

2.2 The MEOR technique

MEOR is a process to recover the oil remaining in the reservoir using microorganisms. Although the idea seems easy, it is necessary to understand the science involved, due to the presence of chemical, biological and physical processes. This idea was proposed by Beckman in 1926, but it was until 1947 that ZoBell and his research group did several experiments and settled the basis for applying microorganisms for oil recovery (Lazar et al. 2007). Fig. 2.2.1 shows a simplified diagram for applying MEOR to a reservoir.

Figure 2.2.1 General diagram of the MEOR technique in an oil reservoir. On the left well, bacteria and nutrients are injected, meanwhile the oil is extracted on the right well. Inside the reservoir, the bioproducts change the properties of the porous medium and fluids, allowing to increase the production.

2.2.1 Strategies

Regarding the MEOR process, there are three general strategies for his application (Weihong et al. 2009)

- **Injection of nutrients to stimulate indigenous microorganisms**
  If there are indigenous microorganisms inside the reservoir capable of contributing in the recovery, our purpose is to use them. However, it is first necessary to study the reservoir in order to detect if any useful microorganisms is present and after choose the way to stimulate the microorganisms so that their actions modify the rock and fluid properties (Weihong et al. 2009).

- **Injection of exogenous microorganisms and nutrients**
  If there are not microorganisms inside the reservoir that could improve the oil extraction, the next evident idea is to inject both microorganisms and nutrients to the reservoir. Notwithstanding, these exogenous microorganism should be capable to live with the indigenous microorganisms and to adapt to the reservoir conditions (Bryant 1991). Furthermore, the transport of the exogenous microorganisms could be a problem, requiring that these microorganisms have a minimal absorption to the reservoir rock material, in order that they disperse efficiently inside the reservoir (Weihong et al. 2009). In spite of this, one advantage is that we can design a nutrient package specifically for these exogenous microorganism in order to stimulate their growing and metabolism (Youssef et al. 2007).

◇ **Injection of *ex situ*-produced metabolites**
If there are not microorganisms able to live inside the reservoir, the following idea is to generate the bioproducts outside the reservoir and after inject them into the reservoir. However, transport inside the reservoir is also a problem due to a loss (absorption) of bioproducts along the reservoir (Weihong et al. 2009). Despite this, we can produce biosurfactants and polymers from economical renewable sources (Maneerat 2005).

2.2.2 Mechanisms

The bioproducts formed due to microbial activity are surfactants, polymers, solvents, acids and gases. In Sen 2008, it is summarize the different effects due to the microbial activity. Table 2.2.1 shows these effects.

Table 2.2.1 Effects using MEOR.

Biomass	Selective plugging and wettability alteration.
Surfactants	Emulsification and de-emulsification through reduction of interfacial tension.
Polymers	Injectivity profile and viscosity modification, selective plugging.
Solvents	Rock dissolution for better permeability, oil viscosity reduction.
Acids	Permeability increase, emulsification.
Gases	Increased pressure, oil swelling, interfacial tension and viscosity reduction.

The main purpose of using these microbes is to modify the rock and fluid properties in order to enhance the oil recovery. To accomplish this, we have the following performances (Patel et al. 2015)

◇ **Selective plugging**
The water flows inside the reservoir through the paths that need less energy, leaving some of them with feasible oil but not water flow. For reaching these new paths, we use the biomass and polymers to lock these paths where the water already drove the oil.

◇ **Wettability alteration**
Given that water and oil are immiscible fluids, it is more difficult to mobilize the oil due to the water flow. However, using surfactants we can increase the ability of water to mix together, improving the sweep efficiency and increasing the production (Patel et al. 2015).

◇ **Bioacids/solvents/gases**
Regarding the non-interconnection between all pores, there are some zones inside the reservoir where the oil is isolated. To reach these zones, we can remove these rocks in order to access this oil. Hence, we can modify the permeability and porosity of the porous medium due to the effect of acids and solvents formed from microbial activity (Patel et al. 2015). Furthermore, stimulating microbes that produce gases, we increase the reservoir pressure, and also this gas can dissolve into the oil, reducing its viscosity and increasing the sweep efficiency (Lazar et al. 2007, Sen 2008, Patel et al. 2015).

◇ **Degradation, clean-up of build up**
In relation with heavy crude oil, some microbes are capable of consuming hydrocarbons, leading to make the oil less viscous and easier to recover (Patel et al. 2015).

◇ **Surface tension alteration: biosurfactants**
In order to improve the oil recovery, lowering the surface and interfacial tension between the rock, water and oil is a possibility. To do this, we can use surfactants produced from microbes. These biosurfactants have the advantage to be biodegradable, temperature tolerant and pH-hardy. Also they are non harmful to humans and lower concentrations of them can produce similar results as chemical surfactants (Patel et al. 2015).

2.2.3 Advantages and adversities

Among all EOR techniques, MEOR is the one we decided to study in this thesis because one of its characteristics is to be environmentally friendly. In Lazar et al. 2007, they highlight advantages of using MEOR technologies. Table 2.2.2 shows some of these advantages.

Table 2.2.2 Advantages of using MEOR.

I	The microbes and nutrients are cheap and easy to produce and handle in the field.
II	Less expensive to implement and easier applied than another EOR method.
III	The cost of the injected fluids are independent on oil prices.
IV	The effects of bacterial activity within the reservoir are magnified over time due to colony growing.

However, there are some problems facing MEOR implementations; some of them in Table 2.2.3 (Lazar et al. 2007).

Table 2.2.3 Disadvantages of using MEOR.

I	Lost injectivity due to wellbore plugging.
II	Complications for dispersion/transport of all necessary components to the target.
III	Promotion of desired metabolic activity in situ.
IV	Preclusion of competition or undesirable secondary activity.

Moreover, each reservoir has different characteristics, so a study in advance is necessary before MEOR implementations (Castorena-Cortés et al. 2012). Despite the disadvantages, we are still optimistic about the benefits from applying MEOR. However, there is a lot of work to do in order to make more field implementations. Today, MEOR research is more complex, including genetically-engineered microorganism for MEOR (GEMEOR) and enzyme-enhanced oil recovery (EEOR), to mention some of the new areas of research (Patel et al. 2015). In order to make possible the use of MEOR and their variants, mathematical modeling and simulation is fundamental.

2.3 Flow in porous media

A material containing pores (voids) and a solid part (skeleton) is called porous medium. The pores can just be filled with one fluid (single-phase, e.g. water), two fluids (two-phases, e.g. oil and water), three fluids (three-phases, e.g. gas, oil and water), etc. The size of petroleum reservoirs is of the order of kilometers and we cannot simulate the whole reservoir. That is why we work with Representative Elementary Volumes (REV), where we assign to each point of the porous medium the property of the REV around the point. This scale has to be large enough in order to contain a representative quantity of voids for defining a mean global property, but small enough for keeping the property local, having a characteristic length from the order of one centimeter to a few centimeters (Nordbotten and Celia 2011). Once we had introduced the concept of REV, we can define mathematically some physical properties in the porous media.

Porosity [ϕ] is a measure of the void space and is given by the ratio of the void volume in REV divided by the volume of REV. According to this definition, the porosity is a dimensionless property with values in the range [0,1]. However, the porosity of most sedimentary rocks is generally lower than 0.5 (Tiab and Donaldson 2003). Moreover, we are interested in the flow trough connected void spaces, which is why we consider just the interconnected pores for the computation of ϕ. Even though the porosity can be a function of several variables (position, time, temperature, depth, ...), in this thesis we consider that the porosity is just a function of position and time ($\phi(\mathbf{x}, t)$). Fig. 2.3.1 shows the porosity as a function of the REV.

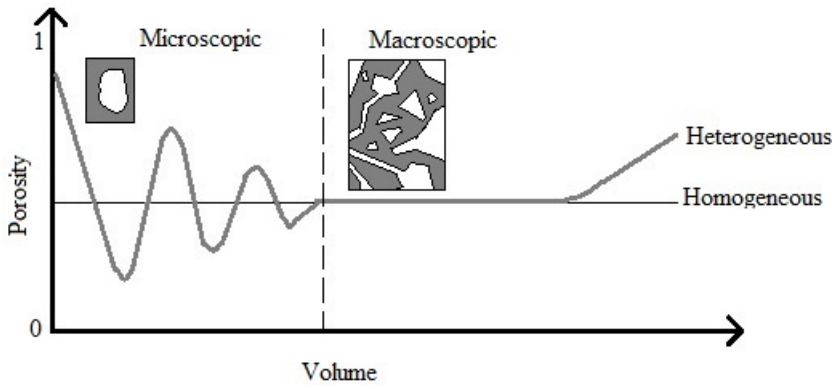

Figure 2.3.1 Porosity as a function of volume (adapted from Engler 2010).

Another common porous medium property is the absolute permeability [$\mathbf{k}$], that is a measure of the ease a liquid passes through the voids. The permeability of a rock depends on the rock grain size, grain shape, grain size distribution, grain packing and the degree of consolidation and cementation (Tiab and Donaldson 2003). The permeability has dimensions of area [L^2] and in the general case is a tensor. However, for simplicity in this thesis we consider examples where the permeability is a scalar and a function of position and time ($\mathbf{k}(\mathbf{x}, t)$). In the oil industry, Darcy is used to measure the permeability (1 Darcy = 0.986923 μm^2). Permeability of petroleum reservoir rocks may range from 0.1 to 1000 or more millidarcies (Tiab and Donaldson 2003). Reservoirs having below 1 mD are considered tight, meanwhile the ones above 250 mD are considered very good quality.

Having defined some properties of the porous medium, now we introduce some properties of the fluid. Density $[\rho]$ is a physical property of matter, being a measure of the relative heaviness of objects with a constant volume. Mathematically, it is given by the ratio of the mass of fluid over the volume of fluid. Density units are $[M/L^3]$. Examples of typical density values for water and oil are 1000 kg/m^3 and 800 kg/m^3 respectively (Li et al. 2011). In this thesis, we consider incompressible fluids (ρ =constant).

Another important property for describing a fluid is its viscosity $[\mu]$. Viscosity is a measure of a fluid's resistance to flow. The unities of viscosity are $[M/(L \cdot T)]$. Examples of typical viscosity values for water and oil are 1 $\times 10^{-3} kg/(m \cdot s)$ and 3.92 $\times 10^{-3} kg/(m \cdot s)$ respectively (Li et al. 2011). In this work, we consider fluids with constant viscosity.

2.4 Darcy's law

In 1856, Henry Darcy published a study of the design of sand filters, where he predicted the quantity of water flowing though these filters, giving the basis for the following equation (Nordbotten and Celia 2011)

$$\mathbf{u} = -\boldsymbol{\kappa} \nabla h \tag{2.1}$$

where $\mathbf{u}$ is a measure of the volumetric flow rate per area of the porous medium with dimensions $[L/T]$ and $\boldsymbol{\kappa}$ is called hydraulic conductivity, being a coefficient of proportionality given by

$$\boldsymbol{\kappa} = \frac{\mathbf{k} \rho g}{\mu} \tag{2.2}$$

where g is the magnitude of gravity. In Eq. (2.1), h is the hydraulic head, which dimension is $[L]$. One way to interpret the hydraulic head is that fluids flow from higher values of h to lower ones. One expression for the hydraulic head is given by

$$h = \frac{p}{\rho g} + z \tag{2.3}$$

where z is measured relative to a given point in the system, but it does not matter where we choose this reference point, because what is relevant is the differences between hydraulic heads. The pressure p is defined as force divided by the area where the force is acting. The dimensions of pressure are $[M/(L \cdot T^2)]$. After defining pressure, it is easier to understand why the flow is from the zones with larger pressure to the lower ones. Substitution of Eqs. (2.3) and (2.2) in (2.1) leads to

$$\mathbf{u} = -\frac{\mathbf{k}}{\mu} \nabla (p - \rho \mathbf{g}) \tag{2.4}$$

where we use the convention that the coordinate z is positive upward.

2.5 Mass conservation

The law of conservation of mass was introduced by Antoine Lavoasier in 1789, stating that mass is neither created nor destroyed in chemical reactions. The Gauss's theorem or divergence theorem is essential for the derivation of the mathematical form of many physical conservation laws, and states

Let $\boldsymbol{f}$ be a continuously differentiable vector field, defined in a volume Ω. Let $\partial\Omega$ be the closed surface forming the boundary of Ω and let $\boldsymbol{n}$ be the unit outward normal to $\partial\Omega$. Then the divergence theorem states that

$$\int_{\Omega} \nabla \cdot \boldsymbol{f}\, dx = \int_{\partial\Omega} \boldsymbol{f} \cdot \boldsymbol{n} dS \tag{2.5}$$

A proof of the theorem can be found in Matthews 1998. For formulating the mass conservation law, intuitively we have that the change of mass in a volume Ω is balanced by the total flow into $\partial\Omega$ through the boundaries and any source/sink term F. Mathematically, we have the following expression

$$\int_{\Omega} \frac{\partial M}{\partial t} dx = -\int_{\partial\Omega} \mathbf{f} \cdot \mathbf{n} dS + \int_{\Omega} F dx \tag{2.6}$$

where M is the mass. Applying the divergence theorem on the second integral and rearranging terms, we obtain

$$\int_{\Omega} \left(\frac{\partial M}{\partial t} + \nabla \cdot \mathbf{f} - F \right) dx = 0 \tag{2.7}$$

The previous integral must hold for any arbitrary Ω, so finally we obtain the differential equation for conservation of mass

$$\frac{\partial M}{\partial t} + \nabla \cdot \mathbf{f} = F \tag{2.8}$$

For example, considering an incompressible fluid of density ρ, porosity ϕ and volumetric flow rate per area $\mathbf{u}$, the conservation law is given by

$$\frac{\partial \phi}{\partial t} + \nabla \cdot \mathbf{u} = \frac{F}{\rho} \tag{2.9}$$

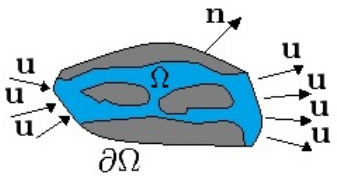

Figure 2.5.1 Volume Ω enclosing a porous media filled with water. Due to the absence of source/sink terms and no reaction presented, all water coming into the left side has to come out of the right side.

2.6 Two-phase flow

Let us consider a porous medium filled with water and oil. In this case, these fluids are immiscible (they do not exchange mass between them). For knowing the amount of a phase in the REV, we introduce the saturation of phase α $[s_\alpha]$ given by the ratio of volume of phase α (in REV) over the volume of voids (in REV), where in this work, we consider gas and oil as non-wetting phases (α =n) and water for the wetting phase (α =w). In the case where the porous medium is just filled with two fluids, we have that $s_n + s_w = 1$.

In the water-oil interface there is a surface free energy due to natural electrical forces, which attract the molecules to the interior of each phase and to the contact surface. This interfacial tension keeps the fluids separated, defined by the quantity of work needed to separate a surface of unit area from both fluids. The ability of a fluid phase to wet a solid surface in the presence of a second immiscible phase is called wettability. In Fig. 2.6.1 we show the three general categories of wettability, where θ is the contact angle at oil-water-solid interface; $\sigma_{\text{Int,os}}$, $\sigma_{\text{Int,ws}}$ and $\sigma_{\text{Int,ow}}$ are the interfacial energy between oil-solid, water-solid and oil-water respectively. The contact angle θ is connected with the interfacial energies by Young's equation $\sigma_{\text{Int,os}} - \sigma_{\text{Int,ws}} = \sigma_{\text{Int,ow}} \cos\theta$.

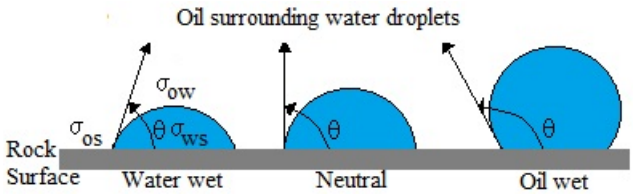

Figure 2.6.1 Different categories of wettability (adapted from Engler 2010).

Capillary pressure p_c is defined as pressure differential between two immiscible fluid phases occupying the same pores caused by interfacial tension between the two phases that must be overcome to initiate flow (Bahadori et al. 2014). Besides, in typical reservoirs, the pores are microscopic and there is interfacial tension between oil-water fluids, these result in capillary pressure influencing considerably in the fluid distributions (Engler 2010). In a small tube, we can compute the p_c as

$$p_c = \frac{2\sigma_{\text{Int}} \cos\theta}{r} \tag{2.10}$$

where r is the tube radius. From this expression, we note the smaller the radius, the larger the capillary pressure. On the macroscale, the capillary pressure is given by

$$p_n - p_w = p_c \tag{2.11}$$

where p_n and p_w are the non-wetting and wetting phase pressure respectively and p_c an empirical function. In standard models, p_c is just considered as a function of the water saturation $p_c(s_w)$. Let us consider a porous medium just filled with water. We inject to the medium oil and after we inject water. Plotting the capillary pressure profile, we obtain the profiles shown in Fig. 2.6.2.

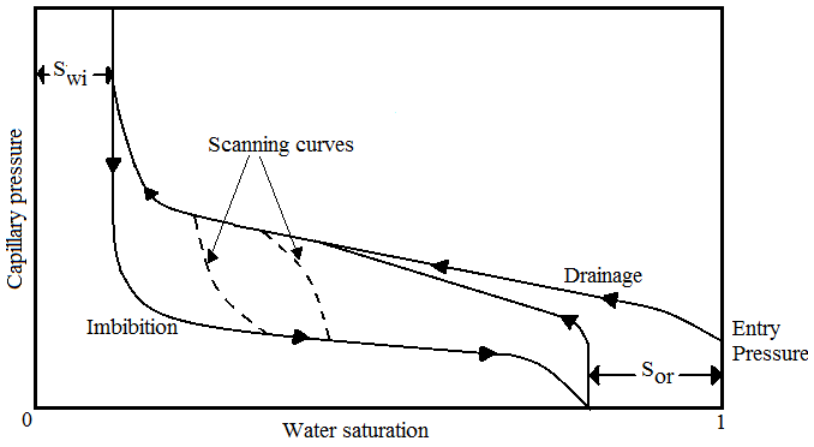

Figure 2.6.2 Capillary pressure profile illustrating hysteresis (borrowed from Nordbotten and Celia 2011).

Drainage is the process when a non-wetting phase displaces the wetting phase, whilst imbibition is when the wetting phase displaces the non-wetting phase. From the plot, we note the presence of an entry pressure p_e, being the minimum pressure needed in order to put the non-wetting phase inside the porous media. In addition, we note that p_c is not a well-defined function because while there is one value of water saturation, there is more than one value of p_c, due to p_c being dependent on the history. This phenomenon presented in some systems is called hysteresis. The explanation for drainage curves having higher capillary pressures while imbibition curves having lower capillary pressure is because pore throats have smaller radii than pore bodies (Eq. 2.10 states that the capillary pressures are inversely proportional to the radius) (Nordbotten and Celia 2011).

Let us consider that the wetting phase is water and the non-wetting phase is oil in Fig. 2.6.2. Intuitively, we could think about extracting all water from the reservoir after drainage, but in reality water saturation can be reduced to 5-40%, at this point the water saturation becomes immobile, defined as irreducible water saturation s_{wi} (Engler 2010). The residual oil saturation s_{or} is the oil that remains in the pores after the imbibition process. In Fig. 2.6.3 we show the displacement of oil by water, where we present schematically the role of s_{wi} and s_{or}

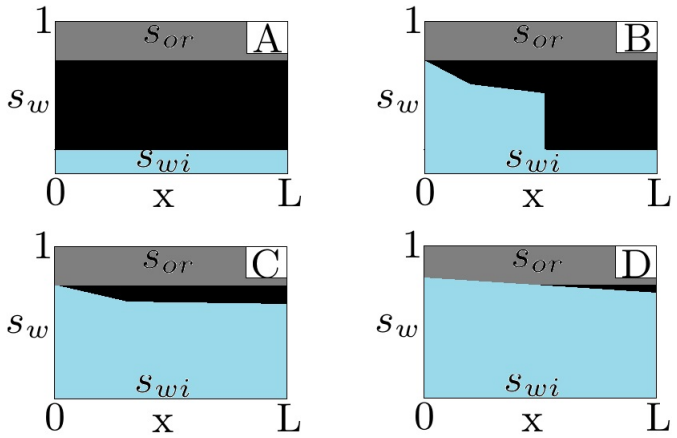

Figure 2.6.3 Oil recovery progression in a porous media in 1D (adapted from Engler 2010).

A At the beginning, the porous medium is filled with some oil $s_n \neq 0$, with some irreducible water $s_w = s_{wi}$ and residual oil $s_{or} \neq 0$.

B We inject water on the left boundary, so on the right boundary we just obtain oil.

C After some time of water injection, water breakthrough is presented, and both oil and water is produced simultaneously.

D If we add some surfactants, we can lower the s_{or}.

The recovery of oil can be analyzed in two stages: before and after water breakthrough. Until water breakthrough, the oil recovery correspond to the water injection. After water breakthrough, there is production of oil and water, so for obtaining the percentage of oil recovered, we use numerical integration. We define the total volume of injected water by $W_i(t) = tQ_T$, where Q_T is the water injection rate. We define the pore volume by $V_p = A\phi L$, where L is the length of the porous medium $[L]$ and A is the cross sectional area $[L^2]$. Using the previous definitions, the number of pore volumes pv injected is given by $pv = \frac{W_i}{V_p}$. The number of pore volume gives a better understanding of the amount of water injected in the reservoir and it is very common to plot the oil recovery in function of pv.

In the beginning of this section, we introduced the definition of absolute permeability, where we emphasized that it is for the case when we have one phase present, being the absolute permeability a property of the rock independent of the phase in question. When we have two fluids, even though they do not mix, just with their own presence they interfere in the flow of each other. Permeability to each phase α is called effective permeability $\mathbf{k}_\alpha$. For modeling this phenomenon, we introduce the relative permeabilities $k_{r,w}(s_w)$ and $k_{r,n}(s_w)$, and we can write the effective permeabilities for each phase

$$\mathbf{k}_w = k_{r,w}(s_w)\mathbf{k} \qquad\qquad \mathbf{k}_n = k_{r,n}(s_w)\mathbf{k} \tag{2.12}$$

Due to p_c, $k_{r,w}$ and $k_{n,w}$ are empirical functions depending on the porous media and phases, it is useful to visualize their profile for some popular parameterizations. In the present work, we use the capillary pressure and relative permeability parameterizations shown in Table 2.6.1. In this table, λ, η, $\varsigma = 1 - 1/\eta$ are parameters and the effective water and oil saturation are given by

$$s_w^* = \frac{s_w - s_{wi}}{1 - s_{or} - s_{wi}} \qquad\qquad s_n^* = \frac{s_n - s_{or}}{1 - s_{or} - s_{wi}} \tag{2.13}$$

Table 2.6.1 Capillary pressure and relative permeability parameterizations.

Van Genuchten 1980	Brooks and Corey 1964
$p_c(s_w^*) = p_e(s_w^{*-1/\varsigma} - 1)^{1/\eta}$	$p_c(s_w^*) = p_e s_w^{*-1/\lambda}$
$k_{r,w}(s_w^*) = \sqrt{s_w^*}[1 - (1 - s_w^{*1/\varsigma})^\varsigma]^2$	$k_{r,w}(s_w^*) = s_w^{*2}$
$k_{r,n}(s_w^*) = \sqrt{1 - s_w^*}(1 - s_w^{*1/\varsigma})^{2\varsigma}$	$k_{r,n}(s_n^*) = s_n^{*2}$

In Fig. 2.6.4 we show the capillary pressure and relative permeabilities profiles with some value parameterizations we consider in this thesis.

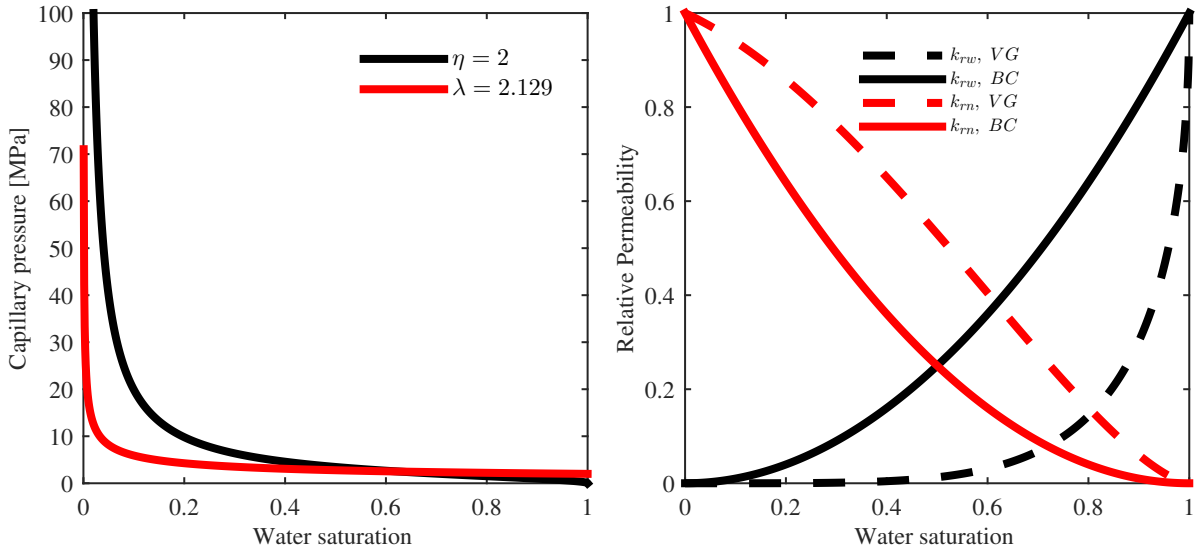

Figure 2.6.4 Examples of capillary pressure and relative permeability profiles. VG and BC are abbreviations of Van Genuchten and Brooks-Corey respectively. For the capillary pressure, we set $P_e = 2$ MPa.

Now we introduce the definition of phase mobilities

$$\lambda_w = \frac{k_{r,w}}{\mu_w} \qquad \lambda_n = \frac{k_{r,n}}{\mu_n} \tag{2.14}$$

Once we defined the phase mobilities, we can write the Darcy's law and the mass conservation equations for each phase

$$\begin{aligned} \frac{\partial \phi s_w}{\partial t} + \nabla \cdot \mathbf{u}_w &= \frac{F_w}{\rho_w} \qquad & \mathbf{u}_w &= -\lambda_w \mathbf{k}(\nabla p_w - \rho_w \mathbf{g}) \\ \frac{\partial \phi s_n}{\partial t} + \nabla \cdot \mathbf{u}_n &= \frac{F_n}{\rho_n} \qquad & \mathbf{u}_n &= -\lambda_w \mathbf{k}(\nabla p_n - \rho_n \mathbf{g}) \end{aligned} \tag{2.15}$$

In the next section we rewrite the previous set of equations in just two equations, where the primary variables are the average pressure p and the water saturation s_w.

2.7 Average pressure formulation

In the previous section, we provided two mass conservation and two flux equations. In addition, the relation of both pressure though the capillary pressure $p_n - p_w = p_c$ and the constriction for the phase saturation $s_w + s_n = 1$. If we consider that p_c is just a function of water saturation, then we have a set of 6 equations with 6 unknowns. In this work we consider the average pressure formulation for solving this system.

We define the average pressure p as

$$p = \frac{p_w + p_n}{2} \tag{2.16}$$

From the definition of capillary pressure, we have the relation $p_n - p_w = p_c$. Using both relations, we can write p_w and p_n as follows

$$p_w = p - \frac{1}{2}p_c \qquad p_n = p + \frac{1}{2}p_c \tag{2.17}$$

Substitution of the previous relations in the flux equations $\mathbf{u}_w$ and $\mathbf{u}_n$ in Eq. (2.15) leads to

$$\mathbf{u}_w = -\lambda_w \mathbf{k}(\nabla(p - \frac{1}{2}p_c) - \rho_w \mathbf{g}) \qquad \mathbf{u}_n = -\lambda_n \mathbf{k}(\nabla(p + \frac{1}{2}p_c) - \rho_n \mathbf{g})$$

Summing the last two equations and defining $\lambda_\Sigma = \lambda_n + \lambda_w$ and $\lambda_\Delta = \lambda_n - \lambda_w$, we can write the total flux $\mathbf{u}_\Sigma = \mathbf{u}_w + \mathbf{u}_n$ as

$$\mathbf{u}_\Sigma = -\mathbf{k}(\lambda_\Sigma \nabla p + \frac{1}{2}\lambda_\Delta \nabla p_c - (\lambda_w \rho_w + \lambda_n \rho_n)\mathbf{g})$$

Now, summing the two mass conservation equations in Eq. (2.15) leads to

$$\frac{\partial \phi(s_w + s_n)}{\partial t} + \nabla \cdot \mathbf{u}_\Sigma = \sum_{\alpha=w,n} \frac{F_\alpha}{\rho_\alpha} \tag{2.18}$$

Using that $s_w + s_n = 1$ and substituting the total flux (2.7) in the previous equation, we get the equation we called "the pressure equation"

$$\frac{\partial \phi}{\partial t} + \nabla \cdot (-\mathbf{k}(\lambda_\Sigma \nabla p + \frac{1}{2}\lambda_\Delta \nabla p_c - (\lambda_w \rho_w + \lambda_n \rho_n)\mathbf{g})) = \sum_{\alpha=w,n} \frac{F_\alpha}{\rho_\alpha} \tag{2.19}$$

On the other hand, substitution of Eq. (2.17) in the mass conservation equation for the wetting-phase, it leads to the equation we called "the saturation equation"

$$\frac{\partial \phi s}{\partial t} - \nabla \cdot (\lambda_w \mathbf{k}(\nabla(p - \frac{1}{2}p_c) - \rho_n \mathbf{g})) = \frac{F_w}{\rho_w} \tag{2.20}$$

Then, given proper boundary and initial conditions for the average pressure and water saturation, we can solve the pressure and saturation equations, obtaining the profiles for the pressure, saturation and flux of the wetting and non-wetting phases.

2.8 Interfacial area

Considering a porous medium filled with two fluids, the surface where they make contact is called interfacial area. Mathematically, we compute the specific interfacial area a_{wn} as a ratio of the interfacial area in the REV over the volume of REV, resulting in units of [1/L]. In this work we refer to the specific interfacial area as interfacial area. For understanding better the importance of a_{wn}, let us consider Fig. 2.8.1.

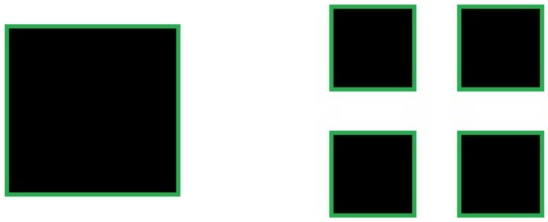

Figure 2.8.1 Example comparing the interfacial area given the same amount of oil. When we split the square in four pieces, the interfacial area increases by a factor of 2. Then, using biosurfactants, the more interfacial area is presented, the more oil we can mobilize from the reservoir.

When Darcy made his experiments and deduced his law, he just considered a single-phase flow. In the case of two-phase flow, we just extend Darcy's law for two variables, but we may expect there are more forces involve than the gradient of the hydraulic head. In Hassanizadeh and Gray 1990, they developed equations of momentum balance for phases and interfaces, based on thermodynamic principles. The two-phase flow equations are a particular case of these equations and in this thesis for modeling the interface between oil and water we use the following equation (Niessner and Hassanizadeh 2008a)

$$\frac{\partial a_{wn}}{\partial t} + \nabla \cdot (a_{wn}\mathbf{v}_{wn}) = E_{wn} \qquad \text{with} \qquad \mathbf{v}_{wn} = -\mathbf{k}_{wn}\nabla a_{wn} \tag{2.21}$$

where $\mathbf{v}_{wn}$ is the interfacial velocity $[L/T]$, E_{wn} is the rate of production of specific interfacial area $[L^3/T]$ and $\mathbf{k}_{wn}$ is the interfacial permeability $[L^3/T]$. In standard models, we give $p_n - p_w = p_c(s_w)$ as an empirical function with fitting parameters, in order to have a relation between both pressures and solve the system. However, we mentioned that this capillary pressure relation presents hysteresis. Following the thermodynamic approach in Hassanizadeh and Gray 1993, they proposed that including the interfacial area in the capillary pressure relation eliminates the hysteresis under equilibrium conditions. Fig. 2.8.2 shows experimental interfacial area profiles reported by Porter et al. 2010, where they focused on measuring directly p_c, s_w and a_{wn} during drainage and imbibition; after they compared with those predicted from a thermodynamic model, finding reasonable approximations, giving a practical tool for constructing these surfaces from $p_c - s_w$ curves, being just necessary either the data from the drainage or imbibition process (Chen et al. 2007).

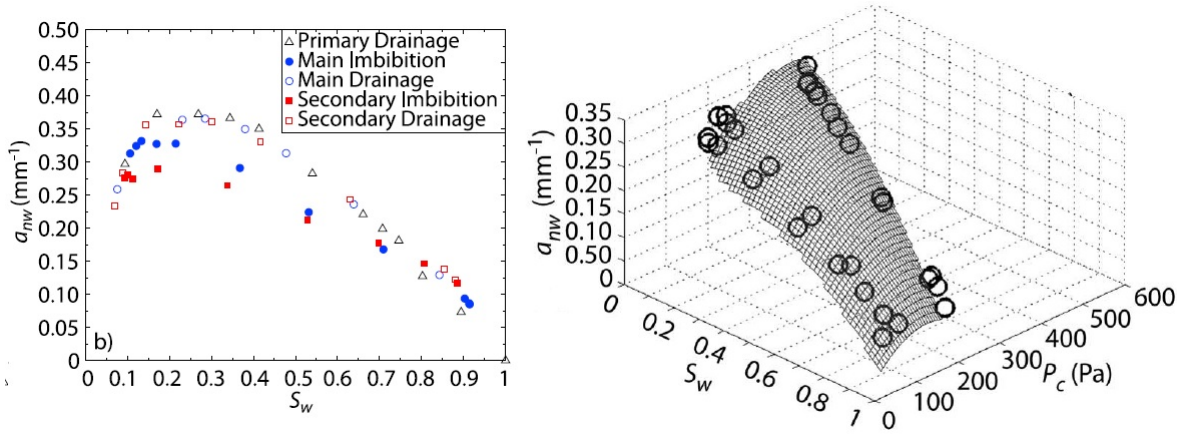

Figure 2.8.2 Examples of experimental interfacial area profiles (Porter et al. 2010). The first plot shows the hysteresis in the interfacial area while the second plot shows the interfacial area surface $a_{wn}(s_w, p_c)$.

Because we consider the oil-water interfacial area $a_{wn}(s_w, p_c)$ in this work, we have to provide a relation $p_n - p_w = p_c(a_{wn}, s_w)$ that accounts for interfacial forces. This relation can be produced by fitting surfaces to $a_{wn} - s_w - p_c$ data coming from models or experiments. In Niessner and Hassanizadeh 2008a, they used a bi-quadratic relationship. However, this relation does not fulfill the requirements $a_{wn}(0, p_c) = a_{wn}(1, p_c) = 0$. In this work, we use the next relation (Joekar-Niasar and Hassanizadeh 2012)

$$a_{wn}(s_w, p_c) = \alpha_1 s_w^{\alpha_2}(1 - s_w)^{\alpha_3} p_c^{\alpha_4} \tag{2.22}$$

with α_1, α_2, α_3 and α_4 constants. From the given parameterization (2.22), we can isolate the capillary pressure

$$p_c(s_w, a_{wn}) = \alpha_1^{-1/\alpha_4} s_w^{-\alpha_2/\alpha_4}(1 - s_w)^{-\alpha_3/\alpha_4} a_{wn}^{1/\alpha_4} \tag{2.23}$$

In order to better visualize this parameterization, in Fig. 2.8.3 we show the interfacial area surface using the values from Joekar-Niasar and Hassanizadeh 2012 α_1=6.462, α_2=3.057e^{-12}, α_3=1.244, α_4=-0.963.

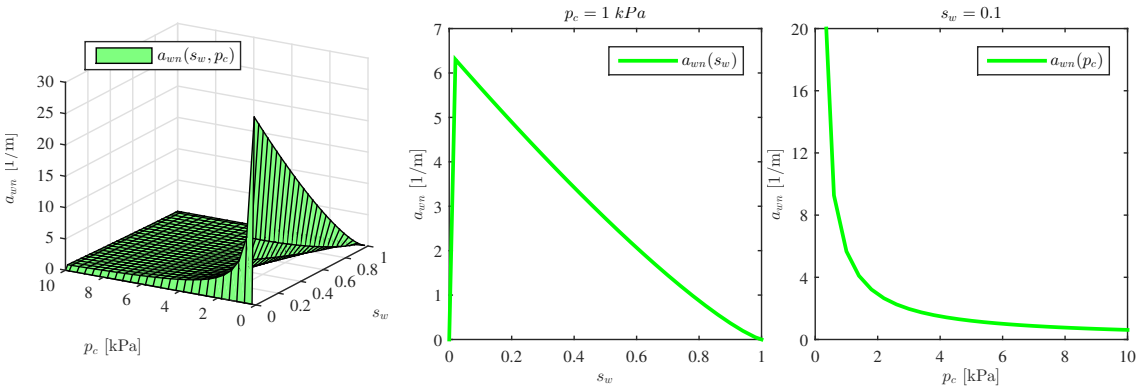

Figure 2.8.3 Interfacial area profile in Joekar-Niasar and Hassanizadeh 2012.

For solving the interfacial area equation, we need to provide the mathematical expression for the production/destruction rate of interfacial area E_{wn}. However, we could not find information about this term apart from Niessner and Hassanizadeh 2008a, where they proposed a relation based on physical arguments. It is clear that when the reservoir is filled with just one phase, there is not interfacial area. When we start to inject the other phase, we start to generate interfacial area until we have a maximum interfacial area value. After this saturation value, if we increase the saturation the interfacial area decreases. Moreover, the faster the change in saturation, the larger the rate of change of interfacial area. Then, we consider the following production/destruction rate of interfacial area

$$E_{wn} = -e_{wn}\frac{\partial s_w}{\partial t} \tag{2.24}$$

where e_{wn} is a parameter characterizing the strength of change of specific interfacial area due to a change of saturation, with unites $[1/L]$. Moreover, to estimate this parameter, they neglected the interfacial area flux in Eq. 2.21, thus after using the chain rule for the time derivative in Eq. 2.21, we have

$$\frac{\partial a_{wn}}{\partial p_c}\left(\frac{dp_c}{ds_w}\right)_{\text{line}}\frac{\partial s_w}{\partial t} + \frac{\partial a_{wn}}{\partial s_w}\frac{\partial s_w}{\partial t} = -e_{wn}\frac{\partial s_w}{\partial t} \tag{2.25}$$

Rearranging terms, the expression for e_{wn} results

$$e_{wn} = -\frac{\partial a_{wn}}{\partial p_c}\left(\frac{dp_c}{ds_w}\right)_{\text{line}} - \frac{\partial a_{wn}}{\partial s_w} \tag{2.26}$$

where the path $\left(\frac{dp_c}{ds_w}\right)_{\text{line}}$ is in general unknown, but in the main drainage and imbibition curves, p_c is a known function of s_w. In addition, it is possible to compute this derivative for $e_{wn} = 0$. For all other paths, we interpolate using these three values of e_{wn} (Niessner and Hassanizadeh 2008a).

Experimental investigations focused on simultaneously measuring p_c, s_w and a_{wn} are often difficult, expensive and subject to limitations, thus only a few have been reported in the literature, indicating a need for further experimental studies characterizing the relationship $a_{wn}(s_w, p_c)$ (Youssef et al. 2003, Chen et al. 2007, Porter et al. 2010).

2.9 Transport equations

In Chapter 2 we mentioned the MEOR technique, involving the addition of bacteria and nutrients inside the oil reservoir in order to produce biosurfactants and reduce the interfacial tension, leading to enhanced oil recovery. The movement of these components in the water is controlled by advective and diffusion processes.

The advection-difussion equation can be derived from the conservation of mass (2.8)

$$\frac{\partial c}{\partial t} + \nabla \cdot \mathbf{j} = R \tag{2.27}$$

where c is the concentration of mass transferred and $\mathbf{j}$ is the total flux given by $\mathbf{j} = \mathbf{j}_{\text{dif}} + \mathbf{j}_{\text{adv}} = -D\nabla c + \mathbf{u}c$ (Bennett 2012). Dispersion causes spreading of c, where we have mechanical and molecular dispersion (diffusion). Diffusion describes the spread of particles through random motion, going from higher concentration to lower concentration, described by Fick's Law, while mechanical dispersion is due to every path has different geometry inside the porous medium, so not all c components travel in the average flow velocity, leading to faster and slower transport of c. Advection causes transport of c due to the flow movement, in this cases the water flow.

For describing the movement of bacteria, nutrients and bioproducts, we consider the following transport equations (Kim 2006, Li et al. 2011)

$$\begin{aligned}
\frac{\partial(C_b\phi s_w)}{\partial t} - \nabla \cdot \left(\mathbf{D}_b s_w \phi \nabla C_b - \mathbf{u}_w C_b - \phi \mathbf{v}_g C_b\right) &= R_b \\
\frac{\partial(C_n\phi s_w)}{\partial t} - \nabla \cdot \left(\mathbf{D}_n s_w \phi \nabla C_n - \mathbf{u}_w C_n\right) &= R_n \\
\frac{\partial(C_p\phi s_w)}{\partial t} - \nabla \cdot \left(\mathbf{D}_p s_w \phi \nabla C_p - \mathbf{u}_w C_p\right) &= R_p
\end{aligned}$$

where the reaction rate terms are given by

$$R_b = -k_1\phi s_w C_b + k_2\rho_b\sigma_1 - k_3\phi s_w C_b + g_{1\,\max}\frac{C_n}{K_{b/n}+C_n}\phi s_w C_b - d_1\phi s_w C_b - \frac{R_p}{Y_{p/b}}$$

$$R_n = -\frac{R_p}{Y_{p/n}} - Y_n(\phi s_w C_b + \rho_b\sigma)$$

$$R_p = \mu_{\mathrm{p}\,\max}\frac{C_n - C_n^*}{K_{p/n}+C_n-C_n^*}(\phi s_w C_b + \rho_b\sigma)$$

and in the general case the dispersion coefficients are given by

$$D_{\beta,ij} = \delta_{ij}\alpha_{\beta,T}|\mathbf{u}| + (\alpha_{\beta,L}-\alpha_{\beta,T})\frac{u_i u_j}{|\mathbf{u}|} + \delta_{ij}D_\beta^{\mathrm{eff}} \qquad \beta = \{b,n,p\} \tag{2.28}$$

where the fluid velocity of the aqueous phase is given by $\mathbf{u} = \frac{\mathbf{u}_w}{\phi s_w}$. In this work we consider that biosurfactants are the only bioproducts. Table 2.9.1 shows a brief description of the previous parameters (Kim 2006, Li et al. 2011).

Table 2.9.1 Descriptions and units in the SI for the parameters used in the transport equations.

Parameter	Description
C_b, C_n, C_p	Concentrations of bacteria, nutrients and biosurfactants $[M/L^3]$
v_g	Settling velocity of bacteria $[L/T]$
k_1	Reversible rate of bacterial attachment to the rock surface $[1/T]$
k_2	Bacterial detachment rate $[1/T]$
k_3	Irreversible rate of bacterial attachment to the rock surface $[1/T]$
d_1	Bacterial decay rate coefficient $[1/T]$
ρ_b	Density of bacteria $[M/L^3]$
σ_1	Volumetric fractions of bacteria attached reversibly $[-]$
σ_2	Volumetric fractions of bacteria attached irreversibly $[-]$
$Y_{p/b}$	Biosurfactant yield coefficient per unit bacteria $[-]$
$Y_{p/n}$	Biosurfactant yield coefficient per unit nutrient $[-]$
Y_n	Maintenance energy+bacterial growth yield coefficient representing nutrient consumed $[1/T]$
$g_{1\max}$	Maximum bacterial growth rate coefficient $[1/T]$
$\mu_{\mathrm{p}\,\max}$	Maximum specific biomass production rate $[1/T]$
$K_{b/n}$	Half-saturation constant for concentration of specific growth rate $[M/L^3]$
$K_{p/n}$	Half-saturation constant for production of biosurfactants by consuming nutrient+substrate $[M/L^3]$
C_n^*	Critical nutrient concentration for metabolism $[M/L^3]$
$\alpha_{b,L}$, $\alpha_{n,L}$, $\alpha_{p,L}$	Longitudinal dispersivity of bacteria, nutrients and biosurfactants $[L]$
$\alpha_{b,T}$, $\alpha_{n,T}$, $\alpha_{p,T}$	Transverse dispersivity of bacteria, nutrients and biosurfactants $[L]$
D_b^{eff}, D_n^{eff}, D_p^{eff}	Effective diffusion coefficients of bacteria, nutrients and biosurfactants in the water phase $[L^2/T]$

Let us analyses the reaction terms for the transport equations. Regarding the bacterial clogging, we consider both scenarios: reversible k_1 and irreversible k_3 attachment to the rock, resulting in a detachment rate k_2. For modeling the growth of bacteria, we use the Monod-type model (Skjaelaaen 2010)

$$g_1 = g_{1\max}\frac{C_n}{K_{b/n} + C_n} \tag{2.29}$$

where $g_{1\max}$ is the observed maximum growth rate and $K_{b/n}$ the half saturation constant, being the nutrient concentration level when $g_1 = \frac{1}{2}g_{1\max}$. On the other hand, we consider a linear death of bacteria, given by d_1. Due to nutrients and bacteria being involved in the generation of biosurfactants, we introduce the yield coefficients $\frac{1}{Y_{p/b}} + \frac{1}{Y_{p/n}} = 1$. For the nutrients consumed for bacteria, we consider the yield coefficient Y_n, which we included in the R_n term. Considering now the biosurfactants source term, we need to model the production in function of nutrients and bacteria. We consider that the production rate is given by (Lacerda et al. 2012)

$$\mu_p = \mu_{\text{p max}}\frac{C_n - C_n^*}{K_{p/n} + C_n - C_n^*} \tag{2.30}$$

We notice that this function has the same structure than the Monod-type model, but we included the term C_n^*, in order to model a need of minimum C_n for obtaining biosurfactants.

The pressure, saturation and interfacial area equations are coupled with these transport equation under the following assumptions (Li et al. 2011)

1. The two-phase flows are incompressible and immiscible.
2. Both viscosities are constants.
3. We neglect the presence of dissolved salt in the wetting phase.
4. The system is isothermal.

2.10 Bioclogging

In Chapter 2, we introduced the idea of bioclogging as a mechanism for MEOR. In Kim 2006, a transport model that incorporates reversible/irreversible attachment to the solid matrix and growth/decay of bacteria is presented, where changes in porosity and permeability due to bacterial deposition and/or growth are also included. Following this model, the mass balance equations for bacteria deposited reversibly and irreversibly on the solid matrix are given by

$$\begin{aligned}\frac{\partial(\rho_b\sigma_1)}{\partial t} &= R_1\\ \frac{\partial(\rho_b\sigma_2)}{\partial t} &= R_2\end{aligned} \tag{2.31}$$

with

$$\begin{aligned} R_1 &= k_1(\phi_0 - \sigma)C_b - k_2\rho_b\sigma_1 + g_1\rho_b\sigma_1 - d_1\rho_b\sigma_1 \\ R_2 &= k_3(\phi_0 - \sigma)C_b + g_1\rho_b\sigma_2 - d_1\rho_b\sigma_2 \end{aligned} \tag{2.32}$$

where the modify porosity is defined as $\phi = \phi_0 - \sigma = \phi_0 - \sigma_1 - \sigma_2$. This model describe the changes of porosity in function of the position and time. In this model the growth and decay rate coefficients for the bacteria deposited and suspended are supposed to be equal.

Apart from reduction of the porosity due to bacteria clogging, the rock's ability to allow phases to flux is affected. For including the changes of permeability, we consider the parametric model (Clement et al. 1996), which states that reduction of porosity leads to reduction of permeability as the following relation

$$k = k_0\left(\frac{\phi}{\phi_0}\right)^C \tag{2.33}$$

where we take the value for the parameter $C = 19/6$ from Clement et al. 1996, which is founded in the idea that bioclogging is due to radius reduction instead of raise of micro-colonies.

2.11 Interfacial tension

One of the main objectives of applying MEOR is to reduce the s_{or} via surfactant effect on the oil-water interfacial tension. There exist several experiments showing the impact of surfactants in reducing the interfacial tension (Youssef et al. 2003, Wu et al. 2013). Common initial interfacial area values are of the order of 10^{-2} mN/m and we aim to lower this value $\leq 10^{-3}$ mN/m (Yuan et al. 2015). In order to model mathematically this behavior, we need a function $\sigma_{\text{Int}}(C_{\text{ps}})$ that under values of a critical surfactant concentration, the interfacial tension does not decrease but over this critical surfactant concentration, the interfacial tension decreases until a minimal interfacial tension value, persisting this value despite we increase the surfactant concentration. One mathematical model fulfilling these requirements is given by (Nielsen et al. 2010)

$$\sigma^*_{\text{Int}} = \sigma_{\text{Int}}\frac{-\tanh(l_3 * C_p - l_2) + 1 + l_1}{-\tanh(-l_2) + 1 + l_1} \tag{2.34}$$

where l_1, l_2 and l_3 are fitting parameters, which define the efficiency of the surfactant, moderating the concentration where the interfacial tension drops dramatically and the minimal interfacial tension achieved after the surfactant action (Nielsen et al. 2015).

2.12 Capillary number

The residual oil saturation after water flooding is believed to be distributed through the pores in the petroleum reservoir in the form of immobile globules, being the capillary and viscous interactions the main forces acting on these globules (Donaldson et al. 1989). The capillary number N_{Ca} relates the surface tension and viscous forces acting in the interface and is given by

$$N_{\text{Ca}} = \frac{u_w \mu_w}{\sigma^*_{\text{Int}}} \tag{2.35}$$

At the end of water flooding, the capillary number is in the range 10^{-6} to 10^{-7} (Donaldson et al. 1989). In order to increase the capillary number, from Eq. 2.35 we observe that increasing the flow rate, the water viscosity or lowering the interfacial tension are the three possibilities. In Li et al. 2011, they implemented a biological and hydrogeological finite element model, resulting in a functional relation between s_{or} and N_{Ca}, demonstrating that MEOR could improve the oil extraction if we can obtain a capillary number between 10^{-5} and 10^{-1}.

2.13 Residual oil saturation

Formerly, we mentioned that the surfactants reduce the oil-water interfacial tension, allowing to enhance oil recovery. In order to model the amount of residual oil saturation recovered using biosurfactants, we consider an irreducible residual oil saturation $s_{or}^{\min}$. On the other hand, the capillary number N_{Ca} is inversely proportional to the interfacial tension σ_{Int}. Then, for modeling the residual oil saturation reduction due to biosurfactant effects, one possibility is to give a parameterization where when the capillary number increases, the s_{or} decreases until a irreducible value of oil saturation.

For relating the residual oil saturation and the capillary number, in this thesis we use the following relation (Li et al. 2007)

$$s_{or}(t + \Delta t) = \min\left(s_{or}(t), s_{or}^{\min} + (s_{or}^{\max} - s_{or}^{\min})[1 + (T_1 N_{\text{Ca}}(t))^{T_2}]^{\frac{1}{T_2}-1}\right) \tag{2.36}$$

where $s_{or}^{\min}$ and $s_{or}^{\max}$ are the maximum and minimum residual oil saturation and both T_1 and T_2 are fitting parameters estimated from the experimental data.

Giving the mathematical expressions for the interfacial area reduction σ^*_{Int}, the capillary number N_{Ca} and the residual oil saturation reduction $s_{or}(t)$, we can account in our model the effect of the biosurfactants in improving the oil recovery.

2.14 Two-phase flow model with transport equations including bioclogging and interfacial area

In summary, the next equations represent our model, and in the next two chapters we show one way to deal with the discretization and boundary conditions in 1-D and 2-D domains.

$$\frac{\partial \phi}{\partial t} - \nabla \cdot (\mathbf{k}(\lambda_\Sigma \nabla p + \tfrac{1}{2}\lambda_\Delta \nabla p_c - (\lambda_w \rho_w + \lambda_n \rho_n)\mathbf{g})) = \sum_{\alpha=w,n} \frac{F_\alpha}{\rho_\alpha} \quad \text{in } \Omega$$

$$\frac{\partial \phi s_w}{\partial t} - \nabla \cdot (\lambda_w \mathbf{k}(\nabla(p - \tfrac{1}{2}p_c) - \rho_n \mathbf{g})) = \frac{F_w}{\rho_w} \quad \text{in } \Omega$$

$$\frac{\partial a_{wn}}{\partial t} - \nabla \cdot (a_{wn}\mathbf{k}_{wn}\nabla a_{wn}) = E_{wn} \quad \text{in } \Omega$$

$$\frac{\partial (C_b \phi s_w)}{\partial t} - \nabla \cdot \left(\mathbf{D}_b s_w \phi \nabla C_b - \mathbf{u}_w C_b - \phi \mathbf{v}_g C_b \right) = R_b \quad \text{in } \Omega$$

$$\frac{\partial (C_n \phi s_w)}{\partial t} - \nabla \cdot \left(\mathbf{D}_n s_w \phi \nabla C_n - \mathbf{u}_w C_n \right) = R_n \quad \text{in } \Omega$$

$$\frac{\partial (C_p \phi s_w)}{\partial t} - \nabla \cdot \left(\mathbf{D}_p s_w \phi \nabla C_p - \mathbf{u}_w C_p \right) = R_p \quad \text{in } \Omega$$

$$\frac{\partial \rho_b \sigma_1}{\partial t} = R_1 \quad \text{in } \Omega$$

$$\frac{\partial \rho_b \sigma_2}{\partial t} = R_2 \quad \text{in } \Omega$$

$$\mathbf{k} = \mathbf{k}_0 \left(\frac{\phi}{\phi_0} \right)^C \quad \text{in } \Omega$$

$$\sigma^*_{\text{Int}} = \sigma_{\text{Int}} \frac{-\tanh(l_3 * C_p - l_2) + 1 + l_1}{-\tanh(-l_2) + 1 + l_1} \quad \text{in } \Omega$$

$$s_{or} = \min\left(s_{or}(t), s_{or}^{\min} + (s_{or}^{\max} - s_{or}^{\min})[1 + (T_1 N_{Ca})^{T_2}]^{\frac{1}{T_2}-1}\right) \quad \text{in } \Omega$$

Initial conditions for $s_w,\ p,\ a_{wn},\ C_b,\ C_n,\ C_p,\ \phi,\ \mathbf{k},\ \sigma_1,\ \sigma_2$ in Ω

Boundary conditions for $s_w,\ p,\ a_{wn},\ C_b,\ C_n,\ C_p$ on $\partial\Omega$

Parametrizations for $k_{r,w} = k_{r,w}(s), \quad k_{r,n} = k_{r,n}(s), \quad p_c = p_c(s_w, a_{wn})$

Chapter 3

Discretization of the model

For solving numerically the two-phase flow model in a given domain, it is necessary to discretize the equations and the space and time domains. The reason for partitioning both space and time is that computers cannot work with the continuum, so we divide the space and time domains in a finite number of elements. In order to achieve the discretization of equations, we use one finite volume method, the TPFA. In this chapter we present the theory and techniques for discretizing and solving numerically the mathematical model.

3.1 Space and time discretization

Numerical methods have been developed since a long time ago, contributing to different techniques to partition a domain. This partition could be formed for elements of different shapes and sizes; it depends on the problem. For example, if there is a zone in the domain where we want more resolution in the results, we should consider a finer partition in this region.

For discretizing the space domain, we consider a uniform cell-centered grid with half-cells at the boundaries. For example, in Fig. 3.1.1 we show such discretization in a 1-D domain of length L with step Δx.

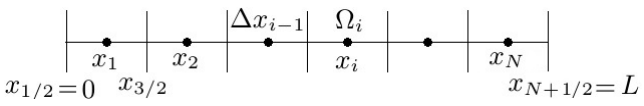

Figure 3.1.1 Cell-centered grid in 1D. We label the middle points x_i of the elements Ω_i.

Fig. 3.1.2 shows a uniform cell-centered grid in a 2D domain of length L and width W.

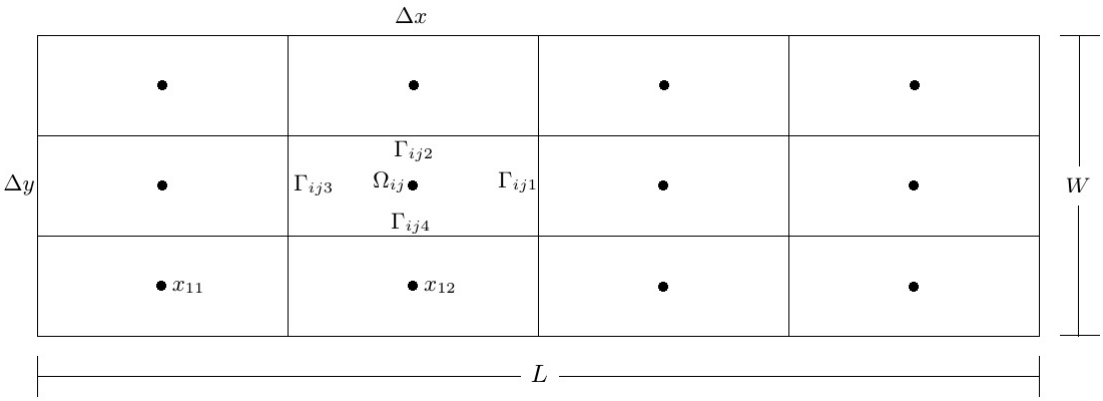

Figure 3.1.2 Gridding in a rectangular domain of size $L \times W$.

The purpose of defining a partition is to find a numerical solution of the discrete problem in the points $\{x_i\}$, where by raising the number of elements, we make better approximations to the solution of the continuous problem.

Because time is also a continuous variable, we have to use a discretization technique. For doing this, we consider a uniform discretization from the initial time t_0 until the final time T with Δt step. In Fig. 3.1.3 we show such discretization.

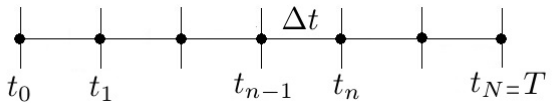

Figure 3.1.3 Vertex-centered grid in 1D. We label the vertex points t_n and the size step Δt.

3.2 Approximations for the derivatives, integrals and parameterizations

Once we have the discretization of space and time, we need to discretize the derivatives and integrals. For doing this, we consider an arbitrary function $f(x)$ and its Taylor expansion (Canuto and Tabacco 2008)

$$\begin{aligned} f(x+\Delta x) &= f(x) + f'(x)\Delta x + \frac{\Delta x^2}{2} f''(x) + O(\Delta x^3) \\ f(x-\Delta x) &= f(x) - f'(x)\Delta x + \frac{\Delta x^2}{2} f''(x) + O(\Delta x^3) \end{aligned} \tag{3.1}$$

From the previous equations, we isolate $f'(x)$ and get

$$f'(x) = \frac{f(x+\Delta x) - f(x)}{\Delta x} + O(\Delta x) \qquad f'(x) = \frac{f(x) - f(x-\Delta x)}{\Delta x} + O(\Delta x) \tag{3.2}$$

Now, subtracting the second equation from the first equation in (3.1) and isolating $f'(x)$, we obtain

$$f'(x) = \frac{f(x+\Delta x) - f(x-\Delta x)}{2\Delta x} + O(\Delta x^2) \Longrightarrow f'(x) = \frac{f(x+\frac{\Delta x}{2}) - f(x-\frac{\Delta x}{2})}{\Delta x} + O(\Delta x^2) \tag{3.3}$$

In this thesis we consider functions of two variables $f(x, y)$. Generalization of these functions can be followed from the previous analysis, having as results such as

$$\frac{\partial f}{\partial x}(x,y) \approx \frac{f(x+\Delta x, y) - f(x,y)}{\Delta x} \qquad \frac{\partial f}{\partial y}(x,y) \approx \frac{f(x, y+\frac{\Delta y}{2}) - f(x, y-\frac{\Delta y}{2})}{\Delta y} \tag{3.4}$$

Both of the last expressions are used in this work for approximating the derivatives. The derivative approximation of first order $O(\Delta x)$ is used on the boundaries of the spatial domain and time derivatives, while the second order approximation $O(\Delta x^2)$ is used in the cell-centered grid.

Now, we focus on the time variable. Let us consider the following differential partial equation

$$\frac{\partial u}{\partial t}(x,t) = F(u,t) \tag{3.5}$$

We use the next notation $u_i^n \equiv u(x_i, t_n)$. Using the derivative discretization, we get

$$\frac{u^{n+1} - u^n}{\Delta t} \approx F(u,t) \Longrightarrow u_i^{n+1} = u_i^n + F(u,t)\Delta t \tag{3.6}$$

The three following methods are use to find an approximation (Olsen-Kettle 2011)

- ◇ Explicit Euler's method $u_i^{n+1} = u_i^n + F(u_i^n, t^n)\Delta t + O(\Delta t)$
- ◇ Implicit Euler's method $u_i^{n+1} = u_i^n + F(u_i^{n+1}, t^{n+1})\Delta t + O(\Delta t)$
- ◇ Crank-Nicolson Scheme $u_i^{n+1} = u_i^n + \frac{1}{2}[F(u_i^{n+1}, t^{n+1}) + F(u_i^n, t^n)]\Delta t + O(\Delta t^2)$

The one that we use in this thesis is the Implicit Euler's method, also known as BE. Although the explicit Euler's method is also of order $O(\Delta t)$ and easier to implement, it is not A-stable (Trefethen and Bau 1997).

After mentioning the mechanisms of approximations for the derivatives, now we study the numerical integration. Let us consider the following integral

$$I[f] = \int_a^b f(x)dx \tag{3.7}$$

where $f(x)$ is a given function and $[a, b]$ a finite interval. We look for approximating the integral by

$$I[f] \approx \sum_{i=1}^{n} w_i f(x_i) \tag{3.8}$$

where $x_1 < x_2 < \cdots < x_n$ are distinct nodes and $w_1,\ w_2, \ldots,\ w_n$ the corresponding weights (Dalquist and Bjorck 2008). These weights are determined in order that (3.8) computes exactly the polynomial

with the highest degree possible. Considering a cell-centered grid, in the midpoint rule we approximate $f(x)$ on $[x_{i-1/2}, x_{i+1/2}]$ by

$$f_i = f(x_i) \qquad x_i = \frac{1}{2}(x_{i-1/2} + x_{i+1/2}) \tag{3.9}$$

leading to the approximation

$$\int_{x-1/2}^{x+1/2} f(x)dx \approx f_i \Delta x \tag{3.10}$$

Finally, after taking into account every sub interval $[x_{i-1/2}, x_{i+1/2}]$, the composite midpoint rule is given by (Dalquist and Bjorck 2008)

$$\int_a^b f(x)dx = \Delta x \sum_{i=1}^{n} f_i + \frac{(b-a)\Delta x^2}{24} f''(\xi), \quad \xi \in [a, b] \tag{3.11}$$

Even though the midpoint rule just uses one function value for the approximation, it computes exact integral when $f(x)$ is a polynomial of degree 1. Generalization of the midpoint rule to a 2-D domain like in Fig. 3.1.2 leads to

$$\int_{ay}^{by}\int_{ax}^{bx} f(x,y)dxdy = \Delta x \Delta y \sum_{j=1}^{m}\sum_{i=1}^{n} f_{ij} \tag{3.12}$$

Once we have introduced these methods of approximations, we proceed with the TPFA.

3.3 Two-point flux approximation

When we use finite difference methods in order to approximate PDEs, we replace the operator derivatives by differences between points on a discrete set of points in the domain. On the other hand, when we consider finite volume methods, they are derived from conservation of quantities over cell volumes (Jorg et al. 2009). These methods are widely used for numerically solving PDEs; we use both on them in this work.

Let us consider the following differential equation on a domain Ω (Lunde 2006)

$$-\nabla \cdot c\nabla y = F \tag{3.13}$$

Our aim is to find the solution for y $\forall x \in \Omega$. First, we consider a partition of our domain $\Omega = \bigcup \Omega_k$, where Ω_k denotes a grid cell in Ω. We integrate Eq. (3.13) in the control volume Ω_k

$$-\int_{\Omega_k} \nabla \cdot c\nabla y dx = \int_{\Omega_k} F dx \tag{3.14}$$

Let us focus on the left integral. Using the divergence theorem, we can write this integral as

$$-\int_{\Omega_k} \nabla \cdot c\nabla y dx = -\int_{\partial\Omega_k} c\nabla y \cdot \mathbf{n} dS \tag{3.15}$$

In the general case, the boundary $\partial\Omega_k$ could be part of several control volume boundaries. For example, in the 3-D case considering a quadrangular partition, there are six control volumes sharing part of the same boundary. Let us consider the 2-D case (which the 1-D case can be derived from) shown in Fig. (3.1.2). In this case, we have four boundaries $\gamma_{i+1,j} = \Omega_{i+1,j} \cap \Omega_{ij}$, $\gamma_{i,j+1} = \Omega_{i,j+1} \cap \Omega_{ij}$, $\gamma_{i-1,j} = \Omega_{i-1,j} \cap \Omega_{ij}$ and $\gamma_{i,j-1} = \Omega_{i,j-1} \cap \Omega_{ij}$. Having found the boundaries, we can approximate ∇y using two points: one in the current control volume Ω_i and the other in the corresponding adjacent control volume. This way to approximate the gradient is called two-point flux approximation. Using the previous idea, we approximate the gradient as

$$\nabla y \approx 2\frac{y_{i+1,j} - y_{ij}}{\Delta x_{i+1,j} + \Delta x_{ij}} \quad \text{on} \quad \gamma_{i+1,j} \tag{3.16}$$

where $y_{i+1,j}$ and y_{ij} correspond to the average value in the control volume $\Omega_{i+1,j}$ and Ω_{ij} respectively, and $\Delta x_{i+1,j}$ and Δx_{ij} correspond to the distance from the middle points of $\Omega_{i+1,j}$ and Ω_{ij} to the boundary $\gamma_{i+1,j}$. Using this approximation and taking into account the sign after the inner product with the normal vectors $\mathbf{n}$, we write Eq. (3.14) as

$$\begin{aligned} &- 2\frac{y_{i+1,j} - y_{ij}}{\Delta x_{i+1,j} + \Delta x_{ij}} \int_{\gamma_{i+1,j}} c dS - 2\frac{y_{i,j+1} - y_{ij}}{\Delta x_{i,j+1} + \Delta x_{ij}} \int_{\gamma_{i,j+1}} c dS - 2\frac{y_{i-1,j} - y_{ij}}{\Delta x_{i-1,j} + \Delta x_{ij}} \int_{\gamma_{i-1,j}} c dS \\ &- 2\frac{y_{i,j-1} - y_{ij}}{\Delta x_{i,j-1} + \Delta x_{ij}} \int_{\gamma_{i,j-1}} c dS = \int_{\Omega_{ij}} F dx \end{aligned} \tag{3.17}$$

Now, we consider $\widetilde{c}$ as an approximate value of the parameter c on the boundary (in the next section we explain methods of approximation for this parameters) and also approximate the right integral using numerical integration. We finally write

$$\begin{aligned} &- 2\widetilde{c}_{i+1,j}\frac{y_{i+1,j} - y_{ij}}{\Delta x_{i+1,j} + \Delta x_{ij}}|\gamma_{i+1,j}| - 2\widetilde{c}_{i,j+1}\frac{y_{i,j+1} - y_{ij}}{\Delta x_{i,j+1} + \Delta x_{ij}}|\gamma_{i,j+1}| - 2\widetilde{c}_{i-1,j}\frac{y_{i-1,j} - y_{ij}}{\Delta x_{i-1,j} + \Delta x_{ij}}|\gamma_{i-1,j}| \\ &- 2\widetilde{c}_{i,j-1}\frac{y_{i,j-1} - y_{ij}}{\Delta x_{i,j-1} + \Delta x_{ij}}|\gamma_{i,j-1}| = \widetilde{F}_{ij}|\Omega_{ij}| \end{aligned} \tag{3.18}$$

Applying the same procedure to all control volumes in Ω, it leads to a linear system of the form $Ay = b$. To make this system positive definite, we add a positive constant to the first diagonal element of A (Lunde 2006). Moreover, this system would have a unique solution if appropriate parameterizations, boundary and initial conditions are given.

3.4 Approximations of the parameters on the integral boundaries

In the previous section, it was necessary to use an approximation of the parameter c on the boundaries, as we consider a cell centered grid and we do not know the values on the walls. Depending on the parameter, we should consider different technique approximations, in order to get stability and correct results (Aziz and Settari 1979).

Regarding the permeability of the medium, we approximate k by the harmonic mean (Aavatsmark 2002)

$$k_{i+1/2} = \frac{2(\Delta x_{i+1} + \Delta x_i)}{\frac{\Delta x_{i+1}}{k_{i+1}} + \frac{\Delta x_i}{k_i}} \tag{3.19}$$

The reason for considering this harmonic mean comes from the computation of an effective permeability when we consider a layered system with different values of permeability and a flux perpendicular to these layers, finding that the effective permeability of a system with two layers is given by Eq. (3.19) (Nordbotten and Celia 2011).

Considering now the phases mobilities, one way to approximate them is using the upstream weighting (Chen et al. 2006)

$${}_r\lambda_{i+1/2} = \begin{cases} {}_r\lambda(s_i) & \text{if flow is from } i \text{ to } i+1 \\ {}_r\lambda(s_{i+1}) & \text{if flow is from } i+1 \text{ to } i \end{cases} \tag{3.20}$$

For the rest of the parameters (porosity, diffusion, etc) that we need to approximate on the walls, we simply use the average value

$$\xi_{i+1/2} = \frac{\xi_{i+1} + \xi_i}{2} \tag{3.21}$$

3.5 Initial and boundary conditions

In general, PDEs have infinite number of solutions. However, given an oil reservoir problem, we are interested in one particular solution of these PDEs. It is natural to think that we have to provide some information about the reservoir to the PDEs, in order to find a unique solution. These conditions are motivated by the physics, being the initial and boundary conditions (Strauss 2008). An initial condition gives the solution at a certain time t_0 for all points inside the domain Ω. In relation to the boundary, we know information (pressure, saturation, flux, ...) about the reservoir on the walls. For example, we could know the flow through the walls, the amount of bacteria that we are injecting into one part of the boundary, etc. There are several types of boundary conditions, but in this thesis we consider Dirichlet boundary conditions (the value of the solution is known on the boundary), Neumann boundary conditions (the normal derivative is known on the boundary) and flux boundary conditions (the flux is known on the boundary).

For solving our model, we need to give the initial conditions for the following variables

$$p(\mathbf{x},0) = p_0(\mathbf{x}) \quad s_w(\mathbf{x},0) = s_{w,0}(\mathbf{x}) \quad a_{wn}(\mathbf{x},0) = a_{wn,0}(\mathbf{x}) \quad c_b(\mathbf{x},0) = c_{b,0}(\mathbf{x}) \quad c_n(\mathbf{x},0) = c_{n,0}(\mathbf{x})$$
$$c_p(\mathbf{x},0) = c_{p,0}(\mathbf{x}) \quad \sigma_1(\mathbf{x},0) = \sigma_{1,0}(\mathbf{x}) \quad \sigma_2(\mathbf{x},0) = \sigma_{2,0}(\mathbf{x}) \quad \phi(\mathbf{x},0) = \phi_0(\mathbf{x}) \quad \mathbf{k}(\mathbf{x},0) = \mathbf{k}_0(\mathbf{x})$$

Additionally, we need to provide the boundary conditions for the average pressure, water saturation, interfacial area, bacterial, nutrient and biosurfactant concentrations. In the next chapter, we show with details a way to deal with these boundary conditions in 1D and 2D.

3.6 General formulation for solving the model

Once we have the discretization of the space, time and equations, we proceed with the implementation. Prior to this, we introduce the following ideas and concepts that we use in the numerical solver. For solving the pressure, saturation and interfacial area equations, we use an implicit scheme. The use of these iterative formulations is very common, for example in Pop et al. 2004 and List and Radu 2016 they solved the Richards equation using this technique. Regarding the two-phase flow, in Radu et al. 2015b and Radu et al. 2015a they solved the equations using the same iterative scheme. The convergence of this implicit scheme can be followed from Radu et al. 2010, Kumar et al. 2013, Kumar et al. 2014 and Kvashchuk 2015. The notation we use is

$$p_i^{n+1,j} \quad \text{where} \quad p_{\text{current point}}^{\text{solution for time t(n+1), iner iteration}} \tag{3.22}$$

Because we use an iterative scheme, it is indispensable to have a measure of the error. It is known that any norm is equivalent in a finite-dimensional space (Trefethen and Bau 1997), so it is not relevant which the norm we choose because we are interested in measuring the reduction of error. For this work, we use the following L^2-norm

$$\|\mathbf{x}\|_{L^2} = \left(\Delta x \sum_{i=1}^{m} x_i^2\right)^{1/2} \tag{3.23}$$

Once we have a measure for the error, we can proceed with the general idea for solving numerically our model. Extending the Skiftestad 2015's algorithm, we have the following procedure

I We solve the pressure equation using the previous values of saturation and interfacial area.

II We solve the saturation equation using the new value of pressure and the previous value of interfacial area.

III We solve the interfacial area equation using the update value of saturation.

IV We compute the errors $\|^{j+1}\mathbf{p}^{n+1} - {}^{j}\mathbf{p}^{n+1}\|_{L^2}$, $\|^{j+1}\mathbf{s}^{n+1} - {}^{j}\mathbf{s}^{n+1}\|_{L^2}$ and $\|^{j+1}\mathbf{a}^{n+1} - {}^{j}\mathbf{a}^{n+1}\|_{L^2}$.

V If the errors are less than a given tolerance ϵ, we solve the concentration equations. Otherwise, we upgrade the values for the inner iteration ^{j} and we solve again the three equations. If any of the errors get more than ϵ in a given maximum number of iterations MI, either the problem is not well posed or we have to consider smaller time steps.

VI We solve the concentration equation iteratively (this due to the source/sink values depend also in the saturation) until the error is less than ϵ or we reach the MI.

VII If the concentration error is less than ϵ, we solve the bacterial deposited equations and we update the porosity.

VIII After updating the porosity, we compute the new permeability, interfacial tension and residual oil saturation.

IX We move to the next time step. If we have not reach the final time T, we start the process again until we reach the final time T.

X Once we reach the final time, we finally plot the results.

3.7 Flux diagram for solving the model

In Fig. 3.7.1, we show a flux diagram for solving the two-phase model with transport equations including bioclogging and interfacial area.

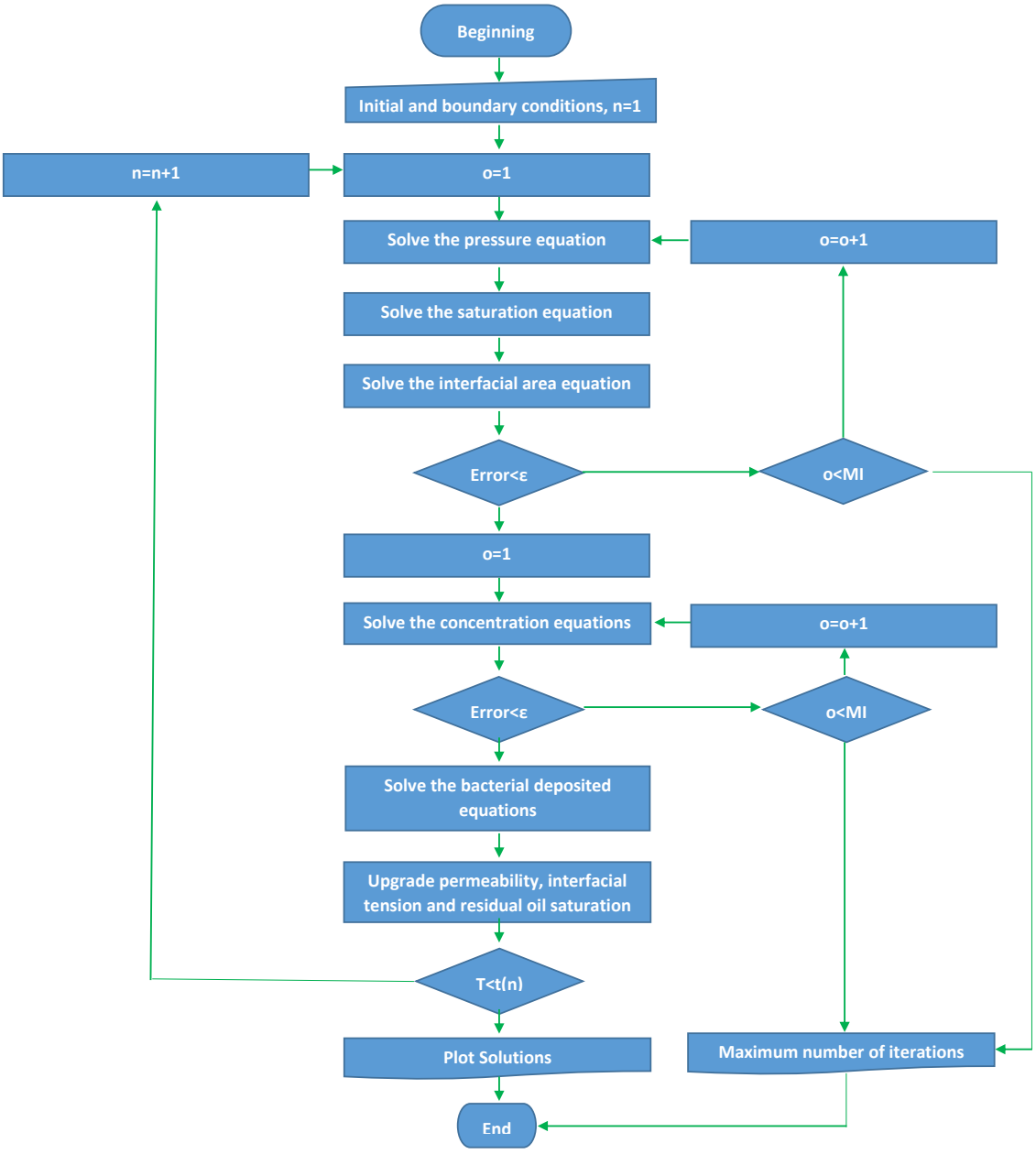

Figure 3.7.1 Flux diagram for solving the two-phase flow model. MI represents the maximun number of iterations and ϵ the error tolerance.

Chapter 4

Implementation of the model in 1-D and 2-D domains

In the previous chapter, we describe some techniques used to discretize partial differential equations in order to give a numerical solution. Once we have the discretization of the problem, we proceed to solve it in 1D and 2D. In this chapter we explain in detail how to implement the equations in 1-D and 2-D rectangular domains with rectangular gridding using cell-centered cells with half-cells on the boundaries. We also compare the numerical results with benchmark simulations and we study the error convergence given analytic solutions.

4.1 1-D formulation

Regarding the spatial location, we are living in a three dimensional space. Then, for specifying a point inside a reservoir, we need three spatial coordinates. However, there are many cases were we can reduce the dimension to 2D or even 1D, using symmetries, approximations, etc. For the 1-D simulation, we consider a porous media of size L. In this case, we just have two boundaries, where we have to provide appropriate conditions in order to get the unique solution.

4.1.1 Pressure equation

We start writing the expression for the pressure equation in 1D

$$\frac{\partial \phi}{\partial t} - \frac{\partial}{\partial x}\big[k\big(\lambda_\Sigma \frac{\partial p}{\partial x} + \frac{1}{2}\lambda_\Delta \frac{\partial p_c}{\partial x} - (\lambda_w \rho_w + \lambda_n \rho_n) g\big)\big] = \sum_{\alpha=w,n} \frac{F_\alpha}{\rho_\alpha} \tag{4.1}$$

We integrate in a control interval $[x_{i-1/2}, x_{i+1/2}]$

$$\int_{x_{i-1/2}}^{x_{i+1/2}} \left(\frac{\partial \phi}{\partial t} - \frac{\partial}{\partial x}\big[k\big(\lambda_\Sigma \frac{\partial p}{\partial x} + \frac{1}{2}\lambda_\Delta \frac{\partial p_c}{\partial x} - (\lambda_w \rho_w + \lambda_n \rho_n) g\big)\big] \right) dx = \int_{x_{i-1/2}}^{x_{i+1/2}} \sum_{\alpha=w,n} \frac{F_\alpha}{\rho_\alpha} dx \tag{4.2}$$

Using the Fundamental Theorem of Calculus for the left integral and the midpoint rule for the right integral

$$\begin{aligned}\frac{\partial \phi_i}{\partial t}\Delta x - \big(k\big(\lambda_\Sigma \frac{\partial p}{\partial x} + \frac{1}{2}\lambda_\Delta \frac{\partial p_c}{\partial x} - (\lambda_w \rho_w + \lambda_n \rho_n) g\big)\big)_{i+1/2} \\ + \big(k\big(\lambda_\Sigma \frac{\partial p}{\partial x} + \frac{1}{2}\lambda_\Delta \frac{\partial p_c}{\partial x} - (\lambda_w \rho_w + \lambda_n \rho_n) g\big)\big)_{i-1/2} = \sum_{\alpha=w,n} \frac{F_{\alpha,i}}{\rho_\alpha}\Delta x\end{aligned} \tag{4.3}$$

Considering the chain rule for p_c

$$\frac{\partial p_c}{\partial x} = \frac{\partial p_c}{\partial s_w}\frac{\partial s_w}{\partial x} + \frac{\partial p_c}{\partial a_{wn}}\frac{\partial a_{wn}}{\partial x} \tag{4.4}$$

Due to the fact that the capillary pressure is a function of the saturation and interfacial area, both of them being unknowns, we should use an inner iteration ^{j} in order to upgrade the values of the functions depending on the saturation and interfacial area and solve this system of equations (pressure, saturation and interfacial area equations) until a stopping criterion is reached. For initializing the iteration, we consider the solution at the previous time step

$$p_i^{n+1,1} = p_i^n, \quad a_{wn,i}^{n+1,1} = a_{wn,i}^n, \quad s_{w,i}^{n+1,1} = s_{w,i}^n, \quad \lambda_i^{n+1,1} = \lambda_i^n, \quad \forall i \tag{4.5}$$

Using Eq. (3.2), we approximate the time derivative for the porosity as $\frac{\partial \phi_i}{\partial t} \approx \frac{\phi_i^n - \phi_i^{n-1}}{\Delta t}$ with $\phi_i^0 = \phi_i^1$. Using the previous considerations and rearranging the terms in order to put on the left hand side the pressure, we get the following system of equations

$$\begin{aligned}&- \frac{p_{i+1}^{n+1,j+1}}{\Delta x}\lambda_{\Sigma,i+1/2}^{n+1,j} k_{i+1/2}^n + p_i^{n+1,j+1}\left(\frac{\lambda_{\Sigma,i+1/2}^{n+1,j} k_{i+1/2}^n}{\Delta x} + \frac{\lambda_{\Sigma,i-1/2}^{n+1,j} k_{i-1/2}^n}{\Delta x}\right) - \frac{p_{i-1}^{n+1,j+1}}{\Delta x}\lambda_{\Sigma,i-1/2}^{n+1,j} k_{i-1/2}^n \\ &= \sum_{\alpha=w,n}\frac{F_{\alpha,i}^{n+1}}{\rho_\alpha}\Delta x - \frac{\phi_i^n - \phi_i^{n-1}}{\Delta t}\Delta x \\ &+ \frac{1}{2}\lambda_{\Delta,i+1/2}^{n+1,j} k_{i+1/2}^n\left(\frac{\partial p_{c,i+1/2}^{n+1,j}}{\partial s_w}\frac{s_{w,i+1}^{n+1,j} - s_{w,i}^{n+1,j}}{\Delta x} + \frac{\partial p_{c,i+1/2}^{n+1,j}}{\partial a_{wn}}\frac{a_{wn,i+1}^{n+1,j} - a_{wn,i}^{n+1,j}}{\Delta x}\right) \\ &+ \frac{1}{2}\lambda_{\Delta,i-1/2}^{n+1,j} k_{i-1/2}^n\left(\frac{\partial p_{c,i-1/2}^{n+1,j}}{\partial s_w}\frac{s_{w,i-1}^{n+1,j} - s_{w,i}^{n+1,j}}{\Delta x} + \frac{\partial p_{c,i-1/2}^{n+1,j}}{\partial a_{wn}}\frac{a_{wn,i-1}^{n+1,j} - a_{wn,i}^{n+1,j}}{\Delta x}\right) \\ &- g[\rho_w(k_{i+1/2}^n \lambda_{w,i+1/2}^{n+1,j} - k_{i-1/2}^n \lambda_{w,i-1/2}^{n+1,j}) + \rho_n(k_{i+1/2}^n \lambda_{n,i+1/2}^{n+1,j} - k_{i-1/2}^n \lambda_{n,i-1/2}^{n+1,j})]\end{aligned} \tag{4.6}$$

Multiplying $\Delta x \Delta t$ in both sides, we finally obtain

$$
\begin{aligned}
&- p_{i+1}^{n+1,j+1}\lambda_{\Sigma,i+1/2}^{n+1,j}k_{i+1/2}^{n}\Delta t \\
&+ p_{i}^{n+1,j+1}\Big(\lambda_{\Sigma,i+1/2}^{n+1,j}k_{i+1/2}^{n} + \lambda_{\Sigma,i-1/2}^{n+1,j}k_{i-1/2}^{n}\Big)\Delta t \\
&- p_{i-1}^{n+1,j+1}\lambda_{\Sigma,i-1/2}^{n+1,j}k_{i-1/2}^{n}\Delta t \\
&= \sum_{\alpha=w,n}\frac{F_{\alpha,i}^{n+1}}{\rho_\alpha}\Delta x^2\Delta t - (\phi_i^n - \phi_i^{n-1})\Delta x^2 \\
&+ \frac{1}{2}\lambda_{\Delta,i+1/2}^{n+1,j}k_{i+1/2}^{n}\Big(\frac{\partial p_{c,i+1/2}^{n+1,j}}{\partial s_w}(s_{w,i+1}^{n+1,j} - s_{w,i}^{n+1,j}) + \frac{\partial p_{c,i+1/2}^{n+1,j}}{\partial a_{wn}}(a_{wn,i+1}^{n+1,j} - a_{wn,i}^{n+1,j})\Big)\Delta t \\
&+ \frac{1}{2}\lambda_{\Delta,i-1/2}^{n+1,j}k_{i-1/2}^{n}\Big(\frac{\partial p_{c,i-1/2}^{n+1,j}}{\partial s_w}(s_{w,i-1}^{n+1,j} - s_{w,i}^{n+1,j}) + \frac{\partial p_{c,i-1/2}^{n+1,j}}{\partial a_{wn}}(a_{wn,i-1}^{n+1,j} - a_{wn,i}^{n+1,j})\Big)\Delta t \\
&- g[\rho_w(k_{i+1/2}^{n}\lambda_{w,i+1/2}^{n+1,j} - k_{i-1/2}^{n}\lambda_{w,i-1/2}^{n+1,j}) + \rho_n(k_{i+1/2}^{n}\lambda_{n,i+1/2}^{n+1,j} - k_{i-1/2}^{n}\lambda_{n,i-1/2}^{n+1,j})]\Delta x\Delta t
\end{aligned}
\tag{4.7}
$$

Defining

$$
\begin{aligned}
a_i &= \lambda_{\Sigma,i+1/2}^{n+1,j}k_{i+1/2}^{n} \qquad 1 \le i \le N-1 \\
b_i &= \sum_{\alpha=w,n}\frac{F_{\alpha,i}^{n+1}}{\rho_\alpha}\Delta x^2\Delta t - (\phi_i^n - \phi_i^{n-1})\Delta x^2 \\
&+ \frac{1}{2}\lambda_{\Delta,i+1/2}^{n+1,j}k_{i+1/2}^{n}\Big(\frac{\partial p_{c,i+1/2}^{n+1,j}}{\partial s_w}(s_{w,i+1}^{n+1,j} - s_{w,i}^{n+1,j}) + \frac{\partial p_{c,i+1/2}^{n+1,j}}{\partial a_{wn}}(a_{wn,i+1}^{n+1,j} - a_{wn,i}^{n+1,j})\Big)\Delta t \\
&+ \frac{1}{2}\lambda_{\Delta,i-1/2}^{n+1,j}k_{i-1/2}^{n}\Big(\frac{\partial p_{c,i-1/2}^{n+1,j}}{\partial s_w}(s_{w,i-1}^{n+1,j} - s_{w,i}^{n+1,j}) + \frac{\partial p_{c,i-1/2}^{n+1,j}}{\partial a_{wn}}(a_{wn,i-1}^{n+1,j} - a_{wn,i}^{n+1,j})\Big)\Delta t \\
&- g[\rho_w(k_{i+1/2}^{n}\lambda_{w,i+1/2}^{n+1,j} - k_{i-1/2}^{n}\lambda_{w,i-1/2}^{n+1,j}) + \rho_n(k_{i+1/2}^{n}\lambda_{n,i+1/2}^{n+1,j} - k_{i-1/2}^{n}\lambda_{n,i-1/2}^{n+1,j})]\Delta x\Delta t
\end{aligned}
$$

we can write the linear system of equations for the pressure in the matrix system $\mathbf{A}\mathbf{p}^{n+1,j+1} = \mathbf{b}$

$$
\begin{pmatrix}
\text{BCs} & & & & & & & \\
-a_1 & a_1+a_2 & a_2 & 0 & 0 & \dots & 0 & 0 \\
0 & -a_2 & a_2+a_3 & -a_3 & 0 & 0 & 0 & 0 \\
\ddots & \ddots & \ddots & \ddots & \ddots & \ddots & \ddots & \ddots \\
\dots & 0 & -a_{i-1} & a_{i-1}+a_i & -a_i & 0 & \dots & 0 \\
\ddots & \ddots & \ddots & \ddots & \ddots & \ddots & \ddots & \ddots \\
0 & 0 & \dots & 0 & 0 & -a_{N-2} & a_{N-2}+a_{N-1} & -a_{N-1} \\
 & & & & & & & \text{BCs}
\end{pmatrix}
\begin{pmatrix} p_1^{n+1,j+1} \\ \vdots \\ p_i^{n+1,j+1} \\ \vdots \\ p_N^{n+1,j+1} \end{pmatrix}
=
\begin{pmatrix} \text{BCs} \\ b_2 \\ \vdots \\ b_i \\ \vdots \\ b_{N-1} \\ \text{BCs} \end{pmatrix}
$$

4.1.2 Saturation equation

We start writing the expression for the saturation equation in 1D

$$
\frac{\partial \phi s_w}{\partial t} - \frac{\partial}{\partial x}\big(\lambda_w k\big(\frac{\partial}{\partial x}\big(p - \frac{1}{2}p_c\big) - \rho_n g\big)\big) = \frac{F_w}{\rho_w} \tag{4.8}
$$

We integrate in a control interval $[x_{i-1/2}, x_{i+1/2}]$

$$
\int_{x_{i-1/2}}^{x_{i+1/2}}\frac{\partial \phi s_w}{\partial t}dx - \int_{x_{i-1/2}}^{x_{i+1/2}}\frac{\partial}{\partial x}\big(\lambda_w k\big(\frac{\partial}{\partial x}\big(p - \frac{1}{2}p_c\big) - \rho_n g\big)\big)dx = \int_{x_{i-1/2}}^{x_{i+1/2}}\frac{F_w}{\rho_w}dx \tag{4.9}
$$

Using the Fundamental Theorem of Calculus for the left integral and the midpoint rule for the right integral

$$\frac{\partial \phi_i s_{w,i}}{\partial t}\Delta x - \big(\lambda_w k\big(\frac{\partial}{\partial x}\big(p - \frac{1}{2}p_c\big) - \rho_n g\big)\big)_{i+1/2} + \big(\lambda_w k\big(\frac{\partial}{\partial x}\big(p - \frac{1}{2}p_c\big) - \rho_n g\big)\big)_{i-1/2} = \frac{F_{w,i}}{\rho_w}\Delta x \tag{4.10}$$

Now we have to approximate the temporal derivative for the saturation. This can be done with the Implicit Euler's method (3.2). Considering the inner iteration ^{j} and the chain rule for the capillarity pressure

$$\begin{aligned}
&\frac{\phi_i^n s_{w,i}^{n+1,j+1} - \phi_i^n s_i^n}{\Delta t}\Delta x \\
&-k_{i+1/2}^n \lambda_{w,i+1/2}^{n+1,j}\Big(\frac{p_{i+1,j+1}^{n+1} - p_i^{n+1,j+1}}{\Delta x} - \frac{1}{2}\Big(\frac{\partial p_{c,i+1/2}^{n+1,j}}{\partial s_w}\frac{s_{w,i+1}^{n+1,j+1} - s_{w,i}^{n+1,j+1}}{\Delta x} \\
&\qquad + \frac{\partial p_{c,i+1/2}^{n+1,j}}{\partial a_{wn}}\frac{a_{wn,i+1}^{n+1,j} - a_{wn,i}^{n+1,j}}{\Delta x}\Big) - \rho_n g\Big) \\
&-k_{i-1/2}^n \lambda_{w,i-1/2}^{n+1,j}\Big(\frac{p_{i-1}^{n+1,j+1} - p_i^{n+1,j+1}}{\Delta x} - \frac{1}{2}\Big(\frac{\partial p_{c,i-1/2}^{n+1,j}}{\partial s_w}\frac{s_{w,i-1}^{n+1,j+1} - s_{w,i}^{n+1,j+1}}{\Delta x} \\
&\qquad + \frac{\partial p_{c,i-1/2}^{n+1,j}}{\partial a_{wn}}\frac{a_{wn,i-1}^{n+1,j} - a_{wn,i}^{n+1,j}}{\Delta x}\Big) - \rho_n g\Big) \\
&= \frac{F_{w,i}^{n+1}}{\rho_w}\Delta x
\end{aligned} \tag{4.11}$$

Rearranging terms and multiplying $\Delta x \Delta t$ in both sides

$$\begin{aligned}
&s_{w,i+1}^{n+1,j+1} k_{i+1/2}^n \lambda_{w,i+1/2}^{n+1,j} \frac{\partial p_{c,i+1/2}^{n+1,j}}{\partial s_w}\frac{\Delta t}{2} \\
&+ s_{w,i}^{n+1,j+1}\Big(\phi_i^n \Delta x^2 - \big(k_{i+1/2}^n \lambda_{w,i+1/2}^{n+1,j}\frac{\partial p_{c,i+1/2}^{n+1,j}}{\partial s_w} + k_{i-1/2}^n \lambda_{w,i-1/2}^{n+1,j}\frac{\partial p_{c,i-1/2}^{n+1,j}}{\partial s_w}\big)\frac{\Delta t}{2}\Big) \\
&+ s_{w,i-1}^{n+1,j+1} k_{i-1/2}^n \lambda_{w,i-1/2}^{n+1,j} \frac{\partial p_{c,i-1/2}^{n+1,j}}{\partial s_w}\frac{\Delta t}{2} \\
&= \frac{F_{w,i}^{n+1}}{\rho_w}\Delta x^2 \Delta t + \phi_i^n s_{w,i}^n \Delta x^2 \\
&+ k_{i+1/2}^n \lambda_{w,i+1/2}^{n+1,j}(p_{i+1}^{n+1,j+1} - p_i^{n+1,j+1} - \frac{\partial p_{c,i+1/2}^{n+1,j+1}}{\partial a_{wn}}\frac{a_{wn,i+1}^{n+1,j} - a_{wn,i}^{n+1,j}}{2} - \rho_n g \Delta x)\Delta t \\
&+ k_{i-1/2}^n \lambda_{w,i-1/2}^{n+1,j}(p_{i-1}^{n+1,j+1} - p_i^{n+1,j+1} - \frac{\partial p_{c,i-1/2}^{n+1,j}}{\partial a_{wn}}\frac{a_{wn,i}^{n+1,j} - a_{wn,i-1}^{n+1,j}}{2} - \rho_n g \Delta x)\Delta t
\end{aligned} \tag{4.12}$$

Defining

$$\begin{aligned}
d_i &= k_{i+1/2}^n \lambda_{w,i+1/2}^{n+1,j} \frac{\partial p_{c,i+1/2}^{n+1,j}}{\partial s_w}\frac{\Delta t}{2} \qquad 1 \le i \le N-1 \\
e_i &= \frac{F_{w,i}^{n+1}}{\rho_w}\Delta x^2 \Delta t + \phi_i^n s_{wi}^n \Delta x^2 \\
&+ k_{i+1/2}^n \lambda_{w,i+1/2}^{n+1,j}(p_{i+1}^{n+1,j+1} - p_i^{n+1,j+1} - \frac{\partial p_{c,i+1/2}^{n+1,j}}{\partial a_{wn}}\frac{a_{wn,i+1}^{n+1,j} - a_{wn,i}^{n+1,j}}{2} - \rho_n g \Delta x)\Delta t \\
&+ k_{i-1/2}^n \lambda_{w,i-1/2}^{n+1,j}(p_{i-1}^{n+1,j+1} - p_i^{n+1,j+1} - \frac{\partial p_{c,i-1/2}^{n+1,j}}{\partial a_{wn}}\frac{a_{wn,i}^{n+1,j} - a_{wn,i-1}^{n+1,j}}{2} - \rho_n g \Delta x)\Delta t
\end{aligned}$$

we can write the linear system of equations for the saturation equation in the matrix system $\mathbf{Bs}^{n+1,j+1} = \mathbf{e}$

$$\mathbf{B}\begin{pmatrix} s_1^{n+1,j+1} \\ \vdots \\ s_i^{n+1,j+1} \\ \vdots \\ s_N^{n+1,j+1} \end{pmatrix} = \begin{pmatrix} \text{BCs} \\ e_2 \\ \vdots \\ e_i \\ \vdots \\ e_{N-1} \\ \text{BCs} \end{pmatrix}$$

$$\mathbf{B} = \begin{pmatrix} \text{BCs} & & & & & & & \\ d_1 & \Delta x^2\phi_2^n - d_1 - d_2 & d_2 & 0 & 0 & \dots & 0 & 0 \\ 0 & d_2 & \Delta x^2\phi_3^n - d_2 - d_3 & d_3 & 0 & 0 & 0 & 0 \\ \ddots & \ddots & \ddots & \ddots & \ddots & \ddots & \ddots & \ddots \\ \dots & 0 & d_{i-1} & \Delta x^2\phi_i^n - d_{i-1} - d_i & d_i & 0 & \dots & 0 \\ \ddots & \ddots & \ddots & \ddots & \ddots & \ddots & \ddots & \ddots \\ 0 & 0 & \dots & 0 & 0 & d_{N-2} & \Delta x^2\phi_{N-1}^n - d_{N-2} - d_{N-1} & d_{N-1} \\ & & & & & & & \text{BCs} \end{pmatrix}$$

4.1.3 Interfacial equation

We start writing the expression for the interfacial area equation in 1D

$$\frac{\partial a_{wn}}{\partial t} - \frac{\partial}{\partial x}\left(a_{wn}k_{wn}\frac{\partial a_{wn}}{\partial x}\right) = E_{wn} \tag{4.13}$$

We integrate in a control interval $[x_{i-1/2}, x_{i+1/2}]$

$$\int_{x_{i-1/2}}^{x_{i+1/2}} \frac{\partial a_{wn}}{\partial t}dx - \int_{x_{i-1/2}}^{x_{i+1/2}} \frac{\partial}{\partial x}\left(a_{wn}k_{wn}\frac{\partial a_{wn}}{\partial x}\right)dx = \int_{x_{i-1/2}}^{x_{i+1/2}} E_{wn}dx \tag{4.14}$$

Using the midpoint rule and the Fundamental Theorem of Calculus

$$\frac{\partial a_{wn}}{\partial t}\Delta x - \left(a_{wn}k_{wn}\frac{\partial a_{wn}}{\partial x}\right)_{i+1/2} + \left(a_{wn}k_{wn}\frac{\partial a_{wn}}{\partial x}\right)_{i-1/2} = E_{wn,i}\Delta x \tag{4.15}$$

Considering again the inner iteration ^{j}, the approximation for the temporal derivative, and the chain rule

$$\begin{aligned} \frac{a_{wn,i}^{n+1,j+1} - a_{wn,i}^{n}}{\Delta t}\Delta x &- k_{wn,i+1/2}^{n} a_{wn,i+1/2}^{n+1,j}\left(\frac{a_{wn,i+1}^{n+1,j+1} - a_{wn,i}^{n+1,j+1}}{\Delta x}\right) \\ &- k_{wn,i-1/2}^{n} a_{wn,i-1/2}^{n+1,j}\left(\frac{a_{wn,i-1}^{n+1,j+1} - a_{wn,i}^{n+1,j+1}}{\Delta x}\right) \\ &= E_{wn,i}^{n+1}\Delta x \end{aligned} \tag{4.16}$$

Rearranging terms and multiplying $\Delta x \Delta t$ in both sides

$$\begin{aligned} & -a_{wn,i+1}^{n+1,j+1} k_{wn,i+1/2}^{n} a_{wn,i+1/2}^{n+1,j} \Delta t \\ & a_{wn,i}^{n+1,j+1} (\Delta x^2 + (k_{wn,i+1/2}^{n} a_{wn,i+1/2}^{n+1,j} + k_{wn,i-1/2}^{n} a_{wn,i-1/2}^{n+1,j}) \Delta t) \\ & -a_{wn,i-1}^{n+1,j+1} k_{wn,i-1/2}^{n} a_{wn,i-1/2}^{n+1,j} \Delta t \\ & = (E_{wn,i}^{n+1} \Delta t + a_{wn,i}^{n}) \Delta x^2 \end{aligned} \tag{4.17}$$

Defining

$$\begin{aligned} q_i &= k_{wn,i+1/2}^{n} a_{wn,i+1/2}^{n+1,j} \Delta t \qquad 1 \leq i \leq N-1 \\ r_i &= (E_{wn,i}^{n+1} \Delta t + a_{wn,i}^{n}) \Delta x^2 \end{aligned}$$

we can write the linear system of equations for the saturation equation in the matrix system $\mathbf{Q}\mathbf{a}^{n+1,j+1} = \mathbf{r}$

$$\mathbf{Q} \begin{pmatrix} a_{wn,1}^{n+1,j+1} \\ \vdots \\ a_{wn,i}^{n+1,j+1} \\ \vdots \\ a_{wn,N}^{n+1,j+1} \end{pmatrix} = \begin{pmatrix} \text{BCs} \\ r_2 \\ \vdots \\ r_i \\ \vdots \\ r_{N-1} \\ \text{BCs} \end{pmatrix}$$

$$\mathbf{Q} = \begin{pmatrix} \text{BCs} & & & & & & & \\ -q_1 & \Delta x^2 + q_1 + q_2 & -q_2 & 0 & 0 & \dots & 0 & 0 \\ 0 & -q_2 & \Delta x^2 + q_2 + q_3 & -q_3 & 0 & 0 & 0 & 0 \\ \ddots & \ddots & \ddots & \ddots & \ddots & \ddots & \ddots & \ddots \\ \dots & 0 & -q_{i-1} & \Delta x^2 + q_{i-1} + q_i & -q_i & 0 & \dots & 0 \\ \ddots & \ddots & \ddots & \ddots & \ddots & \ddots & \ddots & \ddots \\ 0 & 0 & \dots & 0 & 0 & -q_{N-2} & \Delta x^2 + q_{N-2} + q_{N-1} & -q_{N-1} \\ & & & & & & \text{BCs} & \end{pmatrix}$$

4.1.3.1 Boundary conditions

In the following pages, we show a way to deal with boundary conditions for the pressure and saturation equation. It is analogous for the interfacial area.

4.1.3.1.1 Dirichlet boundary conditions

Let us suppose that we have Dirichlet boundary conditions for the pressure equation on the right boundary ($p(L,t) = p_R(t)$). Because we consider a cell-centered grill, we do not know the value of the pressure derivative on the right boundary, but we know the pressure. So one way to deal with Dirichlet boundary conditions is to modify the size of the two boundary cells (Thomas 1995) as follows

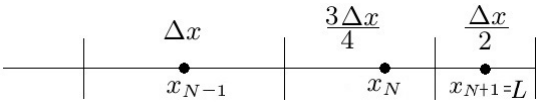

Figure 4.1.1 Modification in a half-cell for Dirichlet boundary conditions in 1D. We observe the change of size for implementing the condition.

Then, considering a half cell on the right boundary, the integration results

$$\begin{aligned}
&-\lambda^{n+1,j}_{\Sigma,N+1/2}k^n_{N+1/2}\frac{p^{n+1}_R-p^{n+1,j+1}_N}{\frac{\Delta x}{2}}+\lambda^{n+1,j}_{\Sigma,N-1/2}k^n_{N-1/2}\frac{p^{n+1,j+1}_N-p^{n+1}_{N-1}}{\Delta x}\\
&=\sum_{\alpha=w,n}\frac{F^{n+1}_{\alpha,N}}{\rho_\alpha}\frac{3\Delta x}{4}-\frac{\phi^n_N-\phi^{n-1}_N}{\Delta t}\Delta x\\
&+\frac{1}{2}\lambda^{n+1,j}_{\Delta,N+1/2}k^n_{N+1/2}\left(\frac{p^{n+1,j}_{c,N+1/2}}{\partial s_w}\frac{s^{n+1,j}_{w,N+1}-s^{n+1,j}_{wN}}{\frac{\Delta x}{2}}+\frac{\partial p^{n+1,j}_{c,N+1/2}}{\partial a_{wn}}\frac{a^{n+1,j}_{wn,N+1}-a^{n+1,j}_{wn,N}}{\frac{\Delta x}{2}}\right)\\
&+\frac{1}{2}\lambda^{n+1,j}_{\Delta,N-1/2}k^n_{N-1/2}\left(\frac{\partial p^{n+1,j}_{c,N-1/2}}{\partial s_w}\frac{s^{n+1,j}_{w,N-1}-s^{n+1,j}_{w,N}}{\Delta x}+\frac{\partial p^{n+1,j}_{c,N-1/2}}{\partial a_{wn}}\frac{a^{n+1,j}_{wn,N-1}-a^{n+1,j}_{wn,N}}{\Delta x}\right)\\
&-g[\rho_w(k^n_{N+1/2}\lambda^{n+1,j}_{w,N+1/2}-k^n_{N-1/2}\lambda^{n+1,j}_{w,N-1/2})+\rho_n(k^n_{N+1/2}\lambda^{n+1,j}_{n,N+1/2}-k^n_{N-1/2}\lambda^{n+1,j}_{n,N-1/2})]
\end{aligned}\tag{4.18}$$

From the last equation, we just rearrange terms and we implement in the last row in the matrix system for the pressure. Nevertheless, we need the value of $s^{n+1,j}_{w,N+1}$. If we have for the the saturation equation on the right boundary Dirichlet condition, we already know the value $s^{n+1,j}_{w,N+1}=s_w(L,t)\ \ \forall t$. If instead we have a Neumann boundary condition ($s'_w(L,t)=q_R(t)$), we approximate the value as

$$q^{n+1}_R=\frac{s^{n+1,j}_{w,N+1}-s^{n+1,j}_{w,N}}{\frac{\Delta x}{2}}\quad\Rightarrow\quad s^{n+1,j}_{w,N+1}=q^{n+1}_R\frac{\Delta x}{2}+s^{n+1,j}_{w,N}\tag{4.19}$$

4.1.3.1.2 Neumann boundary conditions

Let us suppose that we have Neumann boundary conditions for the saturation on the right boundary ($s'_w(L,t)=q_R(t)$). Because we considered a uniform cell-centered grid, we already know the value for the derivative on the boundary, so after integration and substitution we get

$$\begin{aligned}
&\frac{\phi^n_N s^{n+1,j}_{w,N}-\phi^n_N s^n_{w,N}}{\Delta t}\Delta x\\
&-k^n_{N+1/2}\lambda^{n+1,j}_{w,N+1/2}\Big(\frac{p^{n+1,j+1}_{N+1}-p^{n+1,j+1}_N}{\frac{\Delta x}{2}}-\frac{1}{2}\Big(\frac{\partial p^{n+1,j}_{c,N+1/2}}{\partial s_w}q^{n+1}_R\\
&\qquad\qquad+\frac{\partial p^{n+1,j}_{c,N+1/2}}{\partial a_{wn}}\frac{a^{n+1,j}_{wn,N+1}-a^{n+1,j}_{wn,N}}{\frac{\Delta x}{2}}\Big)-\rho_n g\Big)\\
&-k^n_{N-1/2}\lambda^{n+1,j}_{w,N-1/2}\Big(\frac{p^{n+1,j+1}_N-p^{n+1,j+1}_{N-1}}{\Delta x}-\frac{1}{2}\Big(\frac{\partial p^{n+1,j}_{c,N-1/2}}{\partial s_w}\frac{s^{n+1,j+1}_{w,N-1}-s^{n+1,j+1}_{w,N}}{\Delta x}\\
&\qquad\qquad+\frac{\partial p^{n+1,j}_{c,N-1/2}}{\partial a_{wn}}\frac{a^{n+1,j}_{wn,N-1}-a^{n+1,j}_{wn,N}}{\Delta x}\Big)-\rho_n g\Big)\\
&=\frac{F^{n+1}_{w,N}}{\rho_w}\Delta x
\end{aligned}\tag{4.20}$$

From the last equation, we just rearrange terms and we implement in the last row in the system matrix for the saturation. For computing the mobilities and derivatives of capillary pressure on the boundary,

we need to approximate the saturation on the right boundary. We use the following approximation

$$s_{w,N+1}^{n+1,j+1} = q_R^{n+1}\frac{\Delta x}{2} + s_{w,N}^{n+1,j+1} \tag{4.21}$$

4.1.3.1.3 Flux boundary conditions

Now, let us suppose that we have flux boundary conditions on the right boundary ($\mathbf{n}\cdot_\Sigma \mathbf{u}(L,t) = q_R(t)$). Because we consider a uniform cell-centered grid, we already know the value of the total flux on the boundary, so after integration and substitution we get

$$\frac{\partial \phi_N}{\partial t}\Delta x + q_R(t) + \big(k\big(\lambda_\Sigma \frac{\partial p}{\partial x} + \frac{1}{2}\lambda_\Delta \frac{\partial p_c}{\partial x} - (\lambda_w\rho_w + \lambda_n\rho_n)g\big)\big)_{N-1/2} = \sum_{\alpha=w,n}\frac{F_{\alpha,N}}{\rho_\alpha}\Delta x \tag{4.22}$$

From the last equation, we can just follow the previous method and rearrange terms in order to substitute in the matrix system for the pressure equation. After solving the system, using the expression for the total flux

$$\mathbf{u}_\Sigma = -\mathbf{k}(\lambda_\Sigma \nabla p + \frac{1}{2}\lambda_\Delta \nabla p_c - (\lambda_w\rho_w + \lambda_n\rho_n)\mathbf{g}) \tag{4.23}$$

We approximate the right pressure

$$p_{N+1}^{n+1,j+1} = -\frac{\frac{\Delta x}{2}}{\lambda_{\Sigma,N}^{n+1,j}}\left(\frac{q_R^{n+1}}{k_N^n} + \frac{1}{2}\lambda_{\Delta,N}^{n+1,j} p_{c,N}'^{n+1,j}\frac{s_{w,N+1}^{n+1,j} - s_{w,N}^{n+1,j}}{\frac{\Delta x}{2}} - (\lambda_{w,N}^{n+1,j}\rho_w + \lambda_{n,N}^{n+1,j}\rho_n)g\right) + p_N^{n+1,j+1} \tag{4.24}$$

4.1.4 Validation of the two-phase flow model in 1D

After discretizing the pressure, saturation and interfacial area equations, we should test if the algorithm is working. In this section we test our algorithm with two analytic solutions, computing the error reduction in order to check if the numerical solution approximates to the continuous one, and also with a benchmark simulation.

4.1.4.1 Analytic solution

In this section we present the numerical results for using the previous algorithm given two analytic solutions. First, we test our algorithm just considering the pressure and saturation equations verifying the error reduction, and after we test the algorithm including the interfacial tension equation.

4.1.4.1.1 Example 1

We consider a 1-D domain of size $L = 1$. We test our scheme for the next analytic solutions and parameterizations

$$p(x,t) = tx^2 \qquad s_w(x,t) = e^x + t \qquad p_c(s_w, a_{wn}) = -s_w^2 \qquad k_{r,w}(s_w) = s_w \qquad k_{r,n}(s_w) = 2s_w$$

with Dirichlet boundary conditions for the pressure and saturation, except on the right boundary for the pressure, where we give the flux

$$p(x,0)=0 \qquad p(0,t)=0 \qquad \mathbf{n}\cdot\mathbf{u}_\Sigma(L,t)=-(3(t+e^L)2tL-e^L(t+e^L)^2)$$
$$s_w(x,0)=e^x \qquad s_w(0,t)=1+t \qquad s_w(L,t)=e^L+t$$

We consider

$$k=\rho_w=\phi=\rho_n=\mu_w=\mu_n=1$$

The source/sink terms are given by

$$\frac{F_w}{\rho_w}=\phi-k(2t(xe^x+t+e^x)+(t+e^x)e^{2*x}+(t+e^x)(te^x+2e^{2x}))$$
$$\frac{F_n}{\rho_n}=-\phi-k(4t(xe^x+t+e^x)-2(t+e^x)e^{2x}-2(t+e^x)(te^x+2e^{2x}))$$

We present the results of the analysis of convergence in Table 4.1.1, where we halve the size of the time and space step in each case.

Table 4.1.1 Pressure and saturation errors for the analytic validation in 1D. We test for different mesh sizes and time steps, with $L=1$ and $T=0.1$.

	Δx	Δt	$L_{p,2}$ error	$L_{s,2}$ error	reduction p	reduction s
1	0.2	0.01	0.039244	0.012350		
2	0.1	0.005	0.0090652	0.0024305	4.3291	5.0814
3	0.05	0.0025	0.0021532	5.1367e-004	4.2101	4.7316
4	0.025	0.00125	5.2277e-004	1.1628e-004	4.1189	4.4176
5	0.0125	0.000625	1.2866e-004	2.7555e-005	4.0632	4.2200

From Table 4.1.1 we observe that the error reduction for both pressure and saturation approximates to 4, which is the behavior expected (Iserles 2009).

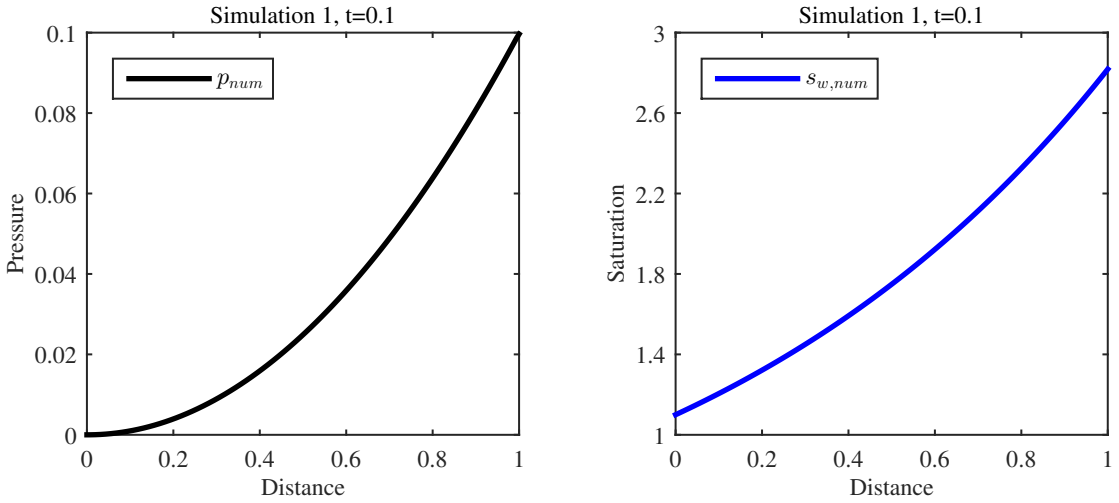

Figure 4.1.2 Pressure and saturation profiles for the analytic validation in 1D. The size partitions we used are dx= 0.025 and dt= 0.00125.

4.1.4.1.2 Example 2

Now, we also consider the interfacial area equation. We test our scheme for the next analytic solutions and parameterizations

$$p(x,t) = tx^2 \qquad s_w(x,t) = e^x + t \qquad a_{wn}(x,t) = t\sin(x)$$
$$p_c(s_w, a_{wn}) = -a_{wn}^2 s_w^2 \qquad k_{r,w}(s_w) = s_w \qquad k_{r,n}(s_w) = 2s_w$$

with Dirichlet boundary conditions for the pressure, saturation and interfacial area, except on the right boundary for the saturation and interfacial area, where we have Neumann conditions

$$p(x,0) = 0 \qquad p(0,t) = 0 \qquad p(L,t) = tL^2$$
$$s_w(x,0) = e^x \qquad s_w(0,t) = 1 + t \qquad \frac{\partial s_w}{\partial x}(L,t) = e^L$$
$$a_{wn}(x,0) = 0 \qquad a_{wn}(0,t) = 0 \qquad \frac{\partial a_{wn}}{\partial x}(L,t) = t\cos(L)$$

where we consider

$$k_{wn} = \rho_w = \phi = \rho_n = \mu_w = \mu_n = 1 \qquad k = 0.001$$

The source/sink terms are given by

$$\begin{aligned}
&\frac{F_w}{\rho_w} = 1 - k(2t(xe^x + e^x + t)\\
&- \frac{1}{2}(e^x(-2t^2(\sin(x)^2 e^x(e^x + t) + \sin(x)\cos(x)(e^x + t)^2)) + (e^x + t)(-2t^2(2\sin(x)\cos(x)e^x(e^x + t)\\
&+ \sin(x)^2 e^x(e^x + t) + \sin(x)^2 e^{2x} + \cos(x)^2(e^x + t)^2 - \sin(x)^2(e^x + t)^2 + 2\sin(x)\cos(x)(e^x + t)e^x))))\\
&\frac{F_n}{\rho_n} = -1 - k(4t(xe^x + e^x + t)\\
&+ (e^x(-2t^2(\sin(x)^2 e^x(e^x + t) + \sin(x)\cos(x)(e^x + t)^2)) + (e^x + t)(-2t^2(2\sin(x)\cos(x)e^x(e^x + t)\\
&+ \sin(x)^2 e^x(e^x + t) + \sin(x)^2 e^{2x} + \cos(x)^2(e^x + t)^2 - \sin(x)^2(e^x + t)^2 + 2\sin(x)\cos(x)(e^x + t)e^x))))\\
&E_{wn} = \sin(x) - k_{wn}t^2(\cos(x)^2 - \sin(x)^2)
\end{aligned}$$

We present the results of the analysis of convergence in Table 4.1.2, where we halve the size of the time and space step in each case. From the table we observe that the error reductions approximates to 2.

Table 4.1.2 Pressure, saturation and interfacial errors for the analytic validation in 1D. We tested for different mesh sizes and time steps, with $L = 1$ and $T = 1$.

	Δx	Δt	$L_{p,2}$ error	$L_{s_w,2}$ error	$L_{a_{wn},2}$ error	red p	red s_w	red a_{wn}
1	0.2	0.1	0.015756	0.0063866	0.0083452			
2	0.1	0.05	0.011011	0.0037196	0.0037359	1.4309	1.7170	2.2338
3	0.05	0.025	0.0072132	0.0020267	0.0017916	1.5265	1.8354	2.0852
4	0.025	0.0125	0.0041720	0.0010494	8.7942e-004	1.7290	1.9312	2.0372
5	0.0125	0.00625	0.0022443	5.3254e-004	4.3587e-004	1.8589	1.9706	2.0176
6	0.00625	0.003125	0.0011639	2.6807e-004	2.1700e-004	1.9282	1.9866	2.0086

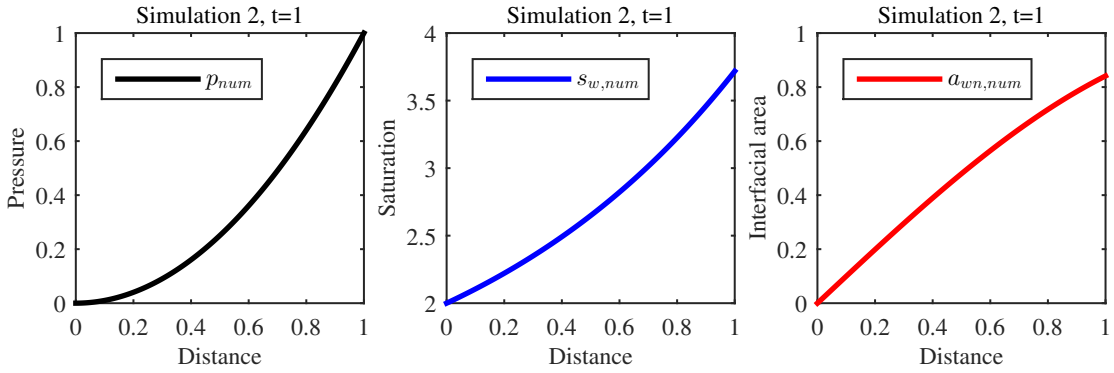

Figure 4.1.3 Pressure, saturation and interfacial area profiles for the analytic validation in 1D. The size partitions we used are dx= 0.025 and dt= 0.0125.

4.1.4.2 Benchmark simulation

We test our algorithm against a numerical simulation made by Amaziane et al. 2009, where the porous medium has a length $L = 100$ m with homogeneous permeability and porosity (the gravity is neglected). The parameters for the simulation are given in Table 4.1.3 where we assume that the gaseous phase is incompressible (Skiftestad 2015).

Table 4.1.3 Model parameters used in the benchmark validation of the two-phase model in 1D.

Parameter	Value	Parameter	Value	Parameter	Value
k	1mD	ϕ	0.1	p_e	2 MPa
μ_n	$9{\cdot}10^{-6}$ Pa·s	s_{wi}	0	L	100 m
μ_w	$0.86{\cdot}10^{-3}$ Pa·s	s_{or}	0	T	45 days
ρ_n	2 kg/m^3	n	2		
ρ_w	996.5 kg/m^3	m	0.5		

In the simulation, we consider that the porous medium is filled with 30% of gas and water is injected on the left boundary. The boundary and initial conditions for the pressure and saturation are the following

$$p(x,0) = 0.5 \text{ MPa} \qquad p(0,t) = 4 \text{ MPa} \qquad p(L,t) = 0.5 \text{ MPa}$$
$$s_w(x,0) = 0.7 \qquad s_w(0,t) = 1 \qquad \frac{\partial s_w}{\partial x}(L,t) = 0$$

Fig. 4.1.4 shows that after 45 days of water injection, we have extracted approximately 30% of the gas. When we compare these results with the ones shown in the paper, we observe that they present the same behavior, despite the fact that we did not consider compressibility in the gaseous phase.

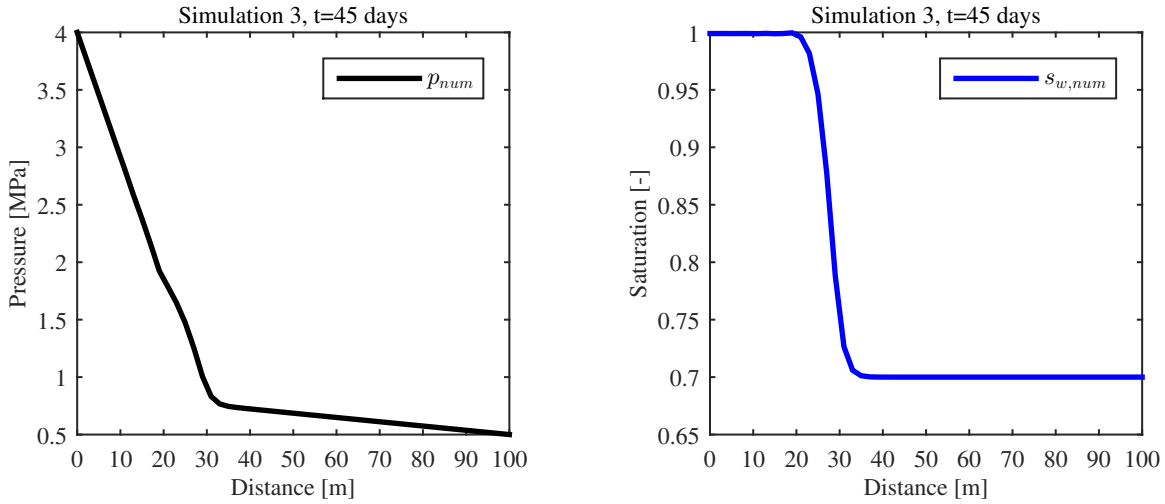

Figure 4.1.4 Pressure and saturation profiles for the benchmark validation in 1D. The size partitions we used are dx=0.5 m and dt= $3.888e^{-6}$ s.

4.1.5 Transport equations

Posterior to solving the pressure, saturation and interfacial area equations, we consider now the discretization of the transport equations. We start writing the transport equations in 1D

$$\begin{aligned}
&\frac{\partial(C_b\phi s_w)}{\partial t} - \frac{\partial}{\partial x}\left(D_b s_w \phi \frac{\partial C_b}{\partial x} - u_w C_b - \phi v_g C_b\right) = R_b \\
&\frac{\partial(C_n\phi s_w)}{\partial t} - \frac{\partial}{\partial x}\left(D_n s_w \phi \frac{\partial C_n}{\partial x} - u_w C_n\right) = R_n \\
&\frac{\partial(C_p\phi s_w)}{\partial t} - \frac{\partial}{\partial x}\left(D_p s_w \phi \frac{\partial C_p}{\partial x} - u_w C_p\right) = R_p
\end{aligned} \tag{4.25}$$

We show the discretization for the bacteria equation, and for getting the discretization for the other two equations, we just change indexes and consider $v_g = 0$.

We integrate in a control interval $[x_{i-1/2}, x_{i+1/2}]$

$$\int_{x_{i-1/2}}^{x_{i+1/2}} \frac{\partial(C_b\phi s_w)}{\partial t} dx - \int_{x_{i-1/2}}^{x_{i+1/2}} \frac{\partial}{\partial x}\left(D_b s_w \phi \frac{\partial C_b}{\partial x} - u_w C_b - \phi v_g C_b\right) dx = \int_{x_{i-1/2}}^{x_{i+1/2}} R_b dx \tag{4.26}$$

Using the Fundamental Theorem of Calculus for the left integrals and the midpoint rule for the right integral

$$\frac{\partial(C_{b,i}\phi_i s_{w,i})}{\partial t}\Delta x_i - \left(D_b s_w \phi \frac{\partial C_b}{\partial x} - u_w C_b - \phi v_g C_b\right)_{i+1/2} + \left(D_b s_w \phi \frac{\partial C_b}{\partial x} - u_w C_b - \phi v_g C_b\right)_{i-1/2} = R_{b,i}\Delta x_i \tag{4.27}$$

Approximating the temporal derivative, using the inner iteration ^{j} and rearranging terms

$$\begin{aligned}
&- C_{b,i+1}^{n+1,j+1}(\frac{1}{\Delta x}D_{b,i+1/2}^{n+1}s_{w,i+1/2}^{n+1}\phi_{i+1/2}^{n} - \frac{1}{2}(u_{w,i+1/2}^{n+1} + \phi_{i+1/2}^{n}v_g))\\
&+ C_{b,i}^{n+1,j+1}(\phi_i^n s_{w,i}^{n+1}\frac{\Delta x}{\Delta t} + \frac{1}{\Delta x}D_{b,i+1/2}^{n+1}s_{w,i+1/2}^{n+1}\phi_{i+1/2}^{n} + \frac{1}{2}(u_{w,i+1/2}^{n+1} + \phi_{i+1/2}^{n}v_g)\\
&\qquad + \frac{1}{\Delta x}D_{b,i-1/2}^{n+1}s_{w,i-1/2}^{n+1}\phi_{i-1/2}^{n} - \frac{1}{2}(u_{w,i-1/2}^{n+1} + \phi_{i-1/2}^{n}v_g))\\
&- C_{b,i-1}^{n+1,j+1}(\frac{1}{\Delta x}D_{b,i-1/2}^{n+1}s_{w,i-1/2}^{n+1}\phi_{i-1/2}^{n} + \frac{1}{2}(u_{w,i-1/2}^{n+1} + \phi_{i-1/2}^{n}v_g))\\
&= R_{b,i}^{n+1,j}\Delta x + C_{b,i}^{n}\phi_i^n s_{w,i}^{n}\frac{\Delta x}{\Delta t}
\end{aligned} \tag{4.28}$$

Multiplying $\Delta x \Delta t$ in both sides

$$\begin{aligned}
&- C_{b,i+1}^{n+1,j+1}(\Delta t D_{b,i+1/2}^{n+1}s_{w,i+1/2}^{n+1}\phi_{i+1/2}^{n} - \frac{\Delta x\Delta t}{2}(u_{w,i+1/2}^{n+1} + \phi_{i+1/2}^{n}v_g))\\
&+ C_{b,i}^{n+1,j+1}(\phi_i^n s_{w,i}^{n+1}\Delta x^2 + \Delta t(D_{b,i+1/2}^{n+1}s_{w,i+1/2}^{n+1}\phi_{i+1/2}^{n} + D_{b,i-1/2}^{n+1}s_{w,i-1/2}^{n+1}\phi_{i-1/2}^{n}\\
&\qquad + \frac{\Delta x}{2}(u_{w,i+1/2}^{n+1} + \phi_{i+1/2}^{n}v_g - u_{w,i-1/2}^{n+1} - \phi_{i-1/2}^{n}v_g))\\
&- C_{b,i-1}^{n+1,j+1}(\Delta t D_{b,i-1/2}^{n+1}s_{w,i-1/2}^{n+1}\phi_{i-1/2}^{n} + \frac{\Delta x\Delta t}{2}(u_{w,i-1/2}^{n+1} + \phi_{i-1/2}^{n}v_g))\\
&= R_{b,i}^{n+1,j}\Delta x^2\Delta t + C_{b,i}^{n}\phi_i^n s_{w,i}^{n}\Delta x^2
\end{aligned} \tag{4.29}$$

Defining

$$\begin{aligned}
f_i &= \Delta t D_{i+1/2}^{n+1}s_{w,i+1/2}^{n+1}\phi_{i+1/2}^{n} \qquad 1 \le i \le N-1\\
g_i &= \frac{\Delta x\Delta t}{2}u_{w,i+1/2}^{n+1} \qquad 1 \le i \le N-1\\
h_i &= \phi_i^n s_{w,i}^{n+1}\Delta x^2\\
i_i &= \frac{\Delta x\Delta t}{2}\phi_i^n v_g
\end{aligned}$$

we can write the three transport equations

$$\begin{aligned}
&- C_{b,i+1}^{n+1,j+1}(f_{b,i} - g_i - i_i)\\
&+ C_{b,i}^{n+1,j+1}(h_i + f_{b,i} + f_{b,i-1} + g_i + i_i - g_{i-1} - i_{i-1})\\
&- C_{b,i-1}^{n+1,j+1}(f_{b,i-1} + g_{i-1} + i_{i-1})\\
&= R_{b,i}^{n+1.j}\Delta x^2\Delta t + C_{b,i}^{n}\phi_i^n s_{w,i}^{n}\Delta x^2
\end{aligned} \tag{4.30}$$

$$\begin{aligned}
&- C_{n,i+1}^{n+1,j+1}(f_{n,i} - g_i)\\
&+ C_{n,i}^{n+1,j+1}(h_i + f_{n,i} + f_{n,i-1} + g_i - g_{i-1})\\
&- C_{n,i-1}^{n+1,j+1}(f_{n,i-1} + g_{i-1})\\
&= R_{n,i}^{n+1.j}\Delta x^2\Delta t + C_{n,i}^{n}\phi_i^n s_{w,i}^{n}\Delta x^2
\end{aligned} \tag{4.31}$$

$$\begin{aligned}
&- C_{p,i+1}^{n+1,j+1}(f_{p,i} - g_i)\\
&+ C_{p,i}^{n+1,j+1}(h_i + f_{p,i} + f_{p,i-1} + g_i - g_{i-1})\\
&- C_{p,i-1}^{n+1,j+1}(f_{p,i-1} + g_{i-1})\\
&= R_{p,i}^{n+1,j}\Delta x^2\Delta t + C_{p,i}^{n}\phi_i^n s_{w,i}^{n}\Delta x^2
\end{aligned} \tag{4.32}$$

Finally, we can write the linear system of equations for the transport equations in the matrix system

$$D\begin{pmatrix} C_{b,1}^{n+1,j+1} \\ \vdots \\ C_{b,i}^{n+1,j+1} \\ C_{n,i}^{n+1,j+1} \\ C_{p,i}^{n+1,j+1} \\ \vdots \\ C_{p,N}^{n+1,j+1} \end{pmatrix} = \begin{pmatrix} \text{BCs} \\ \text{BCs} \\ \text{BCs} \\ R_{b,2}^{n+1,j}\Delta x^2\Delta t + C_{b,2}^{n}\phi_2^n s_{w,2}^n \Delta x^2 \\ \vdots \\ R_{p,N-1}^{n+1,j}\Delta x^2\Delta t + C_{p,N-1}^{n}\phi_{N-1}^n s_{w,N-1}^n \Delta x^2 \\ \text{BCs} \\ \text{BCs} \\ \text{BCs} \end{pmatrix}$$

$$D = \begin{pmatrix} \text{BCs} & & & & & & & & & \\ \text{BCs} & & & & & & & & & \\ \text{BCs} & & & & & & & & & \\ -f_{b,1}-g_1-i_1 & 0 & 0 & h_2+f_{b,2}+f_{b,1}+g_2+i_2-g_1-i_1 & 0 & 0 & -f_{b,2}+g_2+i_2 & \dots & & \\ \ddots & \ddots & \ddots & \ddots & \ddots & \ddots & \ddots & \ddots & & \\ & & & & & & & & \text{BCs} & \\ & & & & & & & & \text{BCs} & \\ & & & & & & & & \text{BCs} & \end{pmatrix}$$

4.1.5.1 Boundary conditions

The implementation of the boundary conditions for the transport equations can be obtained following the same ideas as for the pressure, saturation and interfacial area equations. For the next scenarios, we consider $v_g = 0$.

4.1.5.1.1 Dirichlet boundary conditions

Considering Dirichlet conditions on the left boundary ($C(0,t) = M(t)$), we use a half cell, so we have the following equation

$$\begin{aligned} \frac{C_1^{n+1,j+1}\phi_1^n s_{w,1}^{n+1} - C_1^n\phi_1^n s_{w,1}^n}{\Delta t}\frac{3\Delta x}{4} &- D_{3/2}^{n+1}s_{w,3/2}^{n+1}\phi_{3/2}^n\frac{C_2^{n+1,j+1}-C_1^{n+1,j+1}}{\Delta x} + u_{w,3/2}^{n+1}C_{3/2}^{n+1,j+1} \\ &+ D_{1/2}^{n+1}s_{w,1/2}^{n+1}\phi_{1/2}^n\frac{C_1^{n+1,j+1}-M^{n+1}}{\frac{\Delta x}{2}} - u_{w,1/2}^{n+1}C_{1/2}^{n+1,j+1} \\ &= R_1^{n+1,j}\frac{3\Delta x}{4} \end{aligned} \tag{4.33}$$

In this case, noting that we approximate $C_{1/2}^{n+1,j+1} = \frac{1}{2}(C_1^{n+1,j+1} + M^{n+1})$, we rearrange terms and finally obtain

$$\begin{aligned} &+ C_1^{n+1,j+1}(\phi_1^n s_{w,1}^{n+1}\frac{3\Delta x^2}{4} + \Delta t\left(D_{1/2}^{n+1}s_{w,1/2}^{n+1}\phi_{1/2}^n + 2D_{3/2}^{n+1}s_{w,3/2}^{n+1}\phi_{3/2}^n + \frac{\Delta x}{2}(u_{w,3/2}^{n+1}-u_{w,1/2}^{n+1})\right) \\ &- C_2^{n+1,j+1}(\Delta t D_{3/2}^{n+1}s_{w,3/2}^{n+1}\phi_{3/2}^n - \frac{\Delta x\Delta t}{2}u_{w,3/2}^{n+1}) \\ &= (R_N^{n+1,j}\Delta t + C_1^n\phi_1^n s_{w,1}^n)\frac{3\Delta x^2}{4} + \left(2D_{1/2}^{n+1}s_{w,1/2}^{n+1}\phi_{1/2}^n + u_{w,1/2}^{n+1}\frac{\Delta x}{2}\right)M^{n+1}\Delta t \end{aligned} \tag{4.34}$$

4.1.5.1.2 Neumann boundary conditions

Considering a Neumann condition on the right boundary ($\mathbf{n} \cdot \nabla C = Q(t)$), we use the following approximation for the concentration

$$\frac{C_{N+1/2}^{n+1} - C_N^{n+1}}{\frac{\Delta x}{2}} = Q^{n+1} \Rightarrow C_{N+1/2}^{n+1,j+1} = Q^{n+1}\frac{\Delta x}{2} + C_N^{n+1,j+1} \tag{4.35}$$

When we use the previous expression, the equation to solve on the right boundary becomes

$$\begin{aligned}
&\frac{C_N^{n+1,j+1}\phi_N^n s_{w,N}^{n+1} - C_N^n \phi_N^n s_{w,N}^n}{\Delta t}\Delta x \\
&- D_{N+1/2}^{n+1} s_{w,N+1/2}^{n+1}\phi_{N+1/2}^n Q^{n+1} + u_{w,N+1/2}^{n+1}\left(Q^{n+1}\frac{\Delta x}{2} + C_N^{n+1,j+1}\right) \\
&+ D_{N-1/2}^{n+1} s_{w,N-1/2}^{n+1}\phi_{N-1/2}^n \frac{C_N^{n+1,j+1} - C_{N-1}^{n+1,j+1}}{\Delta x} - u_{w,N-1/2}^{n+1} C_{N-1/2}^{n+1,j+1} \\
&= R_N^{n+1,j}\Delta x
\end{aligned} \tag{4.36}$$

And by rearranging terms, we finally obtain

$$\begin{aligned}
&+ C_N^{n+1,j+1}(\phi_N^n s_{w,N}^{n+1}\Delta x^2 + \Delta t\left(D_{N-1/2}^{n+1} s_{w,N-1/2}^{n+1}\phi_{N-1/2}^n + \frac{\Delta x}{2}(2u_{w,N+1/2}^{n+1} - u_{w,N-1/2}^{n+1})\right) \\
&- C_{N-1}^{n+1,j+1}(\Delta t D_{N-1/2}^{n+1} s_{w,N-1/2}^{n+1}\phi_{N-1/2}^n + \frac{\Delta x \Delta t}{2}u_{w,N-1/2}^{n+1}) \\
&= R_N^{n+1,j}\Delta x^2\Delta t + C_N^n\phi_N^n s_{w,N}^n\Delta x^2 + \left(D_{N+1/2}^{n+1} s_{w,N+1/2}^{n+1}\phi_{N+1/2}^n - u_{w,N+1/2}^{n+1}\frac{\Delta x}{2}\right)Q^{n+1}\Delta x\Delta t
\end{aligned} \tag{4.37}$$

4.1.5.1.3 Flux boundary conditions

Considering flux boundary conditions on the left boundary ($\mathbf{n} \cdot (-\phi s_w D\nabla C + \mathbf{u}_w C) = F(t)$), we get the following system

$$\begin{aligned}
&\frac{C_1^{n+1,j+1}\phi_1^n s_{w,1}^{n+1} - C_1^n\phi_1^n s_{w,1}^n}{\Delta t}\Delta x - D_{3/2}^{n+1} s_{w,3/2}^{n+1}\phi_{3/2}^n\frac{C_2^{n+1,j+1} - C_1^{n+1,j+1}}{\Delta x} + u_{w,3/2}^{n+1}C_{3/2}^{n+1,j+1} - F_l^{n+1} \\
&= R_1^{n+1,j}\Delta x
\end{aligned} \tag{4.38}$$

It is worth emphasizing that we approximate in different ways the values of the concentrations on the boundaries. For the left boundary we have

$$\begin{aligned}
&-\left[-\phi_0^n s_{w,0}^{n+1} D_0^{n+1}\frac{C_1^{n+1} - C_0^{n+1}}{\frac{\Delta x}{2}} + u_{w,0}^{n+1}C_0^{n+1}\right] = F_l^{n+1} \\
&\Rightarrow C_0^{n+1} = \frac{-F_l^{n+1}\Delta x + 2C_1^{n+1}\phi_0^n s_{w,0}^{n+1} D_0^{n+1}}{2\phi_0^n s_{w,0}^{n+1} D_0^{n+1} + u_{w,0}\Delta x}
\end{aligned}$$

Meanwhile for the right boundary

$$\begin{aligned}
&-\phi_N^n s_{w,N}^{n+1} D_N^{n+1}\frac{C_{N+1}^{n+1} - C_N^{n+1}}{\frac{\Delta x}{2}} + u_{w,N}^{n+1}C_N^{n+1} = F_r^{n+1} \\
&\Rightarrow C_{N+1}^{n+1} = \left(u_{w,N}^{n+1}\frac{\Delta x}{2\phi_N^n s_{w,N}^{n+1} D_N^{n+1}} + 1\right)C_N^{n+1} - F_r^{n+1}\frac{\Delta x}{2\phi_N^n s_{w,N}^{n+1} D_N^{n+1}}
\end{aligned}$$

4.1.6 Bioclogging

We start writing the equations for the mass balance equations for bacteria deposited reversibly and irreversibly on the solid matrix

$$\begin{aligned}\frac{\partial(\rho_b\sigma_1)}{\partial t} &= k_1(\phi_0-\sigma)C_b - k_2\rho_b\sigma_1 + g_1\rho_b\sigma_1 - d_1\rho_b\sigma_1\\ \frac{\partial(\rho_b\sigma_2)}{\partial t} &= k_3(\phi_0-\sigma)C_b + g_1\rho_b\sigma_2 - d_1\rho_b\sigma_2\end{aligned} \tag{4.39}$$

We approximate the temporal derivatives using the Implicit Euler's method (3.2)

$$\begin{aligned}\frac{\rho_b\sigma_{1,i}^{n+1}-\rho_b\sigma_{1,i}^{n}}{\Delta t} &= k_1(\phi_{0,i}-\sigma_i^{n+1})C_{b,i}^{n+1} - k_2\rho_b\sigma_{1,i}^{n+1} + g_1\rho_b\sigma_{1,i}^{n+1} - d_1\rho_b\sigma_{1,i}^{n+1}\\ \frac{\rho_b\sigma_{2,i}^{n+1}-\rho_b\sigma_{2,i}^{n}}{\Delta t} &= k_3(\phi_{0,i}-\sigma_i^{n+1})C_{b,i}^{n+1} + g_1\rho_b\sigma_{2,i}^{n+1} - d_1\rho_b\sigma_{2,i}^{n+1}\end{aligned} \tag{4.40}$$

Writing the unknowns on the left hand-side and considering $\sigma = \sigma_1 + \sigma_2$

$$\begin{aligned}\sigma_{1,i}^{n+1}(k_1C_{b,i}^{n+1}\Delta t + \rho_b(1+(k_2+d_1-g_1)\Delta t)) + \sigma_{2,i}^{n+1}k_1C_{b,i}^{n+1}\Delta t &= \rho_b\sigma_{1,i}^{n} + \Delta t k_1\phi_{0,i}C_{b,i}^{n+1}\\ \sigma_{2,i}^{n+1}(k_3C_{b,i}^{n+1}\Delta t + \rho_b(1+(d_1-g_1)\Delta t)) + \sigma_{1,i}^{n+1}k_3C_{b,i}^{n+1}\Delta t &= \rho_b\sigma_{2,i}^{n} + \Delta t k_3\phi_{0,i}C_{b,i}^{n+1}\end{aligned} \tag{4.41}$$

Letting

$$\begin{aligned}a_i &= k_1C_{b,i}^{n+1}\Delta t + \rho_b(1+(k_2+d_1-g_{1\,\max}\frac{C_{n,i}^{n+1}}{K_{b/n}+C_{n,i}^{n+1}})\Delta t)\\ b_i &= k_1C_{b,i}^{n+1}\Delta t\\ c_i &= \rho_b\sigma_{1,i}^{n} + \Delta t k_1\phi_{0,i}C_{b,i}^{n+1}\\ d_i &= k_3C_{b,i}^{n+1}\Delta t\\ e_i &= k_3C_{b,i}^{n+1}\Delta t + \rho_b(1+(d_1-g_{1\,\max}\frac{C_{n,i}^{n+1}}{K_{b/n}+C_{n,i}^{n+1}})\Delta t)\\ f_i &= \rho_b\sigma_{2,i}^{n} + \Delta t k_3\phi_{0,i}C_{b,i}^{n+1}\end{aligned} \tag{4.42}$$

We obtain the update solutions

$$\sigma_{1,i}^{n+1} = \frac{b_if_i - c_ie_i}{b_id_i - a_ie_i} \tag{4.43}$$

$$\sigma_{2,i}^{n+1} = \frac{c_id_i - a_if_i}{b_id_i - a_ie_i} \tag{4.44}$$

Once we solve the previous system, we can update the new porosity

$$\phi = \phi_0 - \sigma = \phi_0 - \sigma_1 - \sigma_2 \geq 0 \tag{4.45}$$

Using the parametric model for the permeability (2.33), we update the new permeability after solving the system for the porosity

$$k_i^{n+1} = k_{0,i}\left(1 - \frac{\sigma_i^{n+1}}{\phi_{0,i}}\right)^C \tag{4.46}$$

Finally, we compute the new interfacial tension, capillary number and residual oil saturation using (2.34), (2.35) and (2.36).

4.1.7 Validation of the concentration formulation in 1D

Once we have achieved the discretization of the transport equations, it is time to verify its functionality. In this section we present the analysis of convergence of the error reduction for an analytic solution and after we test our algorithm with the results from an experiment that considers bioclogging.

4.1.7.1 Analytic solution

We consider a porous medium of length $L = 1$. We test our scheme for the next analytic solutions with Dirichlet boundary conditions

$$C_b(x, y, t) = t \sin x \qquad C_n(x, y, t) = t \sin x \qquad C_p(x, y, t) = e^x \ln(1 + t)$$

We take

$$\phi = s_w = u_w = D_b = D_n = D_p = 1 \qquad v_g = 0$$

The source/sink terms are given by

$$R_b = \sin x(1 + tD_b) + t \cos x \quad R_n = \sin x(1 + tD_n) + t \cos x \quad R_p = e^x \left(\frac{1}{1+t} + \ln(1 + t)(1 - D_p) \right)$$

The reason for considering the same solution for the two first equations is to verify there is not a typo mistake. Fig. 4.1.5 shows the concentration profiles. We present the results of the analysis of convergence in Table 4.1.4, where we halve the size of the time and space steps in each case. From the table, we can conclude that the numerical solver for the transport equations is working.

Table 4.1.4 Concentration errors for the analytic validation of the transport model in 1D. We test for different mesh sizes and time steps, with $L = 1$ and $T = 1$.

	Δx	Δt	$L_{b,2}$ error	$L_{n,2}$ error	$L_{p,2}$ error	red b	red n	red p
1	0.2	0.1	3.0660e-004	3.0660e-004	0.0024336			
2	0.1	0.05	1.0691e-004	1.0691e-004	0.0011409	2.8680	2.8680	2.1329
3	0.05	0.025	3.1458e-005	3.1458e-005	5.4799e-004	3.3983	3.3983	2.0820
4	0.025	0.0125	8.5153e-006	8.5153e-006	2.6793e-004	3.6943	3.6943	2.0452
5	0.0125	0.00625	2.2139e-006	2.2139e-006	1.3240e-004	3.8464	3.8464	2.0237

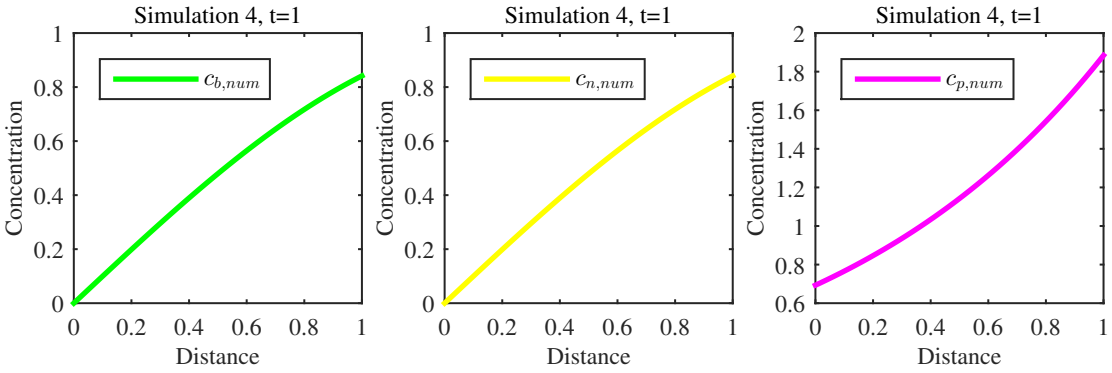

Figure 4.1.5 Concentration profiles for the analytic validation of the transport model in 1D. The size partitions are dx=0.0125 and dt=0.00625.

4.1.7.2 Benchmark simulation

We test our algorithm against a numerical experiment made by Kim 2006. They considered a 40-cm column, where they continuously injected bacteria on one side in order to examine the transport and sorption behavior through the column. The following initial and boundary conditions were used in the experiment

$$C_b(x,0) = \sigma_1(x,0) = \sigma_2(x,0) = 0 \qquad \frac{\partial C_b}{\partial x}(L,t) = 0 \qquad -D_b\frac{\partial C_b}{\partial x}(0,t) + u_w C_b(0,t) = u_w C_{b0}$$

The model parameters used in the numerical experiments are given in Table 4.1.5.

Table 4.1.5 Model parameters used in the benchmark validation of the transport model in 1D.

Parameter	Value	Parameter	Value	Parameter	Value
C_{b0}	4.32 mg·l^{-1}	v_g	1.61×10^{-5} cm·s^{-1}	g_1	1.0×10^{-6} s^{-1}
L	40 cm	ρ_b	1.085×10^{6} mg·l^{-1}	d_1	1.0×10^{-7} s^{-1}
ϕ_0	0.4	k_1	2.28×10^{-5} s^{-1}		
u_w	2.17×10^{-4} cm·s^{-1}	k_2	3.56×10^{-7} s^{-1}		
$\alpha_{b,T}$	0.27 cm	k_3	1.72×10^{-6} s^{-1}		

For the numerical experiment, we partition the domain in 240 elements and consider time intervals of dt=.0026. We present the simulation profiles in Fig 4.1.6

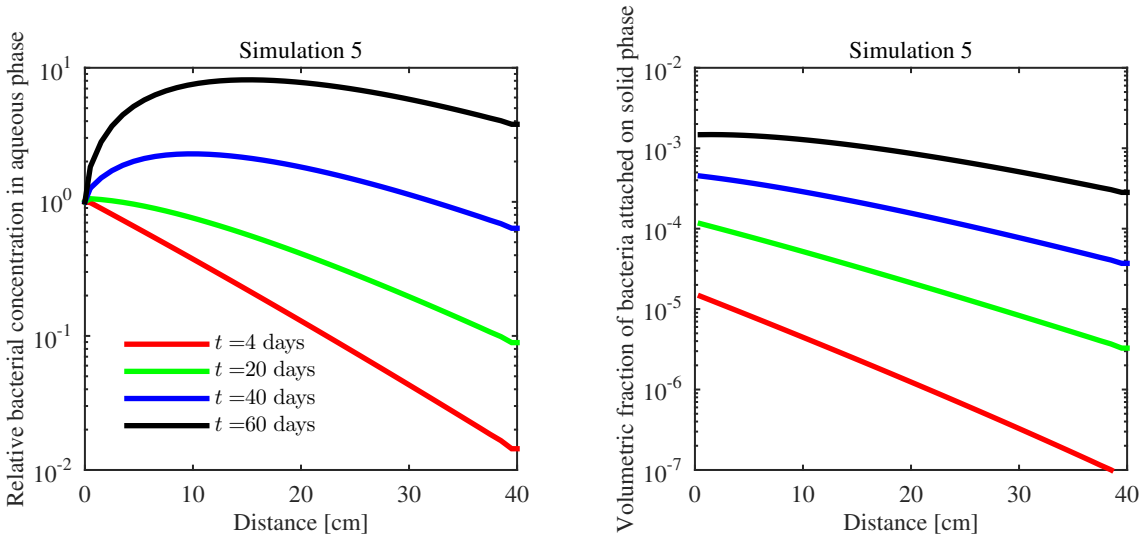

Figure 4.1.6 Concentration profiles for the benchmark validation of the transport model in 1D. On the left plot, we have the relative bacteria concentration in the aqueous phase, while on the right plot, we have the bacteria attached to the solid phase after 4, 20, 40 and 60 days respectively.

In the first plot, we observe an increment of bacterial concentration as time passes, being greater on the left side of the porous medium than on the right because we have greater amount of bacteria attached to the rock on the left as seen in the second plot. Comparison with the simulation results published in Kim 2006 show similar behaviors for the different final times.

4.2 2-D formulation

In this chapter we extend the implementation of our two-flow model to the 2-D case. In this study, we consider rectangular domains with regular rectangular partitions of dimensions $L \times W$. We define the size of the partition in the horizontal direction as Δx and for the vertical direction Δy. Fig. 3.1.2 shows a partition of a rectangular domain, where we label the four boundaries of the element Ω_{ij}. For general nonorthogonal grids, multi-point flux approximation (MPFA) mehtods are used (Aavatsmark 2002, Klausen et al. 2008).

4.2.1 Pressure equation

We start writing the expression for the pressure equation in 2D

$$\frac{\partial \phi}{\partial t} - \nabla \cdot [\mathbf{k}\big(\lambda_\Sigma \nabla p + \frac{1}{2}\lambda_\Delta \nabla p_c - (\lambda_w \rho_w + \lambda_n \rho_n)\mathbf{g}\big)] = \sum_{\alpha=w,n} \frac{F_\alpha}{\rho_\alpha}$$

We integrate in a control square Ω_{ij}

$$\int_{\Omega_{ij}} \left(\frac{\partial \phi}{\partial t} - \nabla \cdot [\mathbf{k}\big(\lambda_\Sigma \nabla p + \frac{1}{2}\lambda_\Delta \nabla p_c - (\lambda_w \rho_w + \lambda_n \rho_n)\mathbf{g}\big)] \right) dx = \int_{\Omega_{ij}} \sum_{\alpha=w,n} \frac{F_\alpha}{\rho_\alpha} dx$$

Using the divergence theorem

$$\int_{\Omega_{ij}} \frac{\partial \phi}{\partial t} dx - \int_{\gamma_{ij}} (\mathbf{k}\big(\lambda_\Sigma \nabla p + \frac{1}{2}\lambda_\Delta \nabla p_c - (\lambda_w \rho_w + \lambda_n \rho_n)\mathbf{g}\big)) \cdot \mathbf{n}\, dS = \int_{\Omega_{ij}} \sum_{\alpha=w,n} \frac{F_\alpha}{\rho \alpha} dx$$

Splitting the left integral

$$\int_{\Omega_{ij}} \frac{\partial \phi}{\partial t} dx - \int_{\gamma_{ij}} \mathbf{k}\lambda_\Sigma \nabla p \cdot \mathbf{n} dS - \int_{\gamma_{ij}} \mathbf{k}\frac{1}{2}\lambda_\Delta \nabla p_c \cdot \mathbf{n}\, dS + \int_{\gamma_{ij}} \mathbf{k}(\lambda_w \rho_w + \lambda_n \rho_n)\mathbf{g} \cdot \mathbf{n} dS = \int_{\Omega_{ij}} \sum_{\alpha=w,n} \frac{F_\alpha}{\rho_\alpha} dx$$

Using the chain rule for the p_c

$$\nabla p_{c,ij} = \frac{\partial p_c}{\partial s_w}(s_{w,ij}, a_{wn,ij}) \nabla s_{w,ij} + \frac{\partial p_c}{\partial a_{wn}}(s_{w,ij}, a_{wn,ij}) \nabla a_{wn,ij}$$

and the TPFA for the gradient

$$(\nabla p \cdot \mathbf{n})\Big|_{\gamma_{ij1}} \approx \frac{(p_{i+1,j} - p_{ij})}{\Delta x} \qquad (\nabla p \cdot \mathbf{n})\Big|_{\gamma_{ij2}} \approx \frac{(p_{i,j+1} - p_{ij})}{\Delta y}$$

$$(\nabla p \cdot \mathbf{n})\Big|_{\gamma_{ij3}} \approx -\frac{(p_{ij} - p_{i-1,j})}{\Delta x} \qquad (\nabla p \cdot \mathbf{n})\Big|_{\gamma_{ij4}} \approx -\frac{(p_{ij} - p_{i,j+1})}{\Delta y}$$

we obtain

$$
\begin{aligned}
&\frac{p_{i+1,j}-p_{ij}}{\Delta x}\int_{\gamma_{ij1}} k\lambda_\Sigma dS+\frac{p_{i,j+1}-p_{ij}}{\Delta y}\int_{\gamma_{ij2}} k\lambda_\Sigma dS\\
&+\frac{p_{i-1,j}-p_{ij}}{\Delta x}\int_{\gamma_{ij3}} k\lambda_\Sigma dS+\frac{p_{i,j-1}-p_{ij}}{\Delta y}\int_{\gamma_{ij4}} k\lambda_\Sigma dS\\
&+\frac{1}{2}\left(\frac{s_{w,i+1,j}-s_{w,ij}}{\Delta x}\int_{\gamma_{ij1}}\frac{\partial p_c}{\partial s_w}k\lambda_\Delta dS+\frac{a_{wn,i+1,j}-a_{wn,ij}}{\Delta x}\int_{\gamma_{ij1}}\frac{\partial p_c}{\partial a_{wn}}k\lambda_\Delta dS\right)\\
&+\frac{1}{2}\left(\frac{s_{w,i,j+1}-s_{w,ij}}{\Delta y}\int_{\gamma_{ij2}}\frac{\partial p_c}{\partial s_w}k\lambda_\Delta dS+\frac{a_{wn,i,j+1}-a_{wn,ij}}{\Delta y}\int_{\gamma_{ij2}}\frac{\partial p_c}{\partial a_{wn}}k\lambda_\Delta dS\right)\\
&+\frac{1}{2}\left(\frac{s_{w,i-1,j}-s_{w,ij}}{\Delta x}\int_{\gamma_{ij3}}\frac{\partial p_c}{\partial s_w}k\lambda_\Delta dS+\frac{a_{wn,i-1,j}-a_{wn,ij}}{\Delta x}\int_{\gamma_{ij3}}\frac{\partial p_c}{\partial a_{wn}}k\lambda_\Delta dS\right)\\
&+\frac{1}{2}\left(\frac{s_{w,i,j-1}-s_{w,ij}}{\Delta y}\int_{\gamma_{ij4}}\frac{\partial p_c}{\partial s_w}k\lambda_\Delta dS+\frac{a_{wn,i,j-1}-a_{wn,ij}}{\Delta y}\int_{\gamma_{ij4}}\frac{\partial p_c}{\partial a_{wn}}k\lambda_\Delta dS\right)\\
&=-\int_{\Omega_{ij}}\sum_{\alpha=w,n}\frac{F_\alpha}{\rho_\alpha}dx+\int_{\Omega_{ij}}\frac{\partial\phi}{\partial t}dx\\
&-\rho_w g\int_{\gamma_{ij2}} k\lambda_w dS+\rho_w g\int_{\gamma_{ij4}} k\lambda_w dS-\rho_n g\int_{\gamma_{ij2}} k\lambda_n dS+\rho_n g\int_{\gamma_{ij4}} k\lambda_n dS
\end{aligned}
$$

Using the mid point rule twice for approximating the integrals for the porosity and for the source/sink term, we approximate the parameters on the boundary, using the inner iteration ^{m} and rearranging the equation

$$
\begin{aligned}
&p_{i+1,j}^{n+1,m+1}k_{i+1/2,j}^{n}\lambda_{\Sigma,i+1/2,j}^{n+1,m}\Delta y^2\Delta t\\
&+p_{i,j+1}^{n+1,m+1}k_{i,j+1/2}^{n}\lambda_{\Sigma,i,j+1/2}^{n+1,m}\Delta x^2\Delta t\\
&+p_{i-1,j}^{n+1,m+1}k_{i-1/2,j}^{n}\lambda_{\Sigma,i-1/2,j}^{n+1,m}\Delta y^2\Delta t\\
&+p_{i,j-1}^{n+1,m+1}k_{i,j-1/2}^{n}\lambda_{\Sigma,i,j-1/2}^{n+1,m}\Delta x^2\Delta t\\
&-p_{ij}^{n+1,m+1}(k_{i+1/2,j}^{n}\lambda_{\Sigma,i+1/2,j}^{n+1,m}\Delta y^2+k_{i,j+1/2}^{n}\lambda_{\Sigma,i,j+1/2}^{n+1,m}\Delta x^2\\
&\qquad+k_{i-1/2,j}^{n}\lambda_{\Sigma,i-1/2,j}^{n+1,m}\Delta y^2+k_{i,j-1/2}^{n}\lambda_{\Sigma,i,j-1/2}^{n+1,m}\Delta x^2)\Delta t\\
&=-\sum_{\alpha=w,n}\frac{F_{\alpha,ij}^{n+1}}{\rho_\alpha}\Delta x^2\Delta y^2\Delta t+(\phi_{ij}^{n}-\phi_{ij}^{n-1})\Delta x^2\Delta y^2\\
&-\frac{1}{2}k_{i+1/2,j}^{n}\lambda_{\Delta,i+1/2,j}^{n+1,m}\left(\frac{\partial p_{c,i+1/2,j}^{n+1,m}}{\partial s_w}(s_{w,i+1,j}^{n+1,m}-s_{w,ij}^{n+1,m})+\frac{\partial p_{c,i+1/2,j}^{n+1,m}}{\partial a_{wn}}(a_{wn,i+1,j}^{n+1,m}-a_{wn,ij}^{n+1,m})\right)\Delta y^2\Delta t\\
&-\frac{1}{2}k_{i,j+1/2}^{n}\lambda_{\Delta,i,j+1/2}^{n+1,m}\left(\frac{\partial p_{c,i,j+1/2}^{n+1,m}}{\partial s_w}(s_{w,i,j+1}^{n+1,m}-s_{w,ij}^{n+1,m})+\frac{\partial p_{c,i,j+1/2}^{n+1,m}}{\partial a_{wn}}(a_{wn,i,j+1}^{n+1,m}-a_{wn,ij}^{n+1,m})\right)\Delta x^2\Delta t\\
&-\frac{1}{2}k_{i-1/2,j}^{n}\lambda_{\Delta,i-1/2,j}^{n+1,m}\left(\frac{\partial p_{c,i-1/2,j}^{n+1,m}}{\partial s_w}(s_{w,i-1,j}^{n+1,m}-s_{w,ij}^{n+1,m})+\frac{\partial p_{c,i-1/2,j}^{n+1,m}}{\partial a_{wn}}(a_{wn,i-1,j}^{n+1,m}-a_{wn,ij}^{n+1,m})\right)\Delta y^2\Delta t\\
&-\frac{1}{2}k_{i,j-1/2}^{n}\lambda_{\Delta,i,j-1/2}^{n+1,m}\left(\frac{\partial p_{c,i,j-1/2}^{n+1,m}}{\partial s_w}(s_{w,i,j-1}^{n+1,m}-s_{w,ij}^{n+1,m})+\frac{\partial p_{c,i,j-1/2}^{n+1,m}}{\partial a_{wn}}(a_{wn,i,j-1}^{n+1,m}-a_{wn,ij}^{n+1,m})\right)\Delta x^2\Delta t\\
&-g[\rho_w(k_{i,j+1/2}^{n}\lambda_{w,i,j+1/2}^{n+1,m}-k_{i,j-1/2}^{n}\lambda_{w,i,j-1/2}^{n+1,m})+\rho_n(k_{i,j+1/2}^{n}\lambda_{n,i,j+1/2}^{n+1,m}-k_{i,j-1/2}^{n}\lambda_{n,i,j-1/2}^{n+1,m})]\Delta x^2\Delta y\Delta t
\end{aligned}
\tag{4.47}
$$

This previous system with initial and boundary conditions allows to solve for the pressure variable.

4.2.2 Saturation equation

We start writing the expression for the saturation equation in 2D

$$\frac{\partial \phi s_w}{\partial t} - \nabla \cdot (\lambda_w \mathbf{k}(\nabla(p - \frac{1}{2}p_c) - \rho_w \mathbf{g})) = \frac{F_w}{\rho_w} \tag{4.48}$$

We integrate in a control square Ω_{ij}

$$\int_{\Omega_{ij}} \left(\frac{\partial \phi s_w}{\partial t} - \nabla \cdot (\lambda_w \mathbf{k}(\nabla(p - \frac{1}{2}p_c) - \rho_w \mathbf{g})) \right) dx = \int_{\Omega_{ij}} \frac{F_w}{\rho_w} dx \tag{4.49}$$

Using the divergence theorem

$$\int_{\Omega_{ij}} \frac{\partial \phi s_w}{\partial t} dx - \int_{\gamma_{ij}} (\lambda_w \mathbf{k}(\nabla(p - \frac{1}{2}p_c) - \rho_w \mathbf{g})) \cdot \mathbf{n} \, dS = \int_{\Omega_{ij}} \frac{F_w}{\rho_w} dV \tag{4.50}$$

Splitting the left integral, using the chain rule for p_c, the approximation of the gradient, the approximation of the temporal derivative and the inner iteration ^{m}, we obtain

$$\begin{aligned}
&\frac{\phi_{ij}^n s_{w,ij}^{n+1,m+1} - \phi_{ij}^n s_{w,ij}^n}{\Delta t} \Delta x \Delta y \\
&- \lambda_{w,i+1/2,j}^{n+1,m} k_{i+1/2,j}^n \frac{p_{i+1,j}^{n+1,m+1} - p_{i,j}^{n+1,m+1}}{\Delta x} \Delta y - \lambda_{w,i,j+1/2}^{n+1,m} k_{i,j+1/2}^n \frac{p_{i,j+1}^{n+1,m+1} - p_{i,j}^{n+1,m+1}}{\Delta y} \Delta x \\
&- \lambda_{w,i-1/2,j}^{n+1,m} k_{i-1/2,j}^n \frac{p_{i-1,j}^{n+1,m+1} - p_{i,j}^{n+1,m+1}}{\Delta x} \Delta y - \lambda_{w,i,j-1/2}^{n+1,m} k_{i,j-1/2}^n \frac{p_{i,j-1}^{n+1,m+1} - p_{i,j}^{n+1,m+1}}{\Delta y} \Delta x \\
&+ \frac{1}{2} \lambda_{w,i+1/2,j}^{n+1,m} k_{i+1/2,j}^n \left(\frac{\partial p_{c,i+1/2,j}^{n+1,m}}{\partial s_w} \frac{s_{w,i+1,j}^{n+1,m+1} - s_{w,ij}^{n+1,m+1}}{\Delta x} + \frac{\partial p_{c,i+1/2,j}^{n+1,m}}{\partial a_{wn}} \frac{a_{wn,i+1,j}^{n+1,m} - a_{wn,ij}^{n+1,m}}{\Delta x} \right) \Delta y \\
&+ \frac{1}{2} \lambda_{w,i,j+1/2}^{n+1,m} k_{i,j+1/2}^n \left(\frac{\partial p_{c,i,j+1/2}^{n+1,m}}{\partial s_w} \frac{s_{w,i,j+1}^{n+1,m+1} - s_{w,ij}^{n+1,m+1}}{\Delta y} + \frac{\partial p_{c,i,j+1/2}^{n+1,m}}{\partial a_{wn}} \frac{a_{wn,i,j+1}^{n+1,m} - a_{wn,ij}^{n+1,m}}{\Delta y} \right) \Delta x \\
&+ \frac{1}{2} \lambda_{w,i-1/2,j}^{n+1,m} k_{i-1/2,j}^n \left(\frac{\partial p_{c,i-1/2,j}^{n+1,m}}{\partial s_w} \frac{s_{w,i-1,j}^{n+1,m+1} - s_{w,ij}^{n+1,m+1}}{\Delta x} + \frac{\partial p_{c,i-1/2,j}^{n+1,m}}{\partial a_{wn}} \frac{a_{wn,i-1,j}^{n+1,m} - a_{wn,ij}^{n+1,m}}{\Delta x} \right) \Delta y \\
&+ \frac{1}{2} \lambda_{w,i,j-1/2}^{n+1,m} k_{i,j-1/2}^n \left(\frac{\partial p_{c,i,j-1/2}^{n+1,m}}{\partial s_w} \frac{s_{w,i,j-1}^{n+1,m+1} - s_{w,ij}^{n+1,m+1}}{\Delta y} + \frac{\partial p_{c,i,j-1/2}^{n+1,m}}{\partial a_{wn}} \frac{a_{wn,i,j-1}^{n+1,m} - a_{wn,ij}^{n+1,m}}{\Delta y} \right) \Delta x \\
&- g \rho_w k_{i,j+1/2}^n \lambda_{w,i,j+1/2}^{n+1,m} \Delta x + g \rho_w k_{i,j-1/2}^n \lambda_{w,i,j-1/2}^{n+1,m} \Delta x \\
&= \frac{F_{w,ij}^{n+1}}{\rho_w} \Delta x \Delta y
\end{aligned} \tag{4.51}$$

Rearranging terms, we finally get the following system of equations

$$
\begin{aligned}
&\frac{1}{2}s_{w,i+1,j}^{n+1,m+1}\lambda_{w,i+1/2,j}^{n+1,m}k_{i+1/2,j}^{n}\frac{\partial p_{c,i+1/2,j}^{n+1,m}}{\partial s_w}\Delta y^2\Delta t\\
+&\frac{1}{2}s_{w,i,j+1}^{n+1,m+1}\lambda_{w,i,j+1/2}^{n+1,m}k_{i,j+1/2}^{n}\frac{\partial p_{c,i,j+1/2}^{n+1,m}}{\partial s_w}\Delta x^2\Delta t\\
+&\frac{1}{2}s_{w,i-1,j}^{n+1,m+1}\lambda_{w,i-1/2,j}^{n+1,m}k_{i-1/2,j}^{n}\frac{\partial p_{c,i-1/2,j}^{n+1,m}}{\partial s_w}\Delta y^2\Delta t\\
+&\frac{1}{2}s_{w,i,j-1}^{n+1,m+1}\lambda_{w,i,j-1/2}^{n+1,m}k_{i,j-1/2}^{n}\frac{\partial p_{c,i,j-1/2}^{n+1,m}}{\partial s_w}\Delta x^2\Delta t\\
-&\frac{1}{2}s_{w,ij}^{n+1,m+1}[-2\phi_{ij}^{n}\Delta x^2\Delta y^2\\
+&(\lambda_{w,i+1/2,j}^{n+1,m}k_{i+1/2,j}^{n}\frac{\partial p_{c,i+1/2,j}^{n+1,m}}{\partial s_w}\Delta y^2+\lambda_{w,i,j+1/2}^{n+1,m}k_{i,j+1/2}^{n}\frac{\partial p_{c,i,j+1/2}^{n+1,m}}{\partial s_w}\Delta x^2\\
+&\lambda_{w,i-1/2,j}^{n+1,m}k_{i-1/2,j}^{n}\frac{\partial p_{c,i-1/2,j}^{n+1,m}}{\partial s_w}\Delta y^2+\lambda_{w,i,j-1/2}^{n+1,m}k_{i,j-1/2}^{n}\frac{\partial p_{c,i,j-1/2}^{n+1,m}}{\partial s_w}\Delta x^2)\Delta t]\\
=&\frac{F_{w,ij}^{n+1}}{\rho_w}\Delta x^2\Delta y^2\Delta t+\phi_{ij}^{n}s_{w,ij}^{n}\Delta x^2\Delta y^2\\
+&\lambda_{w,i+1/2,j}^{n+1,m}k_{i+1/2,j}^{n}\left(p_{i+1,j}^{n+1,m+1}-p_{i,j}^{n+1,m+1}-\frac{1}{2}\frac{\partial p_{c,i+1/2,j}^{n+1,m}}{\partial a_{wn}}(a_{wn,i+1,j}^{n+1,m}-a_{wn,ij}^{n+1,m})\right)\Delta y^2\Delta t\\
+&\lambda_{w,i,j+1/2}^{n+1,m}k_{i,j+1/2}^{n}\left(p_{i,j+1}^{n+1,m+1}-p_{i,j}^{n+1,m+1}-\frac{1}{2}\frac{\partial p_{c,i,j+1/2}^{n+1,m}}{\partial a_{wn}}(a_{wn,i,j+1}^{n+1,m}-a_{wn,ij}^{n+1,m})\right)\Delta x^2\Delta t\\
+&\lambda_{w,i-1/2,j}^{n+1,m}k_{i-1/2,j}^{n}\left(p_{i-1,j}^{n+1,m+1}-p_{i,j}^{n+1,m+1}-\frac{1}{2}\frac{\partial p_{c,i-1/2,j}^{n+1,m}}{\partial a_{wn}}(a_{wn,i-1,j}^{m,n+1}-a_{wn,ij}^{n+1,m})\right)\Delta y^2\Delta t\\
+&\lambda_{w,i,j-1/2}^{n+1,m}k_{i,j-1/2}^{n}\left(p_{i,j-1}^{n+1,m+1}-p_{i,j}^{n+1,m+1}-\frac{1}{2}\frac{\partial p_{c,i,j-1/2}^{n+1,m}}{\partial a_{wn}}(a_{wn,i,j-1}^{n+1,m}-a_{wn,ij}^{n+1,m})\right)\Delta x^2\Delta t\\
+&g\rho_w(k_{i,j+1/2}^{n}\lambda_{w,i,j+1/2}^{n+1,m}-k_{i,j-1/2}^{n}\lambda_{w,i,j-1/2}^{n+1,m})\Delta x^2\Delta y\Delta t
\end{aligned}
$$

4.2.3 Interfacial equation

We start writing the expression for the interfacial area equation in 2D

$$\frac{\partial a_{wn}}{\partial t} - \nabla \cdot (a_{wn}\mathbf{k}_{wn}\nabla a_{wn}) = E_{wn} \tag{4.52}$$

We integrate in a control square Ω_{ij}

$$\int_{\Omega_{ij}} \left(\frac{\partial a_{wn}}{\partial t} - \nabla \cdot (a_{wn}\mathbf{k}_{wn}\nabla a_{wn}) \right) dx = \int_{\Omega_{ij}} E_{wn} dx \tag{4.53}$$

Using the divergence theorem

$$\int_{\Omega_{ij}} \frac{\partial a_{wn}}{\partial t} dx - \int_{\gamma_{ij}} a_{wn}\mathbf{k}_{wn}\nabla a_{wn} \cdot \mathbf{n} dS = \int_{\Omega_{ij}} E_{wn} dx \tag{4.54}$$

Considering again the inner iteration ^{m}, the approximation for the temporal derivative and the chain rule

$$\begin{aligned}
\frac{a^{n+1,m+1}_{wn,ij} - a^{n}_{wn,ij}}{\Delta t}\Delta x\Delta y &- k^{n}_{wn,i+1/2,j} a^{n+1,m}_{wn,i+1/2,j} \frac{a^{n+1,m+1}_{wn,i+1,j} - a^{n+1,m+1}_{wn,ij}}{\Delta x}\Delta y \\
&- k^{n}_{wn,i,j+1/2} a^{n+1,m}_{wn,i,j+1/2} \frac{a^{n+1,m+1}_{wn,i,j+1} - a^{n+1,m+1}_{wn,ij}}{\Delta y}\Delta x \\
&- k^{n}_{wn,i-1/2,j} a^{n+1,m}_{wn,i-1/2,j} \frac{a^{n+1,m+1}_{wn,i-1,j} - a^{n+1,m+1}_{wn,ij}}{\Delta x}\Delta y \\
&- k^{n}_{wn,i,j-1/2} a^{n+1,m}_{wn,i,j-1/2} \frac{a^{n+1,m+1}_{wn,i,j-1} - a^{n+1,m+1}_{wn,ij}}{\Delta y}\Delta x \\
&= E^{n+1}_{wn,ij}\Delta x\Delta y
\end{aligned} \tag{4.55}$$

Rearranging terms and multiplying $\Delta x\Delta y\Delta t$ in both sides, we finally obtain

$$\begin{aligned}
&-a^{n+1,m+1}_{wn,i+1,j} k^{n}_{wn,i+1/2,j} a^{n+1,m}_{wn,i+1/2,j}\Delta y^2\Delta t \\
&-a^{n+1,m+1}_{wn,i,j+1} k^{n}_{wn,i,j+1/2} a^{n+1,m}_{wn,i,j+1/2}\Delta x^2\Delta t \\
&-a^{n+1,m+1}_{wn,i-1,j} k^{n}_{wn,i-1/2,j} a^{n+1,m}_{wn,i-1/2,j}\Delta y^2\Delta t \\
&-a^{n+1,m+1}_{wn,i,j-1} k^{n}_{wn,i,j-1/2} a^{n+1,m}_{wn,i,j-1/2}\Delta x^2\Delta t \\
&\quad a^{n+1,m+1}_{wn,ij}(\Delta x^2\Delta y^2 + ([k^{n}_{wn,i+1/2,j} a^{n+1,m}_{wn,i+1/2,j} + k^{n}_{wn,i-1/2,j} a^{n+1,m}_{wn,i-1/2,j}]\Delta y^2 \\
&\qquad\qquad + [k^{n}_{wn,i,j+1/2} a^{n+1,m}_{wn,i,j+1/2} + k^{n}_{wn,i,j-1/2} a^{n+1,m}_{wn,i,j-1/2}]\Delta x^2)\Delta t) \\
&=(E^{n+1}_{wn,ij}\Delta t + a^{n}_{wn,ij})\Delta x^2\Delta y^2
\end{aligned} \tag{4.56}$$

4.2.3.1 Boundary conditions

The treatment for the boundary conditions is analogous to the 1-D domain, but this time we have more cases for considering the size of the cells on the corners. The next figures show how to deal with them.

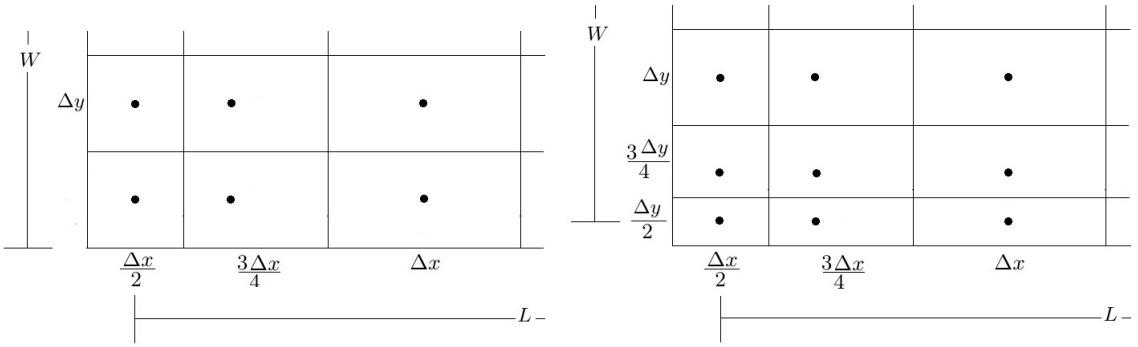

Figure 4.2.1 Modification in half cells for Dirichlet boundary conditions in 2D. In the first domain, we consider a Dirichlet boundary condition on the left and a Neumann\Flux on the bottom, while in the second domain, Dirichlet conditions on both boundaries.

4.2.3.1.1 Dirichlet boundary conditions

Let us suppose that we have Dirichlet boundary conditions on the left and on the bottom sides for the pressure equation ($p(0,y,t) = p_L(y,t)$, $p(x,0,t) = p_B(x,t)$). After integration of the pressure equation, we have

$$
\begin{aligned}
&\Bigg[k^n_{3/2,1}\lambda^{n+1,m}_{\Sigma,3/2,1}\frac{p^{n+1,m+1}_{2,1}-p^{n+1,m+1}_{1,1}}{\Delta x}\\
&\quad+\frac{1}{2}k^n_{3/2,1}\lambda^{n+1,m}_{\Delta,3/2,1}\left(\frac{\partial p^{n+1,m}_{c,3/2,1}}{\partial s_w}\frac{s^{n+1,m}_{w,2,1}-s^{n+1,m}_{w,1,1}}{\Delta x}+\frac{\partial p^{n+1,m}_{c,3/2,1}}{\partial a_{wn}}\frac{a^{n+1,m}_{wn,2,1}-a^{n+1,m}_{wn,1,1}}{\Delta x}\right)\Bigg]\frac{3\Delta y}{4}\\
&+\Bigg[k^n_{1,3/2}\lambda^{n+1,m}_{\Sigma,1,3/2}\frac{p^{n+1,m+1}_{1,2}-p^{n+1,m+1}_{1,1}}{\Delta y}\\
&\quad+\frac{1}{2}k^n_{1,3/2}\lambda^{n+1,m}_{\Delta,1,3/2}\left(\frac{\partial p^{n+1,m}_{c,1,3/2}}{\partial s_w}\frac{s^{n+1,m}_{w,1,2}-s^{n+1,m}_{w,1,1}}{\Delta y}+\frac{\partial p^{n+1,m}_{c,1,3/2}}{\partial a_{wn}}\frac{a^{n+1,m}_{wn,1,2}-a^{n+1,m}_{wn,1,1}}{\Delta y}\right)\\
&+g[\rho_w k^n_{1,3/2}\lambda^{n+1,m}_{w,1,3/2}+\rho_n k^n_{1,3/2}\lambda^{n+1,m}_{n,1,3/2}]\Bigg]\frac{3\Delta x}{4}\\
&+\Bigg[k^n_{1/2,1}\lambda^{n+1,m}_{\Sigma,1/2,1}\frac{p^{n+1}_{L,1}-p^{n+1,m+1}_{1,1}}{\frac{\Delta x}{2}}\\
&\quad+\frac{1}{2}k^n_{1/2,1}\lambda^{n+1,m}_{\Delta,1/2,1}\left(\frac{\partial p^{n+1,m}_{1/2,1,c}}{\partial s_w}\frac{s^{n+1,m}_{w,0,1}-s^{n+1,m}_{w,1,1}}{\frac{\Delta x}{2}}+\frac{\partial p^{n+1,m}_{c,1/2,1}}{\partial a_{wn}}\frac{a^{n+1,m}_{wn,0,1}-a^{n+1,m}_{wn,1,1}}{\frac{\Delta x}{2}}\right)\Bigg]\frac{3\Delta y}{4}\\
&+\Bigg[k^n_{1,1/2}\lambda^{n+1,m}_{\Sigma,1,1/2}\frac{p^{n+1}_{B,1}-p^{n+1,m+1}_{1,1}}{\frac{\Delta y}{2}}\\
&\quad+\frac{1}{2}k^n_{1,1/2}\lambda^{n+1,m}_{\Delta,1,1/2}\left(\frac{\partial p^{n+1,m}_{c,1,1/2}}{\partial s_w}\frac{s^{n+1,m}_{w,1,0}-s^{n+1,m}_{w,1,1}}{\frac{\Delta y}{2}}+\frac{\partial p^{n+1,m}_{c,1,1/2}}{\partial a_{wn}}\frac{a^{n+1,m}_{wn,1,0}-a^{n+1,m}_{wn,1,1}}{\frac{\Delta y}{2}}\right)\\
&\quad-g[\rho_w k^n_{1,1/2}\lambda^{n+1,m}_{w,1,1/2}+\rho_n k^n_{1,1/2}\lambda^{n+1,m}_{n,1,1/2}]\Bigg]\frac{3\Delta x}{4}\\
&=-\sum_{\alpha=w,n}\frac{F^{n+1}_{\alpha,1,1}}{\rho_\alpha}\frac{3\Delta x}{4}\frac{3\Delta y}{4}+\frac{\phi^n_{1,1}-\phi^{n-1}_{1,1}}{\Delta t}\frac{3\Delta x}{4}\frac{3\Delta y}{4}
\end{aligned}
$$

The previous example gives the idea for implementing Dirichlet boundary conditions.

4.2.3.1.2 Flux boundary conditions

Now, let us suppose that we have flux boundary conditions on the right boundary $\mathbf{n}\cdot\mathbf{u}_\Sigma(L,y,t) = q_R(y,t)$. Integration of the pressure equation in one of the right cells, using the divergence theorem, splitting the left integral, and using the boundary condition leads to

$$
\begin{aligned}
&- q_{R,j}^{n+1}\Delta y \\
&+ \Bigg(k_{N,j+1/2}^{n}\lambda_{\Sigma,N,j+1/2}^{n+1,m}\frac{p_{N,j+1}^{n+1,m+1}-p_{N,j}^{n+1,m+1}}{\Delta y} \\
&+ \frac{1}{2}k_{N,j+1/2}^{n}{}^{m}\Delta\lambda_{N,j+1/2}^{n+1}\left[\frac{\partial p_{c,N,j+1/2}^{n+1,m}}{\partial s_w}\frac{(s_{w,N,j+1}^{n+1,m}-s_{w,N,j}^{n+1,m})}{\Delta y}+\frac{\partial p_{c,N,j+1/2}^{n+1,m}}{\partial a_{wn}}\frac{(a_{wn,N,j+1}^{n+1,m}-a_{wn,N,j}^{n+1,m})}{\Delta y}\right] \\
&+ g[\rho_w k_{N,j+1/2}^{n}\lambda_{w,N,j+1/2}^{n+1,m}+\rho_n k_{N,j+1/2}^{n}\lambda_{n,N,j+1/2}^{n+1,m}]\Bigg)\Delta x \\
&+ \Bigg(k_{N-1/2,j}^{n}\lambda_{\Sigma,N-1/2,j}^{n+1,m}\frac{p_{N-1,j}^{n+1,m+1}-p_{N,j}^{n+1,m+1}}{\Delta x} \\
&+ \frac{1}{2}k_{N-1/2,j}^{n}\lambda_{\Delta,N-1/2,j}^{n+1,m}\left[\frac{\partial p_{c,N-1/2,j}^{n+1,m}}{\partial s_w}\frac{(s_{w,N-1,j}^{n+1,m}-s_{w,N,j}^{n+1,m})}{\Delta x}+\frac{\partial p_{c,N-1/2,j}^{n+1,m}}{\partial a_{wn}}\frac{(a_{wn,N-1,j}^{n+1,m}-a_{wn,N,j}^{n+1,m})}{\Delta x}\right]\Bigg)\Delta y \\
&+ \Bigg(k_{N,j-1/2}^{n}\lambda_{\Sigma,N,j-1/2}^{n+1,m}\frac{p_{N,j-1}^{n+1,m+1}-p_{N,j}^{n+1,m+1}}{\Delta y} \\
&+ \frac{1}{2}k_{N,j-1/2}^{n}{}^{m}\Delta\lambda_{N,j-1/2}^{n+1}\left[\frac{\partial p_{c,N,j-1/2}^{n+1,m}}{\partial s_w}\frac{(s_{w,N,j-1}^{n+1,m}-s_{w,N,j}^{n+1,m})}{\Delta y}+\frac{\partial p_{c,N,j-1/2}^{n+1,m}}{\partial a_{wn}}\frac{(a_{wn,N,j-1}^{n+1,m}-a_{wn,N,j}^{n+1,m})}{\Delta y}\right] \\
&- g[\rho_w k_{N,j-1/2}^{n}\lambda_{w,N,j-1/2}^{n+1,m}+\rho_n k_{N,j-1/2}^{n}\lambda_{n,N,j-1/2}^{n+1,m}]\Bigg)\Delta x \\
&= -\sum_{\alpha=w,n}\frac{F_{\alpha,N,j}^{n+1}}{\rho_\alpha}\Delta x\Delta y+\frac{\phi_{N,j}^{n}-\phi_{N,j}^{n-1}}{\Delta t}\Delta x\Delta y
\end{aligned}
$$

Rearranging terms, we finally obtain

$$
\begin{aligned}
&+ p_{N,j+1}^{n+1,m+1}k_{N,j+1/2}^{n}\lambda_{\Sigma,N,j+1/2}^{n+1,m}\Delta x^2\Delta t \\
&+ p_{N-1,j}^{n+1,m+1}k_{N-1/2,j}^{n}\lambda_{\Sigma,N-1/2,j}^{n+1,m}\Delta y^2\Delta t \\
&+ p_{N,j-1}^{n+1,m+1}k_{N,j-1/2}^{n}\lambda_{\Sigma,N,j-1/2}^{n+1,m}\Delta x^2\Delta t \\
&- p_{N,j}^{n+1,m+1}(k_{N,j+1/2}^{n}\lambda_{\Sigma,N,j+1/2}^{n+1,m}\Delta x^2+k_{N-1/2,j}^{n}\lambda_{\Sigma,N-1/2,j}^{n+1,m}\Delta y^2+k_{N,j-1/2}^{n}\lambda_{\Sigma,N,j-1/2}^{n+1,m}\Delta x^2)\Delta t \\
&= -\sum_{\alpha=w,n}\frac{F_{\alpha,N,j}^{n+1}}{\rho_\alpha}\Delta x^2\Delta y^2\Delta t+(\phi_{N,j}^{n}-\phi_{N,j}^{n-1})\Delta x^2\Delta y^2+q_{R,j}^{n+1}\Delta x\Delta y^2\Delta t \\
&- \frac{\Delta t}{2}k_{N,j+1/2}^{n}\lambda_{\Delta,N,j+1/2}^{n+1,m}\left(\frac{\partial p_{c,N,j+1/2}^{n+1,m}}{\partial s_w}(s_{w,N,j+1}^{n+1,m}-s_{w,N,j}^{n+1,m})+\frac{\partial p_{c,N,j+1/2}^{n+1,m}}{\partial a_{wn}}(a_{wn,N,j+1}^{n+1,m}-a_{wn,N,j}^{n+1,m})\right)\Delta x^2 \\
&- \frac{\Delta t}{2}k_{N-1/2,j}^{n}\lambda_{\Delta,N-1/2,j}^{n+1,m}\left(\frac{\partial p_{c,N-1/2,j}^{n+1,m}}{\partial s_w}(s_{w,N-1,j}^{n+1,m}-s_{w,N,j}^{n+1,m})+\frac{\partial p_{c,N-1/2,j}^{n+1,m}}{\partial a_{wn}}(a_{wn,N-1,j}^{n+1,m}-a_{wn,N,j}^{n+1,m})\right)\Delta y^2 \\
&- \frac{\Delta t}{2}k_{N,j-1/2}^{n}\lambda_{\Delta,N,j-1/2}^{n+1,m}\left(\frac{\partial p_{c,N,j-1/2}^{n+1,m}}{\partial s_w}(s_{w,N,j-1}^{n+1,m}-s_{w,N,j}^{n+1,m})+\frac{\partial p_{c,N,j-1/2}^{n+1,m}}{\partial a_{wn}}(a_{wn,N,j-1}^{n+1,m}-a_{wn,N,j}^{n+1,m})\right)\Delta x^2 \\
&- g[\rho_w(k_{N,j+1/2}^{n}\lambda_{w,N,j+1/2}^{n+1,m}-k_{N,j-1/2}^{n}\lambda_{w,N,j-1/2}^{n+1,m}) \\
&\quad+\rho_n(k_{N,j+1/2}^{n}\lambda_{n,N,j+1/2}^{n+1,m}-k_{N,j-1/2}^{n}\lambda_{n,N,j-1/2}^{n+1,m})]\Delta x^2\Delta y\Delta t
\end{aligned}
\tag{4.57}
$$

After solving the system, we approximate the value of the pressure on the right border

$$p_{N+1,j}^{n+1,m+1} = -\frac{\frac{1}{2}\Delta x}{\lambda_{\Sigma,N,j}^{n+1,m}}\left(\frac{q_{R,j}^{n+1}}{k_{N,j}^{n}} + \frac{1}{2}\lambda_{\Delta,N,j}^{n+1,m}\left[\frac{\partial p_{c,N,j}^{n+1,m}}{\partial s_w}\frac{s_{w,N+1,j}^{n+1,m} - s_{w,N,j}^{n+1,m}}{\frac{\Delta x}{2}} + \frac{\partial p_{c,N,j}^{n+1,m}}{\partial a_{wn}}\frac{a_{wn,N+1,j}^{n+1,m} - a_{N,j}^{wn,n+1,m}}{\frac{\Delta x}{2}}\right]\right) + p_{N,j}^{n+1,m+1} \tag{4.58}$$

4.2.3.1.3 Neumann boundary conditions

Let us suppose that we have a Neumann condition on the top boundary for the saturation equation ($\frac{\partial s}{\partial y}(x, W, t) = q_T(x, t)$). Direct substitution of the boundary condition in Eq. (4.51) leads to

$$\begin{aligned}
&\frac{\phi_{i,M}^{n} s_{w,i,M}^{n+1,m+1} - \phi_{i,M}^{n} s_{w,i,M}^{n}}{\Delta t}\Delta x\Delta y \\
&- \left[\lambda_{w,i+1/2,M}^{n+1,m} k_{i+1/2,M}^{n}\frac{p_{i+1,M}^{n+1,m+1} - p_{i,M}^{n+1,m+1}}{\Delta x}\right. \\
&\left. - \frac{1}{2}\lambda_{w,i+1/2,M}^{n+1,m} k_{i+1/2,M}^{n}\left(\frac{\partial p_{c,i+1/2,M}^{n+1,m}}{\partial s_w}\frac{s_{w,i+1,M}^{n+1,m+1} - s_{w,i,M}^{n+1,m+1}}{\Delta x} + \frac{\partial p_{c,i+1/2,M}^{n+1,m}}{\partial a_{wn}}\frac{a_{wn,i+1,M}^{m,n+1} - a_{wn,i,M}^{n+1,m}}{\Delta x}\right)\right]\Delta y \\
&- \left[\lambda_{w,i,M+1/2}^{m,n+1} k_{i,M+1/2}^{n}\frac{p_{i,M+1}^{n+1,m+1} - p_{i,M}^{n+1,m+1}}{\frac{\Delta y}{2}}\right. \\
&- \frac{1}{2}\lambda_{w,i,M+1/2}^{n+1,m} k_{i,M+1/2}^{n}\left(\frac{\partial p_{c,i,M+1/2}^{n+1,m}}{\partial s_w} q_{T,i}^{n+1} + \frac{\partial p_{c,i,M+1/2}^{n+1,m}}{\partial a_{wn}}\frac{a_{wn,i,M+1}^{n+1,m} - a_{wn,i,M}^{n+1,m}}{\frac{\Delta y}{2}}\right) \\
&\left. + g\rho_w k_{i,M+1/2}^{n}\lambda_{\Sigma,i,M+1/2}^{n+1,m}\right]\Delta x \\
&- \left[\lambda_{w,i-1/2,M}^{n+1,m} k_{i-1/2,M}^{n}\frac{p_{i-1,M}^{n+1,m+1} - p_{i,M}^{n+1,m+1}}{\Delta x}\right. \\
&\left. - \frac{1}{2}\lambda_{w,i-1/2,M}^{n+1,m} k_{i-1/2,M}^{n}\left(\frac{\partial p_{c,i-1/2,M}^{n+1,m}}{\partial s_w}\frac{s_{w,i-1,M}^{n+1,m+1} - s_{w,i,M}^{n+1,m+1}}{\Delta x} + \frac{\partial p_{c,i-1/2,M}^{n+1,m}}{\partial a_{wn}}\frac{a_{wn,i-1,M}^{n+1,m} - a_{wn,i,M}^{n+1,m}}{\Delta x}\right)\right]\Delta y \\
&- \left[\lambda_{w,i,M-1/2}^{n+1,m} k_{i,M-1/2}^{n}\frac{p_{i,M-1}^{n+1,m+1} - p_{i,M}^{n+1,m+1}}{\Delta y}\right. \\
&- \frac{1}{2}\lambda_{w,i,M-1/2}^{n+1,m} k_{i,M-1/2}^{n}\left(\frac{\partial p_{c,i,M-1/2}^{n+1,m}}{\partial s_w}\frac{s_{w,i,M-1}^{n+1,m+1} - s_{w,i,M}^{n+1,m+1}}{\Delta y} + \frac{\partial p_{c,i,M-1/2}^{n+1,m}}{\partial a_{wn}}\frac{a_{wn,i,M-1}^{n+1,m} - a_{wn,i,M}^{n+1,m}}{\Delta y}\right) \\
&\left. - g\rho_w k_{i,M-1/2}^{n}\lambda_{\Sigma,i,M-1/2}^{n+1,m}\right]\Delta x \\
&= \frac{F_{w,i,M}^{n+1}}{\rho_w}\Delta x\Delta y
\end{aligned}$$

where we use $s_{w,i,M+1}^{n+1,m} = q_{T,i}^{n+1}\frac{\Delta y}{2} + s_{w,i,M}^{n+1,m}$ in order to compute the mobilities and derivatives of capillary pressure on the top boundary.

4.2.4 Validation of the two-phase flow model in 2D

In this section we present the analysis of convergence of the error reduction for two analytic solutions, where in the first example we do not consider the interfacial area equation, and after we test our algorithm

with the results from a benchmark simulation.

4.2.4.1 Analytic solution

We study the error reduction given two analytic solutions.

4.2.4.1.1 Example 1

We consider a porous medium of dimensions $L = 2$, $W = 0.5$. We test our scheme for the next analytic solutions and parameterizations

$$p(x,y,t) = y\sin(x) + t^2 \qquad s_w(x,y,t) = te^{x+y} + 1 \qquad p_c(s_w) = -\frac{s_w^3}{3}$$
$$k_{r,w}(s_w) = s_w \qquad k_{r,n}(s_w) = 2s_w$$

with Dirichlet boundary conditions for the pressure and saturation and initial conditions given by

$$p(x,y,0) = y\sin(x) \qquad p(0,y,t) = t^2 \qquad p(L,y,t) = y\sin(L) + t^2$$
$$p(x,0,t) = t^2 \qquad p(x,W,t) = W\sin(x) + t^2$$

$$s_w(x,y,0) = 1 \qquad s_w(0,y,t) = te^y + 1 \qquad s_w(L,y,t) = te^{L+y} + 1$$
$$s_w(x,0,t) = te^x + 1 \qquad s_w(x,W,t) = te^{x+W} + 1$$

We consider

$$k = \rho_w = \rho_n = \mu_w = \mu_n = \phi = 1 \qquad g = 0$$

The source/sink terms are given by

$$\frac{F_w}{\rho_w} = \phi e^{x+y} - k[te^{x+y}(y\cos(x) + \sin(x)) - y\sin(x)(te^{x+y} + 1) + te^{x+y}(te^{x+y} + 1)^2(4te^{x+y} + 1)]$$
$$\frac{F_n}{\rho_n} = -\phi e^{x+y} - 2k[te^{x+y}(y\cos(x) + \sin(x)) - y\sin(x)(te^{x+y} + 1) - te^{x+y}(te^{x+y} + 1)^2(4te^{x+y} + 1)]$$

We present the results of the analysis of convergence in Table 4.2.1, where we halve the size of the time and space step in each case. From the table we observe that the error reduction for both pressure and saturation approximates to 4.

Table 4.2.1 Pressure and saturation errors for the analytic validation in 2D. We test for different mesh sizes and time steps, with $L = 2$, $W = 0.5$ and $T = 1$.

	Δx	Δy	Δt	$L_{p,2}$ error	$L_{s,2}$ error	red p	red s
1	0.25	0.125	0.0625	1.9121e-4	0.022499		
2	0.125	0.0625	0.03125	4.7548e-5	0.0064204	4.0213	3.5043
3	0.0625	0.03125	0.015625	1.1923e-5	0.0017886	3.9879	3.5896
4	0.03125	0.015625	0.0078125	2.9963e-6	4.7982e-4	3.9792	3.7277

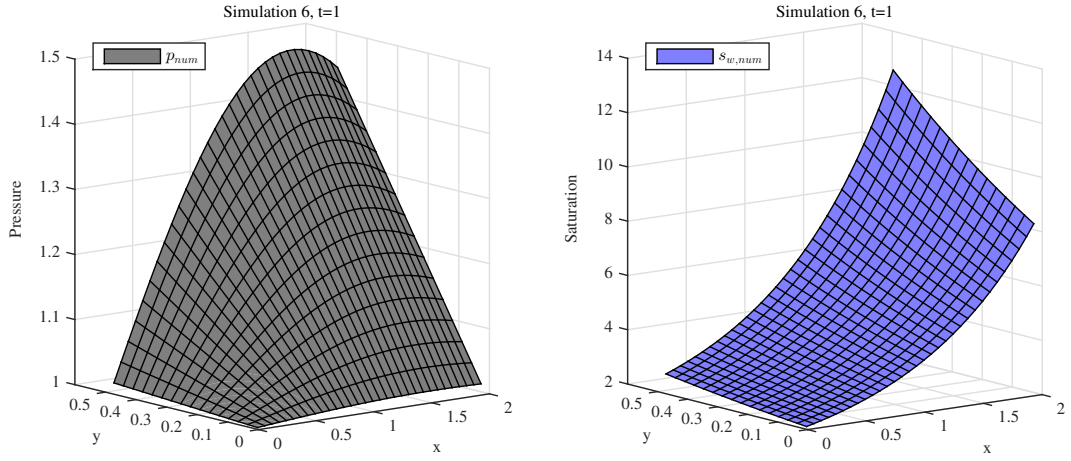

Figure 4.2.2 Pressure and saturation profiles for the analytic validation in 2D. The size partitions are dx=0.0625, dy=0.03125 and dt=0.015625.

4.2.4.1.2 Example 2

We consider a porous medium of dimensions $L = 2$, $W = 1$. We test our scheme for the next analytic solutions and parameterizations

$$p(x,y,t) = x^2y^2t \qquad s_w(x,y,t) = x^2 + y^2 + t \qquad a_{wn}(x,y,t) = e^{txy}$$
$$p_c(s_w, a_{wn}) = -a_{wn}s_w \qquad k_{r,w}(s_w) = s_w \qquad k_{r,n}(s_w) = 2s_w$$

with boundary and initial conditions given by

Pressure

$$p(x,y,0) = 0 \quad \mathbf{n}\cdot\mathbf{u}_\Sigma(0,y,t) = -\frac{1}{2}kyt(y^2+t)^2 \quad \mathbf{n}\cdot\mathbf{u}_\Sigma(x,0,t) = -\frac{1}{2}kxt(x^2+t)^2 p(L,y,t) = L^2y^2t$$
$$\mathbf{n}\cdot\mathbf{u}_\Sigma(x,W,t) = -k(x^2+W^2+t)(6Wtx^2 - \frac{1}{2}e^{txW}(tx(x^2+by^2+t)+2W))$$

Saturation

$$s_w(x,y,0) = x^2 + y^2 \qquad s_w(0,y,t) = y^2 + t$$
$$\mathbf{n}\cdot\nabla s_w(L,y,t) = 2L \qquad \mathbf{n}\cdot\nabla s_w(x,0,t) = 0 \qquad \mathbf{n}\cdot\nabla s_w(x,W,t) = 2W$$

Interfacial area

$$a_{wn}(x,y,0) = 1 \qquad a_{wn}(0,y,t) = 1$$
$$\mathbf{n}\cdot\nabla a_{wn}(L,y,t) = tye^{tyL} \qquad \mathbf{n}\cdot\nabla a_{wn}(x,0,t) = 0 \qquad \mathbf{n}\cdot\nabla a_{wn}(x,W,t) = txe^{txW}$$

where we consider

$$\rho_w = \rho_n = \mu_w = \mu_n = \phi = 1 \qquad k = k_{wn} = 0.001 \qquad g = 0$$

The source/sink terms are given by

$$\frac{F_w}{\rho_w} = 1 - k(8x^2y^2t + 2t(x^2+y^2+t)(x^2+y^2)$$
$$+\frac{1}{2}e^{xyt}(2x(ty(x^2+y^2+t)+2x) + (x^2+y^2+t)(t^2y^2(x^2+y^2+t)+4xyt+2)$$
$$+2y(tx(x^2+y^2+t)+2y) + (x^2+y^2+t)(t^2x^2(x^2+y^2+t)+4xyt+2)))$$
$$\frac{F_n}{\rho_n} = -1 - 2k(8x^2y^2t + 2t(x^2+y^2+t)(x^2+y^2)$$
$$-\frac{1}{2}e^{xyt}(2x(ty(x^2+y^2+t)+2x) + (x^2+y^2+t)(t^2y^2(x^2+y^2+t)+4xyt+2)$$
$$+2y(tx(x^2+y^2+t)+2y) + (x^2+y^2+t)(t^2x^2(x^2+y^2+t)+4xyt+2)))$$
$$E_{wn} = xye^{xyt} - 2k_{wn}t^2e^{2txy}(x^2+y^2)$$

We present the results of the analysis of convergence in Table 4.2.2, where we halve the size of the time and space step in each case

Table 4.2.2 Pressure, saturation and interfacial area errors for the analytic validation in 2D. We test for different mesh sizes and time steps, with $L = 2$, $W = 1$ and $T = 1$.

	Δx	Δy	Δt	$L_{p,2}$ error	$L_{s_w,2}$ error	$L_{a_{wn},2}$ error	red p	red s_w	red a_{wn}
1	0.1	0.2	0.05	0.10551	0.010628	0.060792			
2	0.05	0.1	0.025	0.040402	0.0065931	0.030952	2.6115	1.6120	1.9641
3	0.025	0.05	0.0125	0.016874	0.0035531	0.015515	2.3943	1.8556	1.9950
4	0.0125	0.025	0.00625	0.0076123	0.0018126	0.0077552	2.2167	1.9602	2.0006

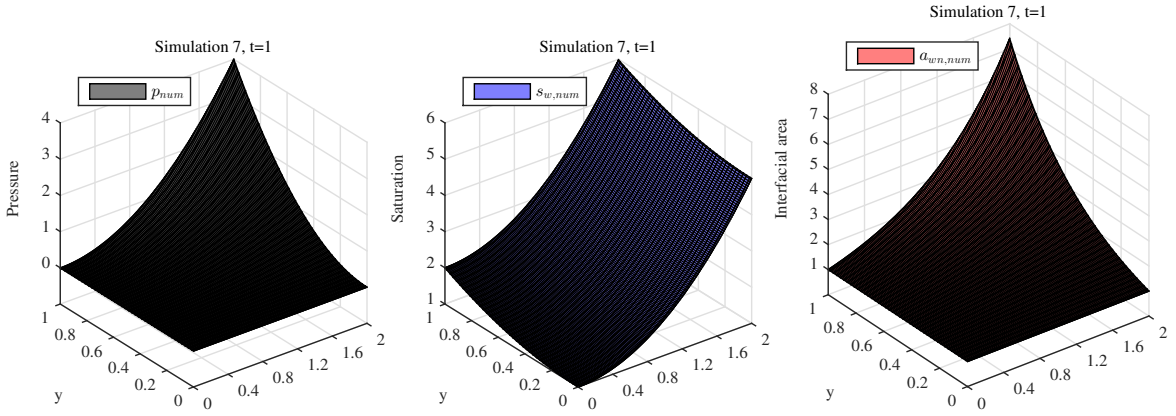

Figure 4.2.3 Pressure, saturation and interfacial area profiles for the analytic validation in 2D. The size partitions are dx=0.0125, dy=0.025 and dt=0.00625.

From the table we observe that the error reduction for the pressure, saturation and interfacial area approximates to 2.

4.2.4.2 Benchmark simulation

We test our algorithm against another numerical simulation made by Amaziane et al. 2009. The parameters for the simulation are given in Table 4.2.3, where we assume again that the gaseous phase is incompressible.

Table 4.2.3 Model parameters used in the benchmark validation in 2D.

Parameter	Value	Parameter	Value	Parameter	Value
k	1mD	ϕ	0.1	p_e	2 MPa
μ_n	$9{\cdot}10^{-6}$ Pa·s	s_{smax}	1	L	100 m
μ_w	$0.86{\cdot}10^{-3}$ Pa·s	s_{sres}	0	W	2 m
ρ_n	2 kg·m^{-3}	n	2	T	45 days
ρ_w	996.5 kg·m^{-3}	m	0.5		

In the simulation, we consider that the porous medium is initial saturated with water and the gas is injected on the left side of the porous medium. The boundary and initial conditions for the pressure and saturation are the following

$$p(x,y,0) = 0.1 \text{ MPa} \quad p(L,y,t) = 0.1 \text{ MPa} \quad \mathbf{n}\cdot\mathbf{u}_\Sigma(x,W,t) = 0 \quad p(0,y,t) = 2 \text{ MPa} \quad \mathbf{n}\cdot\mathbf{u}_\Sigma(x,0,t) = 0$$
$$s_w(x,y,0) = 1 \quad \mathbf{n}\cdot\nabla s_w(L,y,t) = 0 \quad \mathbf{n}\cdot\nabla s_w(x,W,t) = 0 \quad s_w(0,y,t) = 0.4 \quad \mathbf{n}\cdot\nabla s_w(x,0,t) = 0$$

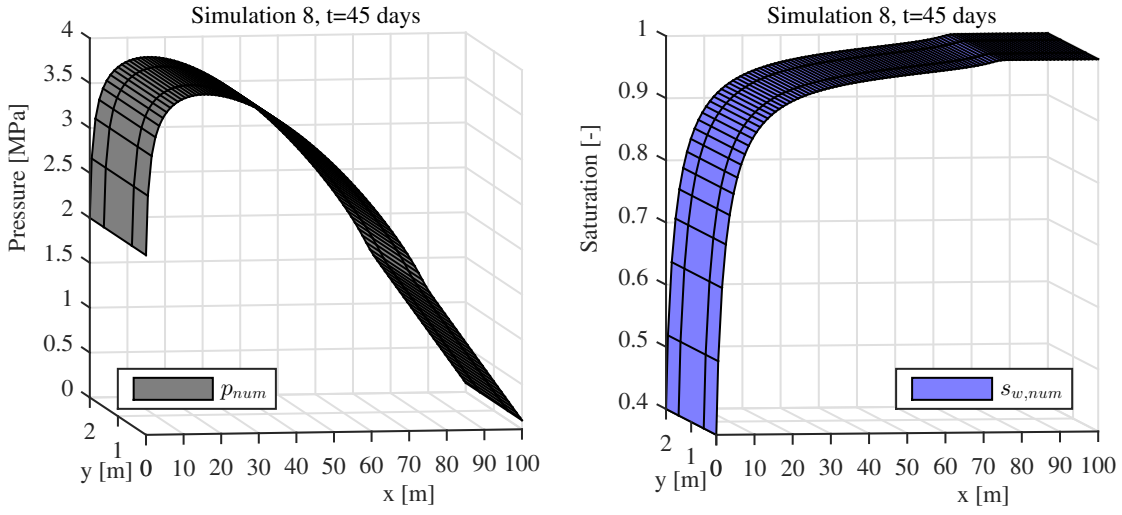

Figure 4.2.4 Pressure and saturation profiles for the benchmark validation in 2D. The size parameters are dx=dy=1 m and dt=3.888e-4.

When we compare these results with the ones shown in the paper, we observe that they present the same behavior. After 45 days of gas injection, we have not reach the breakthrough, which implies we are just extracting water.

4.2.5 Transport equations

Having implemented correctly the algorithm for solving the pressure, saturation and interfacial area equations, we proceed with the transport equations. We start for writing the transport equations in 2D

$$\begin{aligned}
&\frac{\partial(C_b\phi s_w)}{\partial t} - \nabla\cdot(\mathbf{D}_b s_w\phi\nabla C_b - \mathbf{u}_w C_b - \phi\mathbf{v}_g C_b) = R_b\\
&\frac{\partial(C_n\phi s_w)}{\partial t} - \nabla\cdot(\mathbf{D}_n s_w\phi\nabla C_n - \mathbf{u}_w C_n) = R_n\\
&\frac{\partial(C_p\phi s_w)}{\partial t} - \nabla\cdot(\mathbf{D}_p s_w\phi\nabla C_p - \mathbf{u}_w C_p) = R_p
\end{aligned} \tag{4.59}$$

We show the discretization for the bacterial concentration equation and for getting the discretization for the other two equations, we just change indexes and consider $v_g = 0$.

We integrate in a control square Ω_{ij}

$$\int_{\Omega_{ij}}\left(\frac{\partial(C_b\phi s_w)}{\partial t} - \nabla\cdot(\mathbf{D}_b s_w\phi\nabla C_b - \mathbf{u}_w C_b - \phi\mathbf{v}_g C_b)\right)dx = \int_{\Omega_{ij}} R_b\, dx \tag{4.60}$$

Using the divergence theorem for the left integral and the midpoint rule for the right integral

$$\int_{\Omega_{ij}}\frac{\partial(C_b\phi s_w)}{\partial t}dx - \int_{\gamma_{ij}}(\mathbf{D}_b s_w\phi\nabla C_b - \mathbf{u}_w C_b - \phi\mathbf{v}_g C_b)\cdot\mathbf{n}dS = \int_{\Omega_{ij}} R_b\, dx \tag{4.61}$$

By splitting the left integral, using the approximation of the gradient, considering that $\alpha_L = \alpha_T$, the approximation of the temporal derivative and the inner iteration ^{m} we obtain

$$\begin{aligned}
&\frac{C^{n+1,m+1}_{b,ij}\phi^n_{ij}s^{n+1}_{w,ij} - C^n_{b,ij}\phi^n_{ij}s^n_{w,ij}}{\Delta t}\Delta x\Delta y\\
&-D^{n+1}_{b,i+1/2,j}s^{n+1}_{w,i+1/2,j}\phi^n_{i+1/2,j}\frac{C^{n+1,m+1}_{b,i+1,j} - C^{n+1,m+1}_{b,ij}}{\Delta x}\Delta y\\
&-D^{n+1}_{b,i,j+1/2}s^{n+1}_{w,i,j+1/2}\phi^n_{i,j+1/2}\frac{C^{n+1,m+1}_{b,i,j+1} - C^{n+1,m+1}_{b,ij}}{\Delta y}\Delta x\\
&-D^{n+1}_{b,i-1/2,j}s^{n+1}_{w,i-1/2,j}\phi^n_{i-1/2,j}\frac{C^{n+1,m+1}_{b,i-1,j} - C^{n+1,m+1}_{b,ij}}{\Delta x}\Delta y\\
&-D^{n+1}_{b,i,j-1/2}s^{n+1}_{w,i,j-1/2}\phi^n_{i,j-1/2}\frac{C^{n+1,m+1}_{b,i,j-1} - C^{n+1,m+1}_{b,ij}}{\Delta y}\Delta x\\
&+u^{n+1}_{wx,i+1/2,j}\frac{C^{n+1,m+1}_{b,i+1,j} + C^{n+1,m+1}_{b,ij}}{2}\Delta y + u^{n+1}_{wy,i,j+1/2}\frac{C^{n+1,m+1}_{b,i,j+1} + C^{n+1,m+1}_{b,ij}}{2}\Delta x\\
&-u^{n+1}_{wx,i-1/2,j}\frac{C^{n+1,m+1}_{b,i-1,j} + C^{n+1,m+1}_{b,ij}}{2}\Delta y - u^{n+1}_{wy,i,j-1/2}\frac{C^{n+1,m+1}_{b,i,j-1} + C^{n+1,m+1}_{b,ij}}{2}\Delta x\\
&-\phi^n_{i,j+1/2}v_g\frac{C^{n+1,m+1}_{b,i,j+1} + C^{n+1,m+1}_{b,ij}}{2}\Delta y + \phi^n_{i,j-1/2}v_g\frac{C^{n+1,m+1}_{b,i,j-1} + C^{n+1,m+1}_{b,ij}}{2}\Delta x\\
&= R^{n+1,m+1}_{b,ij}\Delta x\Delta y
\end{aligned}$$

Rearranging terms, we obtain the following system

$$
\begin{aligned}
&C_{b,ij}^{n+1,m+1}\{[\phi_{ij}^{n}s_{w,ij}^{n}\Delta x^2\Delta y^2 + D_{b,i+1/2,j}^{n+1}s_{w,i+1/2,j}^{n+1}\phi_{i+1/2,j}^{n} \\
&\quad + D_{b,i-1/2,j}^{n+1}s_{w,i-1/2,j}^{n+1}\phi_{i-1/2,j}^{n} + (u_{wx,i+1/2,j}^{n+1} - u_{wx,i-1/2,j}^{n+1})\frac{\Delta x}{2}]\Delta y^2\Delta t \\
&\quad + [D_{b,i,j+1/2}^{n+1}s_{w,i,j+1/2}^{n+1}\phi_{i,j+1/2}^{n} + D_{b,i,j-1/2}^{n+1}s_{w,i,j-1/2}^{n+1}\phi_{i,j-1/2}^{n} \\
&\quad + (u_{wy,i,j+1/2}^{n+1} - u_{wy,i,j-1/2}^{n+1} - (\phi_{i,j+1/2}^{n} - \phi_{i,j-1/2}^{n})v_g)\frac{\Delta y}{2}]\Delta x^2\Delta t\} \\
&-C_{b,i+1,j}^{n+1,m+1}(D_{b,i+1/2,j}^{n+1}s_{w,i+1/2,j}^{n+1}\phi_{i+1/2,j}^{n} - u_{wx,i+1/2,j}^{n+1}\frac{\Delta x}{2})\Delta y^2\Delta t \\
&-C_{b,i,j+1}^{n+1,m+1}(D_{b,i,j+1/2}^{n+1}s_{w,i,j+1/2}^{n+1}\phi_{i,j+1/2}^{n} - (u_{wy,i,j+1/2}^{n+1} - \phi_{i,j+1/2}^{n}v_g)\frac{\Delta y}{2})\Delta x^2\Delta t \\
&-C_{b,i-1,j}^{n+1,m+1}(D_{b,i-1/2,j}^{n+1}s_{w,i-1/2,j}^{n+1}\phi_{i-1/2,j}^{n} + u_{wx,i-1/2,j}^{n+1}\frac{\Delta x}{2})\Delta y^2\Delta t \\
&-C_{b,i,j-1}^{n+1,m+1}(D_{b,i,j-1/2}^{n+1}s_{w,i,j-1/2}^{n+1}\phi_{i,j-1/2}^{n} + (u_{wy,i,j-1/2}^{n+1} - \phi_{i,j-1/2}^{n}v_g)\frac{\Delta y}{2})\Delta x^2\Delta t \\
&=(R_{b,ij}^{n+1,m}\Delta t + C_{b,ij}^{n}\phi_{ij}^{n}s_{w,ij}^{n})\Delta x^2\Delta y^2
\end{aligned}
$$

Finally, we can write the linear system of equations for the transport equations in the matrix form $\mathbf{M}\mathbf{C}^{n+1,m+1} = \mathbf{R}$, where we consider $\mathbf{C}$ being of the form

$$
\mathbf{C}^{n+1,m+1} = \begin{pmatrix}
C_{b,11}^{n+1,m+1} \\
C_{n,11}^{n+1,m+1} \\
C_{p,11}^{n+1,m+1} \\
C_{b,21}^{n+1,m+1} \\
C_{n,21}^{n+1,m+1} \\
C_{p,21}^{n+1,m+1} \\
\vdots \\
C_{b,N,M}^{n+1,m+1} \\
C_{n,N,M}^{n+1,m+1} \\
C_{p,N,M}^{n+1,m+1}
\end{pmatrix}
$$

The treatment for the boundary conditions can be complete as a generalization of the sections 4.1.5.1 and 4.2.3.1.

4.2.6 Validation of the concentration formulation in 2D

Similar to the 1-D case, we need to run the code and make comparisons with known solutions in order to validate the code's functionality. In this section we present the analysis of convergence of the error reduction for an analytic solution and test our algorithm with the results from an experiment that considers bioclogging.

4.2.6.1 Analytic solution

We consider a rectangular porous medium of dimensions $L = 2$ and $W = 1$. We test our scheme for the next analytic solutions with Dirichlet boundary conditions

$$C_b(x, y, t) = t(\sin x + \cos x) \qquad C_n(x, y, t) = t(\cos x - \sin y) \qquad C_p(x, y, t) = \frac{1}{1 + x + y + t}$$

We consider

$$\phi = s_w = u_{wx} = u_{wy} = D_b = D_n = D_p = 1 \qquad\qquad v_g = 0$$

The source/sink terms are given by

$$R_b = (\sin x + \cos y)(1 + t) - C_n \qquad R_n = (\cos x - \sin y)(1 + t) + C_b \qquad R_p = 2C_p^2(1 - 2C_p)$$

In this example we test the algorithm for the case when the two first transport equations are coupled and the source/sink term for the surfactants are a function of the concentration. We present the results of the analysis of convergence in Table 4.2.4, where we halve the size of the time and space steps in each case. From the table, we can conclude that the numerical solver is working.

Table 4.2.4 Concentration errors for the analytic validation of the transport model in 2D. We test for different mesh sizes and time steps, with $L = 2$, $W = 1$ and $T = 1$.

	Δx	Δy	Δt	$L_{b,2}$ error	$L_{n,2}$ error	$L_{p,2}$ error	red b	red n	red p
1	0.2	0.2	0.1	0.0080298	0.0012655	0.0013173			
2	0.1	0.1	0.05	0.0023322	2.3714e-4	4.4028e-4	3.4431	5.3364	2.9919
3	0.05	0.05	0.025	6.0926e-4	5.1309e-5	1.4079e-4	3.8278	4.6218	3.1273
4	0.025	0.025	0.0125	1.5455e-4	1.2398e-5	4.9410e-5	3.9422	4.1386	2.8494

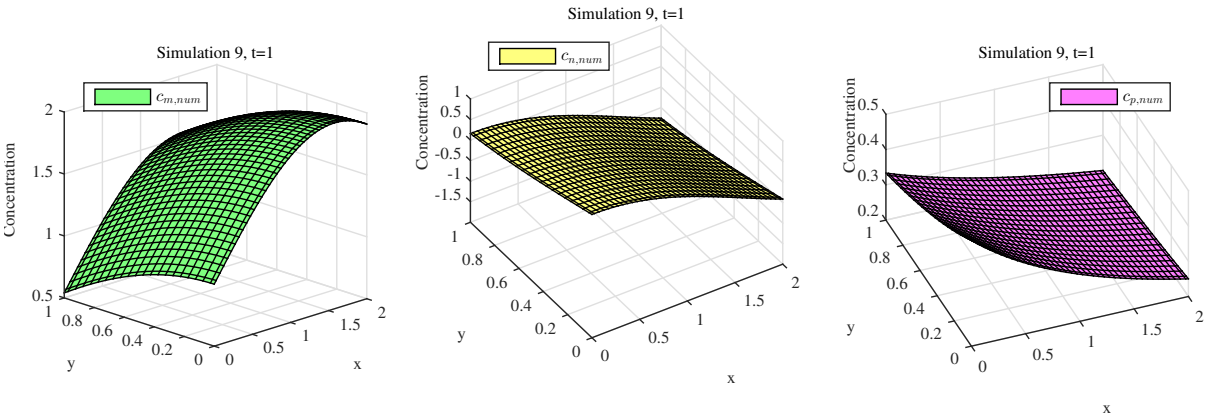

Figure 4.2.5 Concentration profiles for the analytic validation of the transport model in 2D. The size partitions are dx=dy=0.05 and dt=0.025.

4.2.6.2 Benchmark simulation

We test our algorithm against an experiment made by Hendry et al. 1997 and numerical modeled by Kim 2006. In their experiments, bacteria were introduced into the column during t_0 =38.4 hours in order to examine the transport and sorption behavior of *Klebsiella oxytoca*. The following initial and boundary conditions were used in the experiment

$$C_b(x,y,0) = \sigma_1(x,y,0) = \sigma_2(x,y,0) = 0 \quad \mathbf{n}\cdot\nabla C_b(L,y,t) = \mathbf{n}\cdot\nabla C_b(x,0,t) = \mathbf{n}\cdot\nabla C_b(x,W,t) = 0$$

$$\mathbf{n}\cdot(-D_b\nabla C_b(0,y,t) + \mathbf{u}_w C_b(0,y,t)) = \begin{cases} u_w C_{b0} & 0 < t \le t_0 \\ 0 & t > t_0 \end{cases}$$

The model parameters used in the numerical experiment are given in Table 4.2.5.

Table 4.2.5 Model parameters used in the benchmark validation of the transport model in 2D.

Parameter	Value	Parameter	Value	Parameter	Value
C_{b0}	4.32 mg·l^{-1}	v_g	1.61×10^{-5} cm·s^{-1}	g_1	0
L	40 cm	ρ_b	1.085×10^{6} mg·l^{-1}	d_1	0
W	5 cm	k_1	2.28×10^{-5} s^{-1}	ϕ_0	0.4
u_w	2.17×10^{-4} cm·s^{-1}	k_2	3.56×10^{-7} s^{-1}		
$\alpha_{b,T}$	0.27 cm	k_3	1.72×10^{-6} s^{-1}		

For the numerical experiment, we consider a partition of the domain in 82 parts on the horizontal axis, 12 parts on the vertical axis and time intervals of dt=.00009. Fig. 4.2.6 shows the relative bacteria concentration in the end of the column at different times. We observe that after approximately 30 hours of bacteria injection, it is finally observed throughout the whole column. Because we stop injecting bacteria after 38.4 hours, there is a maximum relative bacteria concentration of 10^{-2} and after, the concentration decreases until it reaches a relative concentration of 5×10^{-3} approximately. This behavior is due to the attachment, detachment, growth and death of bacteria. Comparison with the simulation results published in Kim 2006 and Li et al. 2011 indicated the same behavior.

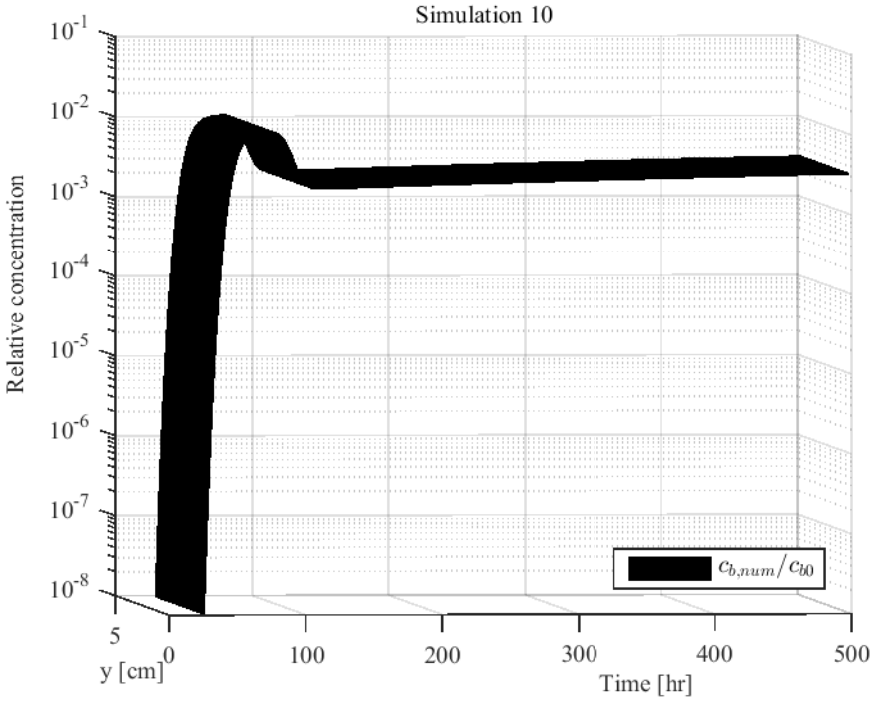

Figure 4.2.6 Concentration profile for the benchmark validation of the transport model in 2D. We show the relative bacteria concentration in the end of the column at different times.

Chapter 5

The effects of MEOR including the oil-water interfacial area

Following all previous work, we can finally perform numerical experiments to study the effects of MEOR considering the oil-water interfacial area. In order to formulate the two-phase flow model with transport equations including bioclogging and interfacial area, we considered the next works: Li et al. 2011 (Transport equations), Clement et al. 1996 and Kim 2006 (bioclogging), Niessner and Hassanizadeh 2008a and Joekar-Niasar and Hassanizadeh 2012 (interfacial area), Nielsen et al. 2010 (reduction of interfacial area) and Li et al. 2007 (reduction of residual oil saturation). In each of these texts, they considered different experimental conditions, having their respective values of parameterizations. The best way to validate our model would be to consider just one experiment in the laboratory, where most of these parameters are estimated. However, we could not find such an experiment in the current literature where they included transport equations, interfacial area and bioclogging. Therefore, when we ran the program using those parameters, it resulted in unreliable scenarios. We then looked for new parameters in order to have a more realistic study case.

In Chapter 2 we introduced a power-law for the interfacial area parameterization $a_{wn} = (s_w, p_c)$ (2.22). In Joekar-Niasar and Hassanizadeh 2012, after fitting the alpha parameters to some experimental data, they obtained $\alpha_1 = 6.462$, $\alpha_2 = 3.057 \times 10^{-12}$, $\alpha_3 = 1.244$ and $\alpha_4 = -0.963$, leading to the approach $s_w^{\alpha_2} \approx 1$. When we consider the previous remarks, the interfacial area expression that we use for the numerical experiments becomes

$$a_{wn}(s_w, p_c) = \alpha_1 (1 - s_w)^{\alpha_3} p_c^{\alpha_4} \tag{5.1}$$

For modeling that biosurfactants are mainly living at the oil-water interface (Kosaric and Varder-Sukan 2015), we introduce a reaction rate of a Monod form in the maximum specific biomass production rate coefficient in order to have a greater biosurfactant concentration in the zones with large interfacial area and null biosurfactant production in the zones with no-interfacial area

$$\mu_{\mathrm{p,max}} = \mu_{\mathrm{pa,max}} \frac{a_{wn}}{K_a + a_{wn}} \tag{5.2}$$

where K_a is a constant with unities [1/m].

We consider that all bioproducts correspond to biosurfactants. In Chapter 2 we mentioned that biosurfactants lower the interfacial tension between water and oil, leading to modification of the residual oil saturation. Regarding the interfacial tension expression (2.34), we choose the parameters from Nielsen et al. 2010. For the residual oil saturation relation (2.36), we consider the following values $s_{or}^{\max} = 0.3$,

$s_{or}^{\min} = 0.08$, $T_1 = 4 \times 10^4$ and $T_2 = 4.5$. Fig. 5.0.7 shows the profiles for the interfacial tension, capillary number and residual oil saturation using the parameters in Table 5.1.3.

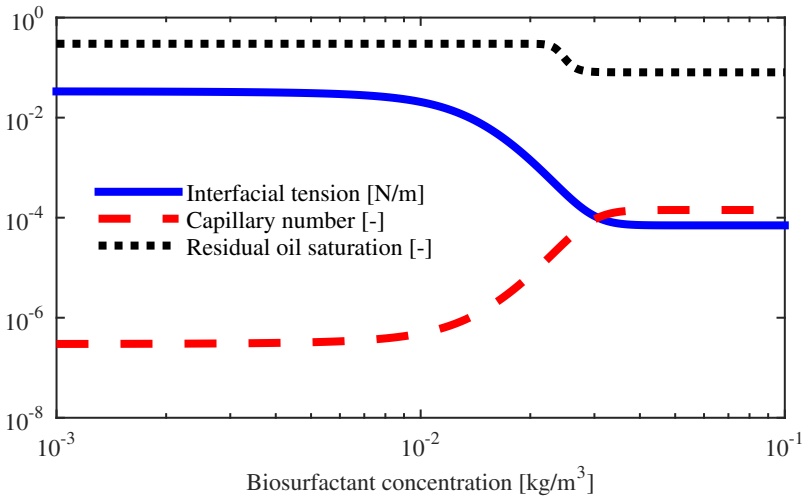

Figure 5.0.7 Interfacial tension, capillary number and residual oil saturation profiles. For the capillary number, we considering a constant water velocity of $2 \times 10^{-5}\ m/s$. We noticed that for these parameter values, the interfacial tension decreases after a biosurfactant concentration of $10^{-2}\ kg/m^3$ and the residual oil saturation decreases from $1 \times 10^{-2}\ kg/m^3$ to $2 \times 10^{-2}\ kg/m^3$.

5.1 Numerical experiments and sensitivity analysis

We consider a porous medium of length $L = 1$ m. We inject water, bacteria and nutrients into the left boundary and oil, water, bacteria, nutrients and biosurfactants flow out through the right boundary. For the water and oil pressures, we take the same conditions as in Li et al. 2011: $p_w(x,0) = 0.981$ kPa and $p_n(x,0) = 9.417$ kPa; leading to an average pressure of $p(x,0) = 5.199$ kPa and initial capillary pressure of $p_c(x,0) = p_n(x,0) - p_w(x,0) = 8.436$ kPa. On the left boundary, we have a flux boundary condition while on the right boundary we consider a constant pressure of 5.199 kPa. We take the same capillary pressure and relative permeability expressions as in Niessner and Hassanizadeh 2008a, corresponding to the Brooks-Corey parameterizations. In order to have the same initial water saturation on the right boundary $s_w(L,0) = 0.2446$, we take $\lambda = 2.129$. In numerical experiments, it is common to consider the same value for the initial residual oil saturation along the porous medium (Nielsen et al. 2010, Li et al. 2011). For studying other scenarios, we consider a porous medium where the residual oil saturation is greater in the opposite side where the water injection occurs. Then, we consider a reservoir with residual oil saturation as a linear function of the position, having on the left boundary a minimum residual oil saturation $s_{or}^{\min} = 0.08$ and on the right boundary a maximum residual oil saturation $s_{or}^{\max} = 0.3$. Therefore, the left boundary condition for the water saturation is $s_w(0,t) = 0.92$. Regarding the right boundary condition for the water saturation, we consider a Neumann condition with zero value. We choose the value for the initial interfacial area evaluating $a_{wn}(x,0) = a_{wn}(s_w(x,0), p_c(s_w(x,0)))$, analogously for the left boundary $a_{wn}(0,t) = a_{wn}(s_w(0,t), p_c(s_w(0,t)))$. We consider that there is neither bacteria nor nutrients initially in the porous media and we inject them on the left boundary. We also consider a no-flux boundary condition for the biosurfactant concentration on the left boundary.

Table 5.1.1 Initial and boundary conditions for the 1-D numerical experiments.

Initial	Left boundary	Right boundary
$p(x,0) = 5199$ Pa	$\mathbf{n} \cdot \mathbf{u}_\Sigma(0,t) = -2.78 \times 10^{-5}$m/s	$p(L,t) = 5199$ Pa
$s_w(x,0) = s_{wi} + (1 - s_{or} - s_{wi})\frac{p_e}{p_c}^\lambda$	$s_w(0,t) = 0.92$	$\mathbf{n} \cdot \nabla s_w(L,t) = 0$
$a_{wn}(x,0) = 452.07\ /m$	$a_{wn}(0,t) = 81.89\ /m$	$\mathbf{n} \cdot \nabla a_{wn}(L,t) = 0$
$C_b(x,y,0) = 0$	$C_b(0,t) = 0.5\ kg/m^3$	$\mathbf{n} \cdot \nabla C_b(L,t) = 0$
$C_n(x,y,0) = 0$	$C_n(0,t) = 0.2\ kg/m^3$	$\mathbf{n} \cdot \nabla C_n(L,t) = 0$
$C_p(x,y,0) = 0$	$\mathbf{n} \cdot (-\phi s_w D_p \nabla C_p(0,t) + \mathbf{u}_w C_p(0,t)) = 0$	$\mathbf{n} \cdot \nabla C_p(L,t) = 0$

Fig. 5.1.1 shows the initial saturation distributions for our numerical experiments.

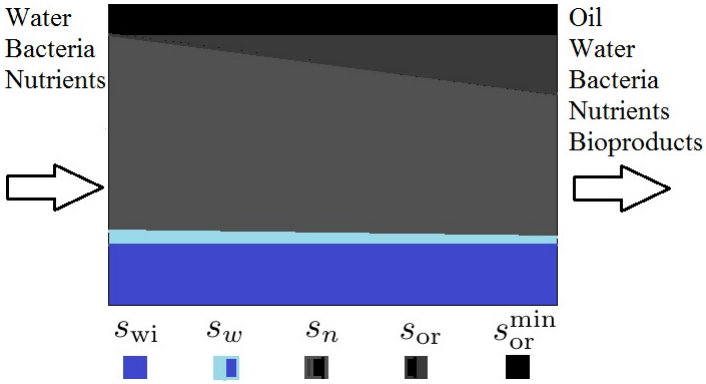

Figure 5.1.1 Initial saturation distributions for the parametric studies in 1-D cores. Our main goal it is to extract the most oil possible $(s_n - s_{or}^{\min})$. In our studies we consider a linear decreasing distribution of residual oil saturation.

After setting the values of the parameters, initial and boundary conditions, we perform numerical tests. We also do a sensitivity analysis in order to identify the critical parameters involved. In Kim 2006 he studied the effects on bioclogging for different injected bacterial concentrations C_b, different reversible attachment rate coefficients k_1, different detachment rate coefficients k_2, different irreversible attachment rate coefficients k_3 and different growth rate coefficients g_1. In Li et al. 2011, they did a similar sensitivity analysis but included the transport equations. Regarding the interfacial area, in El-Amin et al. 2015 they did numerical experiments changing the parameters α_1, α_3 and α_4 in the interfacial area expression $a_{wn}(s_w, p_c)$,however, they just considered the two-phase flow transport equations. About the interfacial area permeability k_{wn}, we could not find studies where they show a sensitivity analysis. Then, in this thesis we focus on the next study cases

- ◇ Reference case. We study the evolution in time of the pressure, saturation, interfacial area, capillary pressure, residual oil saturation, porosity, permeability ratio, bacterial, nutrient and biosurfactant concentrations and oil recovery. The aim of this study is to better understand the influence of the different variables in all modeled processes.

- ◇ Case I. We compare the different profiles until the final time T=10 hr, for different values of k_{wn}. The objective of this sensitivity analysis is to determine the impact of the parameter k_{wn} in the oil recovery. In the literature, we find values of interfacial permeability from $10^{-5}\ m^3/s$ (El-Amin et al. 2015) to $10^{-17}\ m^3/s$ (Niessner and Hassanizadeh 2008a). We set $k_{wn} = 10^{-7}\ m^3/s$ in the reference case.

- ◇ Case II. We test with different values of K_a. This parameter changes the biosurfactant production, having the property of $\mu_{\text{p,max}} = \frac{1}{2}\mu_{\text{pa,max}}$ when $a_{wn} = K_a$. Initially the interfacial area has a value of $a_{wn} = 452.07\ \frac{1}{m}$, thus in the reference case we set $K_a = 250\ \frac{1}{m}$. In order to perform numerical experiments neglecting the interfacial area influence on the biosurfactant production, we can set $K_a = 0$.

- ◇ Case III. The parameter α_1 in the interfacial area parameterization $a_{wn} = \alpha_1(1-s_w)^{\alpha_3} p_c^{\alpha_4}$ influences the magnitude of the interfacial area giving greater values of interfacial area for greater values of α_1. In the literature we find interfacial area values between $10\ \frac{1}{m}$ (Joekar-Niasar and Hassanizadeh 2012) to $1000\ \frac{1}{m}$ (El-Amin et al. 2015). We make a sensitivity analysis of this parameter in this range.

- ◇ Case IV. The parameter α_3 in the interfacial area parameterization $a_{wn} = \alpha_1(1 - s_w)^{\alpha_3} p_c^{\alpha_4}$ gives the dependence on the water saturation. For solving the pressure and saturation equations, we have to calculate the derivatives of $p_c(s_w, a_{wn})$ with respect to s_w and a_{wn}. Therefore, we expect different results in the pressure and saturation profiles.

- ◇ Case V. The parameter α_4 in the interfacial area parameterization $a_{wn} = \alpha_1(1-s_w)^{\alpha_3} p_c^{\alpha_4}$ determines the dependence on the capillary pressure. Analogous to the previous case, the parameter α_4 affects the derivative values of the capillary pressure expression, so we make a sensitivity analysis in order to visualize the impact of this parameter.

Table 5.1.2 shows the different parameters we study in the numerical experiments.

Table 5.1.2 Simulation matrix. $\mu_{\text{p,max}} = \mu_{\text{pa,max}} \frac{a_{wn}}{K_a + a_{wn}}$ $\quad a_{wn}(s_w, p_c) = \alpha_1(1 - s_w)^{\alpha_3} p_c^{\alpha_4}$

Case	$k_{wn}\ \frac{m^3}{s}$	$K_a\ \frac{1}{m}$	α_1	α_3	α_4	Case	$k_{wn}\ \frac{m^3}{s}$	$K_a\ \frac{1}{m}$	α_1	α_3	α_4
Base	10^{-6}	250	6.462	1.244	-0.963						
I	10^{-6} $\frac{1}{2}10^{-7}$ 10^{-7} $\frac{1}{2}10^{-8}$ 10^{-8}	250	6.462	1.244	-0.963	IV	10^{-7}	250	6.462	0.9 1 1.244 1.5 2.5	-0.963
II	10^{-7}	10 100 250 500 1000	6.462	1.244	-0.963	V	10^{-7}	250	6.462	1.244	-0.5 -0.75 -0.963 -1 -1.3
III	10^{-7}	250	0.5 1 6.462 10 20	1.244	-0.963						

Table 5.1.3 summarizes the parameters we use in the numerical experiments.

Table 5.1.3 Model parameters used in the numerical experiments.

Parameter	Value	Parameter	Value
ϕ_0	0.4	μ_w	1×10^{-3} kg/(m · s)
k_0	0.94×10^{-12}m^2	μ_n	3.92×10^{-3} kg/(m · s)
p_e	2740 Pa	C	19/6
λ	2.129	C_n^*	0
K_a	250 $/m$	g	0
$g_{1\ \max}$	2×10^{-5}/s	$\mu_{p\ \max}$	5×10^{-6}/s
d_1	10^{-7}/s	v_g	0
k_1	2.28×10^{-4}/s	F_w	0
k_2	3.56×10^{-7}/s	F_n	0
k_3	1.72×10^{-6}/s	s_{wi}	0.2
$K_{b/n}$	10^{-5} kg/m^3	k_{wn}	10^{-7} m^3/s
$K_{p/n}$	1 kg/m^3	D_b^{eff}	1.5×10^{-9} m^2/s
$Y_{p/b}$	7.944	D_n^{eff}	1.5×10^{-9} m^2/s
$Y_{p/n}$	1.144	D_p^{eff}	1.5×10^{-9} m^2/s
Y_s	5×10^{-6}/s	ρ_w	1000 kg/m^3
$\alpha_{b,T}$	0.01 m	ρ_n	800 kg/m^3
$\alpha_{n,T}$	0.01 m	ρ_b	1600 kg/m^3
$\alpha_{p,T}$	0.01 m	α_1	6.462
l_1	$41 \times 1-^{-4}$	α_2	0
l_2	2	α_3	1.244
l_3	180	α_4	-0.963
T_1	4×10^4	s_{or}^{max}	0.3
T_2	4.5	s_{or}^{min}	0.08
σ_{Int}	3.37×10^{-2} N/m		

5.1.1 Reference case

When we performed the simulation using the parameters from Clement et al. 1996, Kim 2006, Li et al. 2007, Niessner and Hassanizadeh 2008a, Li et al. 2011, Nielsen et al. 2010 and Joekar-Niasar and Hassanizadeh 2012, it resulted in unreliable scenarios. Therefore, we looked for new parameters in order to have a reference case and analyze the results. In this section our model for MEOR is tested using the parameters in Table 5.1.3.

Fig. 5.1.2 shows the profiles for the average pressure, water saturation, interfacial area and capillary pressure. From the pressure profile, we observe that the pressure in the entry decreases over time, due to less pressure is needed after the water has displaced some oil in order to have the same flux. The saturation profiles shows how much water we have put inside the reservoir over time, displacing more oil at the beginning but after the water breakthrough, the recovery becomes slower. In respect to the interfacial area, we notice that it is increassing when s_w is decreasing. This is in accordance to the results from Joekar-Niasar and Hassanizadeh 2012. We also notice that the interfacial value decreases over time, which is the expected behavior due to the porous medium approaching a constant water saturation of 0.92 in the spatial distribution. Analyzing the capillary pressure expression, we observe that over time it presents an expected behavior where the capillary pressure is a decreasing function of the water saturation.

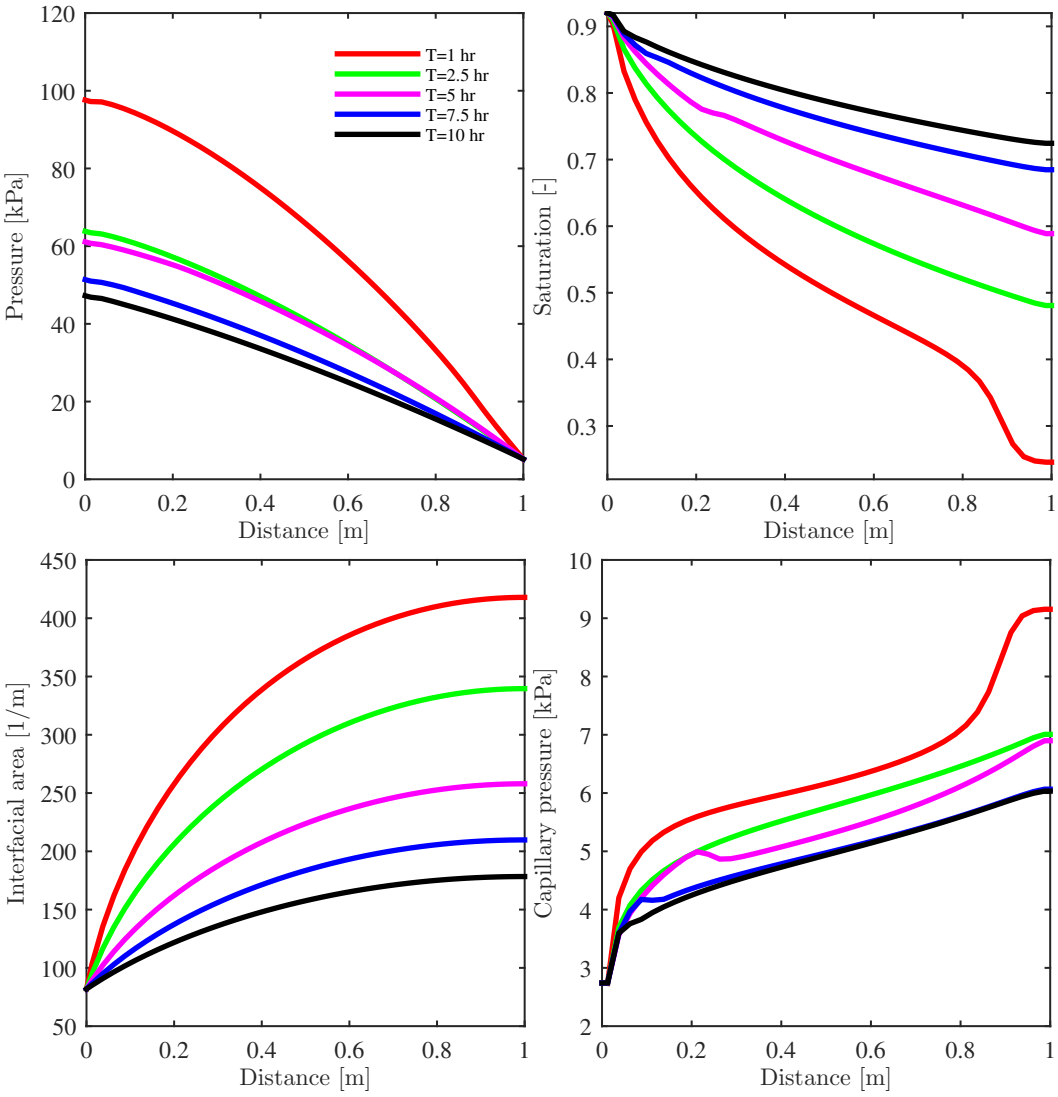

Figure 5.1.2 p, s_w, a_{wn} and p_c profiles in the reference case for different times.

Fig. 5.1.3 shows the different profiles of bacterial, nutrient and biosurfactant concentration and residual oil saturation. Regarding the bacterial concentration, we observe a decreasing behavior in the spatial distribution, due to bacteria death, attachment to the rock or escapement on the right boundary. Nutrients are transported by the water, being consumed by the bacteria in order to reproduce and produce biosurfactants, leading to a decrease in nutrient concentration. The biosurfactant concentration increases over time. The residual oil saturation remains the same for 3.5 hours, but after this the biosurfactant concentration is big enough to start the modification of the residual oil. After 8 hours, we notice that the residual oil saturation almost reaches its lowest value.

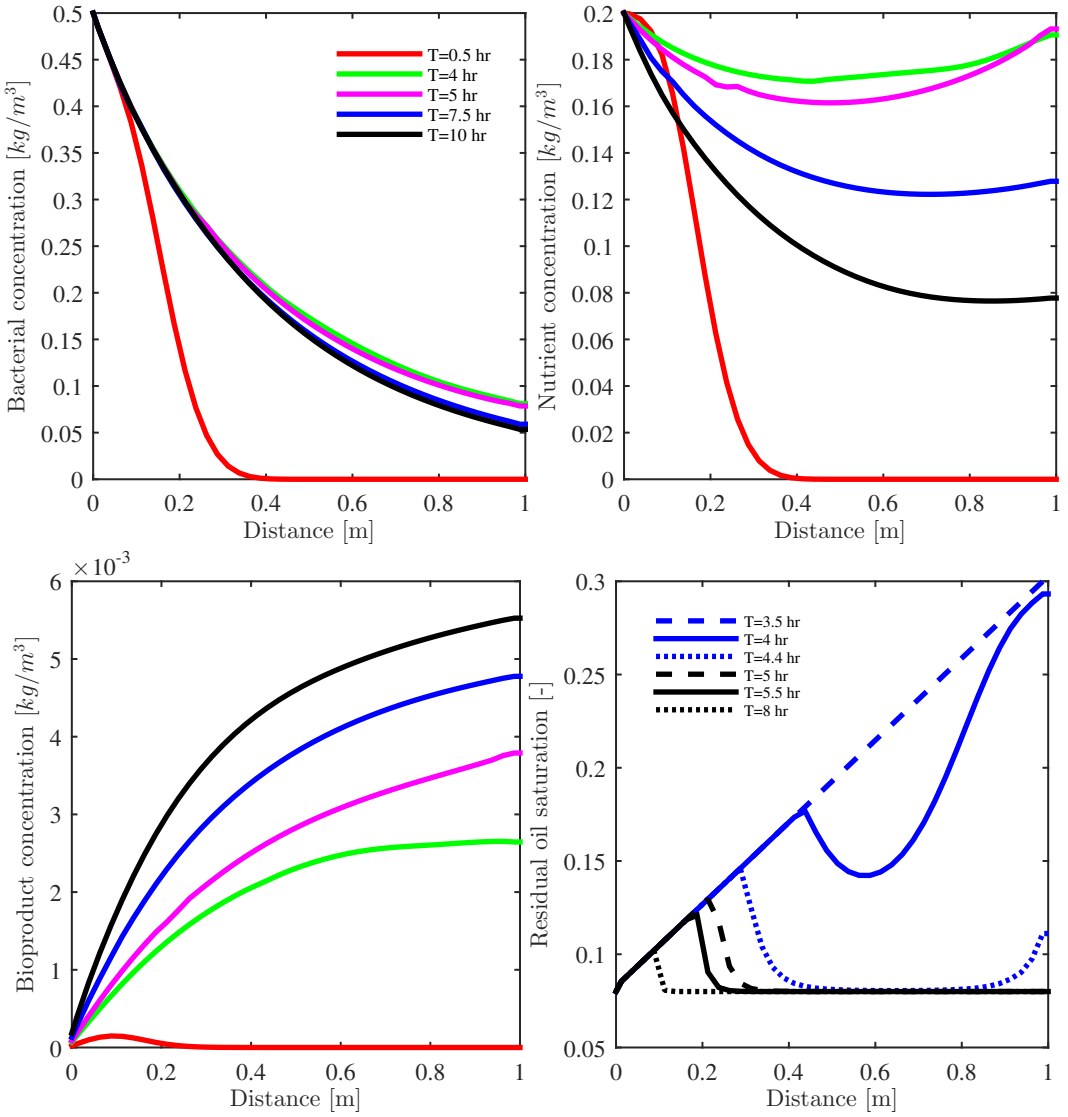

Figure 5.1.3 C_m, C_n, C_p and s_{or} profiles in the reference case.

Fig. 5.1.4 shows the profiles of the porosity and permeability ratio at different time values. Porosity and permeability changes are very small but still we observe the expected behavior of decreasing over time. We used the parameters in Li et al. 2011 for modeling the bioclogging, where they also showed small changes in bioclogging. We notice more bioclogging on the side where we inject the bacteria, which is in accordance with the experiments (Kim 2006).

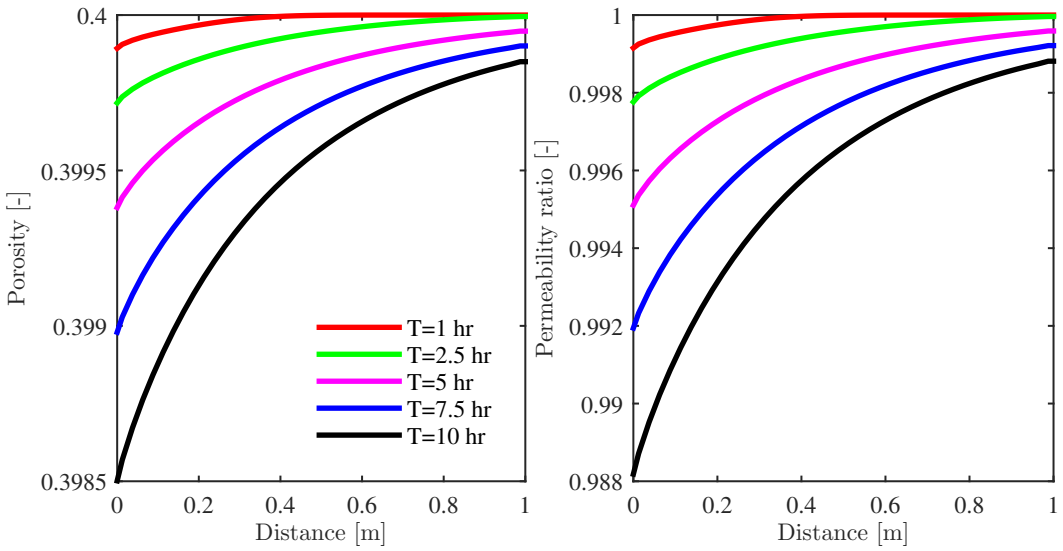

Figure 5.1.4 ϕ and k/k_0 profiles in the reference case.

Fig. 5.1.5 shows the oil recovery after 10 hours of water, bacteria and nutrient injection with and without interfacial area. We observe that after injecting 0.3 pore volume units of water, we reach the water breakthrough and injecting approximately one pore volume units of water, the biosurfactant starts to act, lowering the interfacial tension, extracting the residual oil saturation. Regarding the water flooding, we notice a slight difference between them, resulting in a greater oil recovery after the breakthrough when we consider the interfacial area. In relation with the effects on MEOR, due to the consideration of the maximum specific biomass production rate coefficient $\mu_{\mathrm{p,max}} = \mu_{\mathrm{p,max}} a_{wn}/(K_a + a_{wn})$ as a function of the interfacial area, we have less net production of biosurfactants in comparison to MEOR without interfacial area (in this numerical experiment we consider the same value of $\mu_{\mathrm{p,max}} = \mu_{\mathrm{pa,max}}$). However, after 2.5 pore volumes units of water injected, the oil recovery is the same.

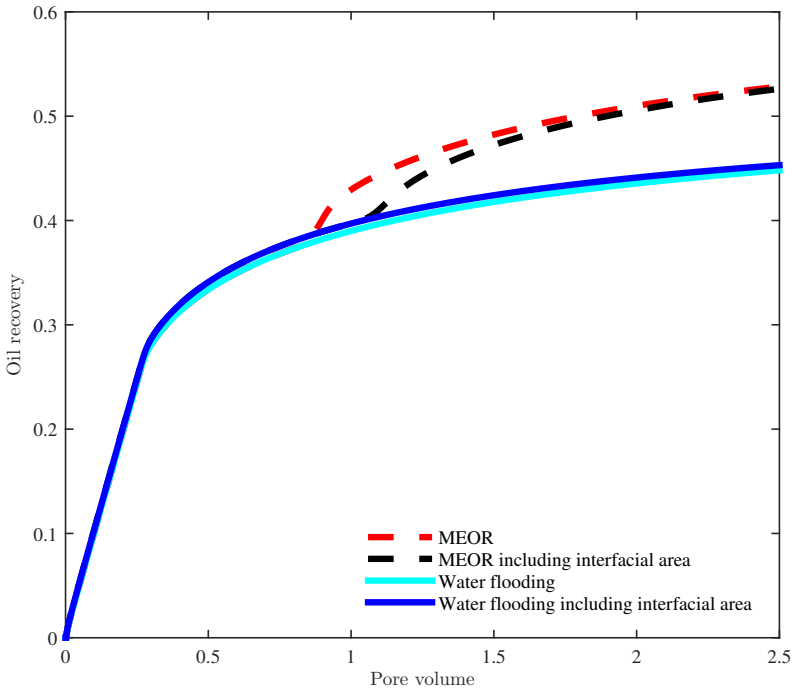

Figure 5.1.5 Comparison of the oil recovery due to biosurfactant action.

5.1.2 Case I: influence of the interfacial permeability k_{wn} in the oil recovery

In order to compare the influence of the interfacial permeability in the different profiles with respect to the reference case, we do a sensitivity analysis for k_{wn}, displaying the results of oil recovery and the different variables in Figs. 5.1.6 and 5.1.7 respectively.

From the interfacial area profile in Fig. 5.1.7, we have that for $k_{wn} = 10^{-6}\ m^3/s$ the interfacial area approximates to an uniform distribution, while for $k_{wn} = 10^{-8}\ m^3/s$ practically we have the same initial distribution of interfacial area. On the other hand, for the capillary pressure we have opposite behavior than the interfacial area, having greater values for $k_{wn} = 10^{-6}\ m^3/s$ and lower for $k_{wn} = 10^{-8}\ m^3/s$. The saturation profiles shows a slower displacement of oil for $k_{wn} = 10^{-6}\ m^3/s$ than $k_{wn} = 10^{-8}\ m^3/s$. In respect to the pressure profiles, we have just slight differences on the left pressure, but the five of them have similar values. From the same figure we observe that the bacterial and nutrient concentration profiles are practically the same, just few nutrient more were consumed for $k_{wn} = 10^{-8}\ m^3/s$, leading to a greater production of biosurfactants. Analyzing the residual oil saturation profiles after 5 hours, we notice that for $k_{wn} = 10^{-8}\ m^3/s$ the biosurfactants have recovered more oil than for $k_{wn} = 10^{-6}\ m^3/s$. This result is expected due to we add the interfacial area dependence to the maximum specific biomass production rate coefficient, giving a greater concentration in the zones with greater interfacial area values.

Fig. 5.1.6 shows the oil recovery in function of the pore volume injected to the reservoir. As mentioned before, we have better oil extraction for smaller values of k_{wn}.

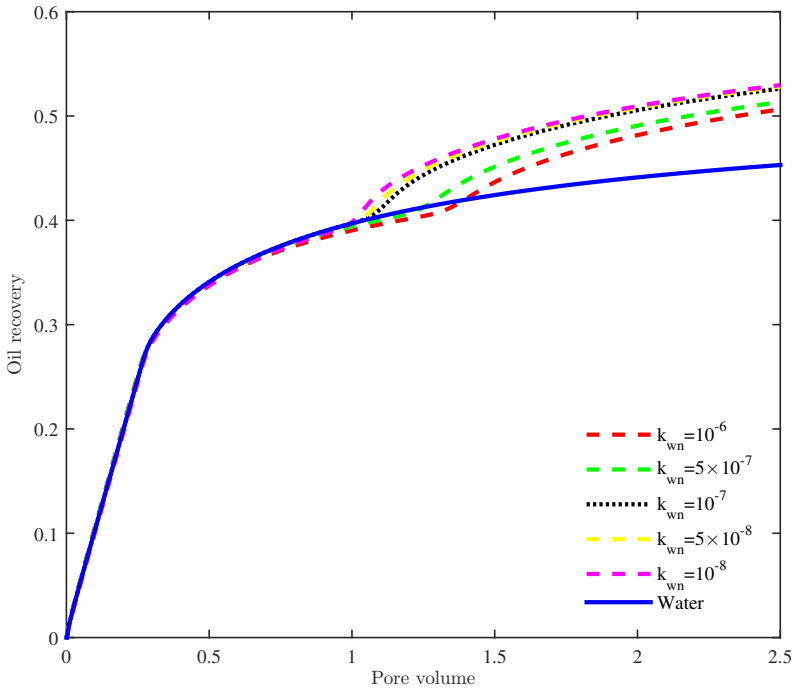

Figure 5.1.6 Comparison of the oil recovery after 10 hours in the parametric study of k_{wn}.

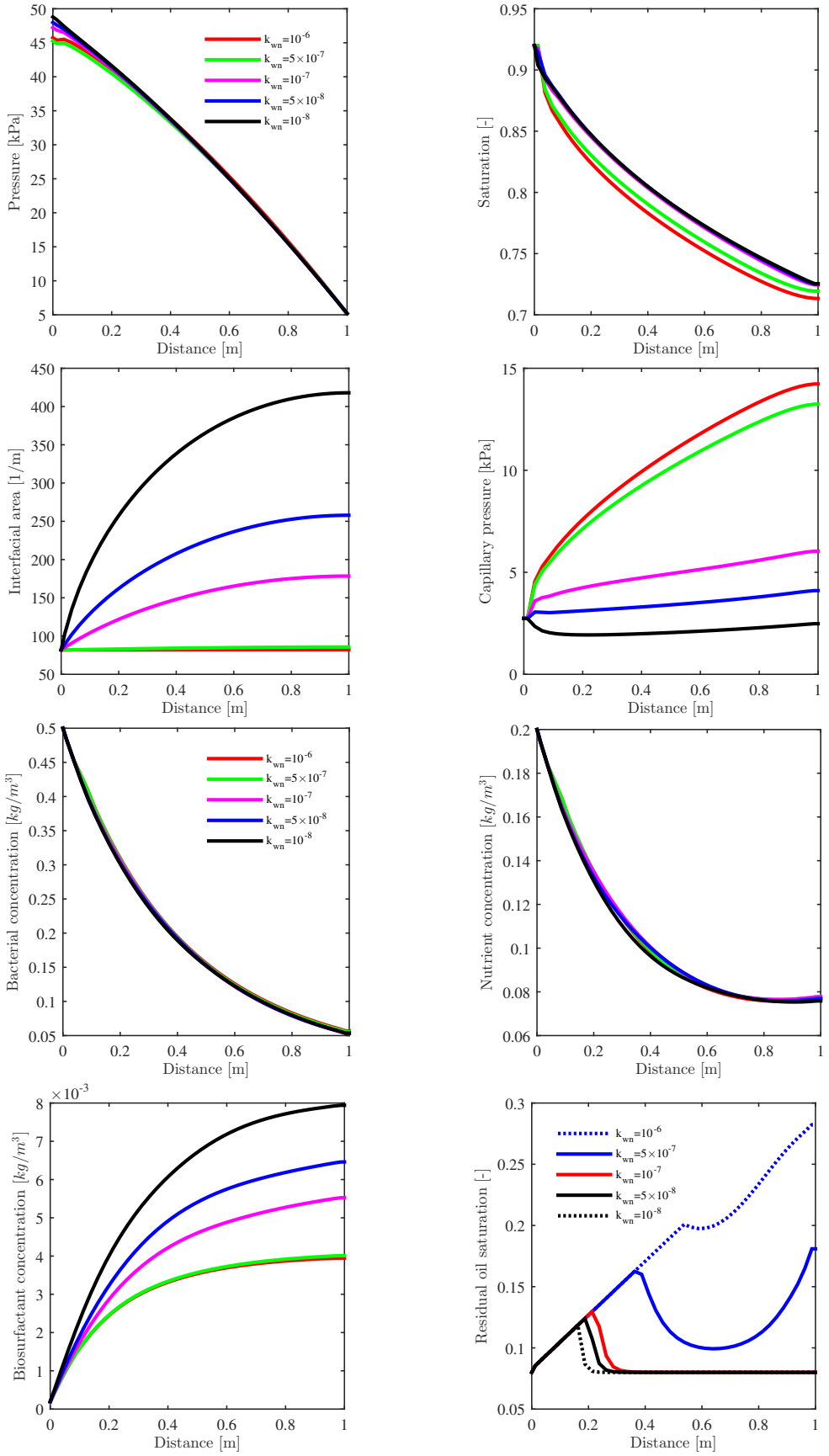

Figure 5.1.7 Profiles in the parametric study of k_{wn}, T=10 hr. For s_{or}, T=5 hr.

5.1.3 Case II: influence of the parameter K_a in the oil recovery

In this case we do a sensitivity analysis for K_a, displaying the results of oil recovery and the different variables in Figs. 5.1.8 and 5.1.9 respectively.

Due to the consideration of the dependence of the interfacial area in the form of the Monod-type model in the maximum specific biomass production rate coefficient, the biosurfactant production is less for greater values of K_a. When analyzing the saturation profile in Fig. 5.1.9, we notice a slower extraction of oil for $K_a = 1000$ and faster extraction for $K_a = 10$ as expected. We notice that the interfacial area profile is the same for the five cases but the capillary pressure changes, having a greater value for $K_a = 1000$. From the same figure we notice that the bacterial concentration profiles have very similar values. For the nutrient concentration, we have a greater consumption for small values of K_a, leading to a larger production of biosurfactants. When analyzing the residual oil saturation profiles after 7 hours, we notice that for $K_a = 10$ the biosurfactants have recovered more oil than for $K_a = 1000$. This result is expected due to the addition of the interfacial area dependence to the maximum specific biomass production rate coefficient, giving a greater concentration for small values of K_a. However, we notice that in our numerical experiment, even though there are three orders of magnitude between the largest and smallest K_a value, both of them have some residual oil recovered after 7 hours. This is due to the values for the parameters in the interfacial tension and residual oil saturation expressions, giving the residual oil saturation reduction in a small range of surfactant concentration, behavior from Fig. 5.0.7.

From Fig. 5.1.8 we have a sooner effect of biosurfactants for small values of K_a and a delayed effect for greater values of K_a. As studied in this case, the parameter K_a allows to modify the production rate of biosurfactants.

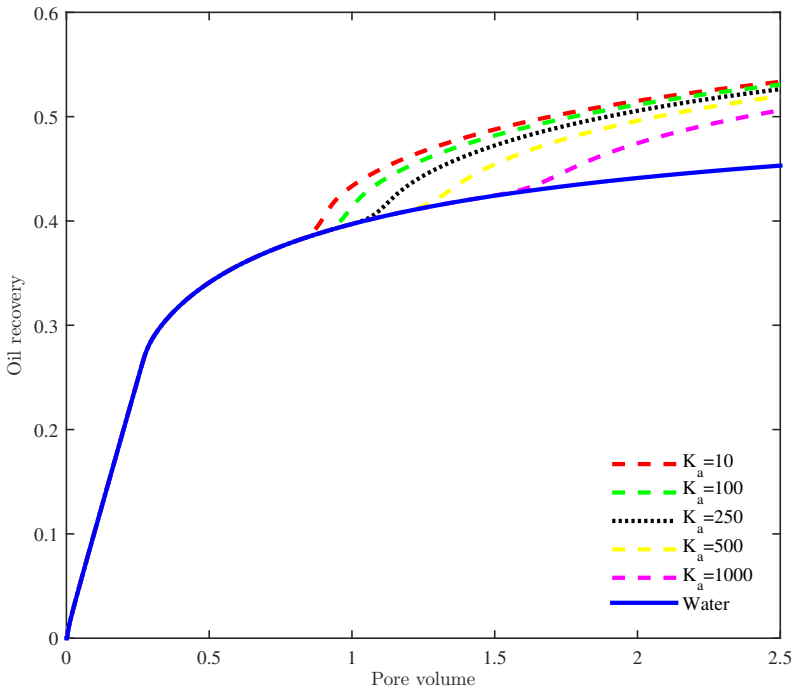

Figure 5.1.8 Comparison of the oil recovery after 10 hours in the parametric study of K_a.

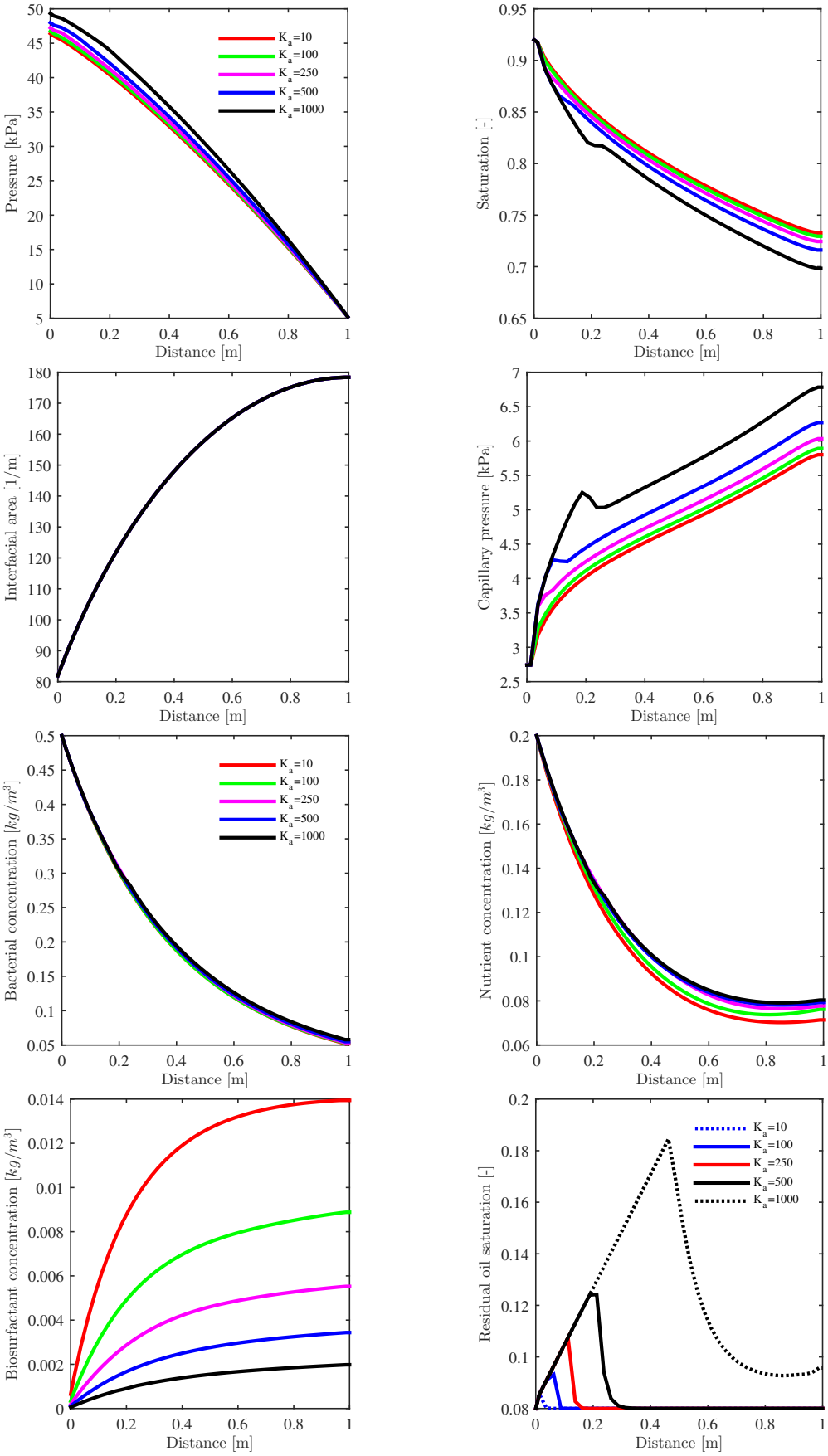

Figure 5.1.9 Profiles in the parametric study of K_a, T=10 hr. For s_{or}, T=7.

5.1.4 Case III: influence of the interfacial area parameter α_1 in the oil recovery

In this case we do a sensitivity analysis for α_1, displaying the results of oil recovery and the different variables in Figs. 5.1.10 and 5.1.11 respectively.

From the interfacial area and capillary pressure profiles in Fig. 5.1.11, we have greater values of interfacial area for larger α_1. We notice a greater extraction of oil for larger values of α_1, that is the expected behavior. From the same figure we notice a slight decrease in bacterial concentration for $\alpha_1 = 20$. We also observe lower nutrient concentration for this value of α_1, having greater biosurfactant production. From the residual oil saturation profile, we notice after 7 hours there is no reduction in residual oil saturation for $\alpha_1 = 0.5$ whereas for $\alpha_1 = 20$ we almost reduce all .

Fig. 5.1.10 shows the oil recovery for the different values of α_1. When $\alpha_1 = 0.5$, we observe that the biosurfactant action starts after 2 pore volume units of water injection. For α_1, the improvement in oil starts after 1.5 pore volume units of water injection. However, for the reference case, $\alpha_1 = 10$ and $\alpha_1 = 20$ the biosurfactant action starts after 1 pore volume unit of water injected. These results are also sensitive to the parameter K_a, which we studied in the previous section.

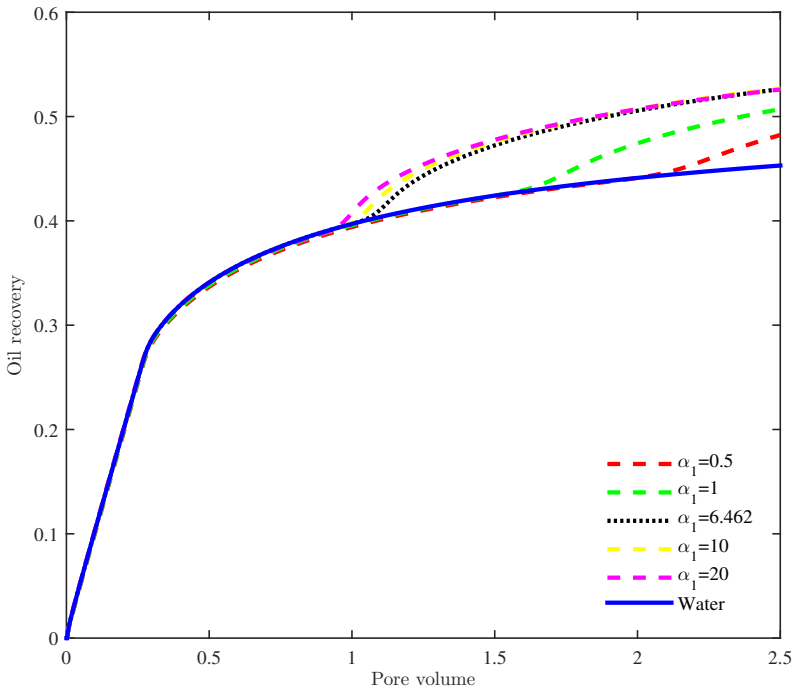

Figure 5.1.10 Comparison of the oil recovery after 10 hours in the parametric study of α_1.

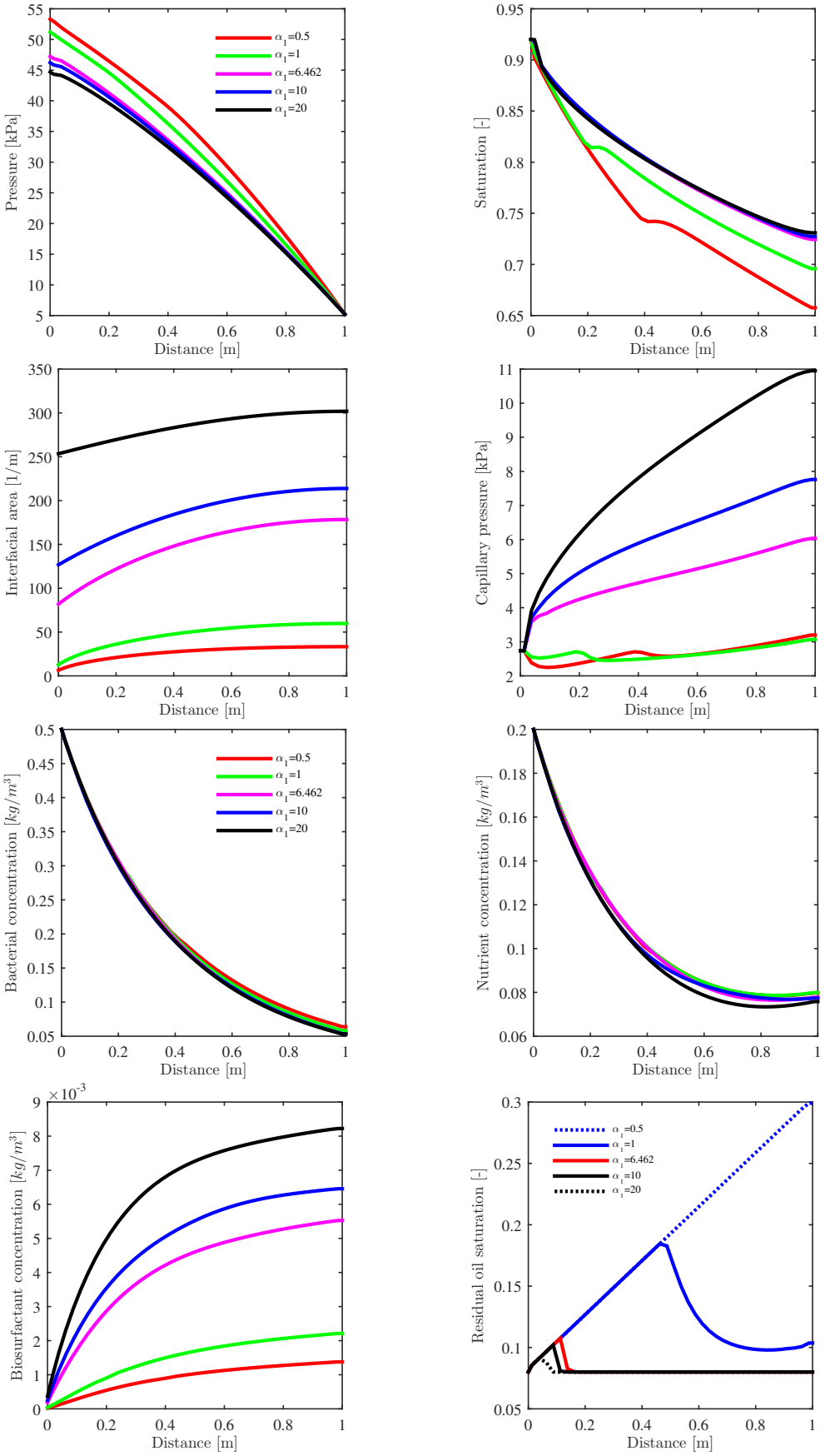

Figure 5.1.11 Profiles in the parametric study of α_1, T=10 hr. For s_{or}, T=7 hr.

5.1.5 Case IV: influence of the interfacial area parameter α_3 in the oil recovery

In this case we do a sensitivity analysis for α_3, displaying the results of oil recovery and the different variables in Figs. 5.1.12 and 5.1.13 respectively. The aim of this study is to determinate the influence of the parameter α_3 in the oil recovery.

Fig. 5.1.13 shows that the interfacial area is more sensitive to changes in the water saturation for greater values of α_3. This behavior is expected due to $(1 - s_w)^{\alpha_3}$ goes to 0 for greater values of α_3 than 1, giving a greater curvature. In the same figure, we have the different profiles for bacterial, nutrient and biosurfactant concentration and residual oil saturation for different values of α_3. We notice a greater biosurfactant production for $\alpha_3 = 0.9$, due to the interfacial area being greater for this value. Regarding the residual oil saturation profile, we have that after four hours of water injection, there is not residual oil recovered for $\alpha = 0.9$.

Analyzing Fig. 5.1.12, we notice that when we increase the value α_3 the biosurfactant action is delayed.

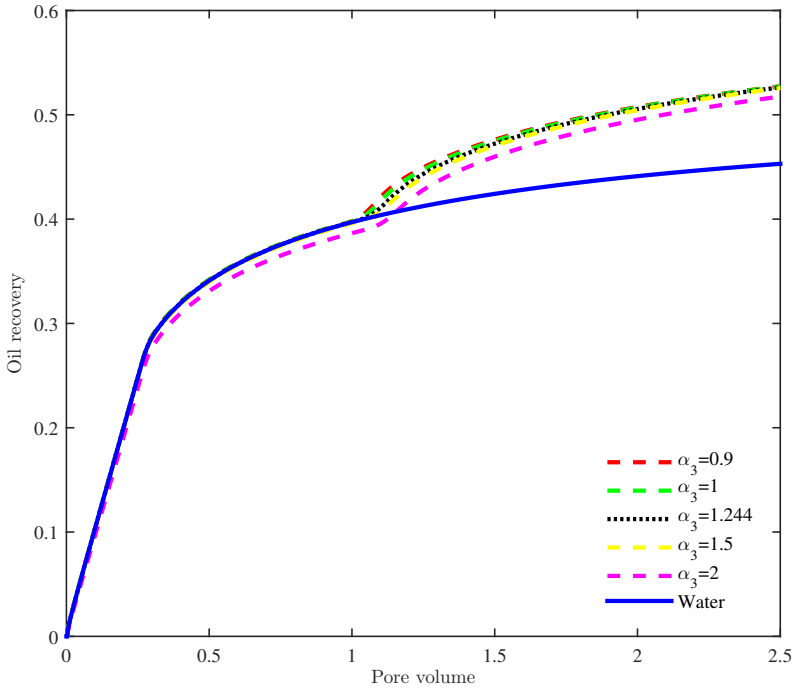

Figure 5.1.12 Comparison of the oil recovery after 10 hours in the parametric study of α_3.

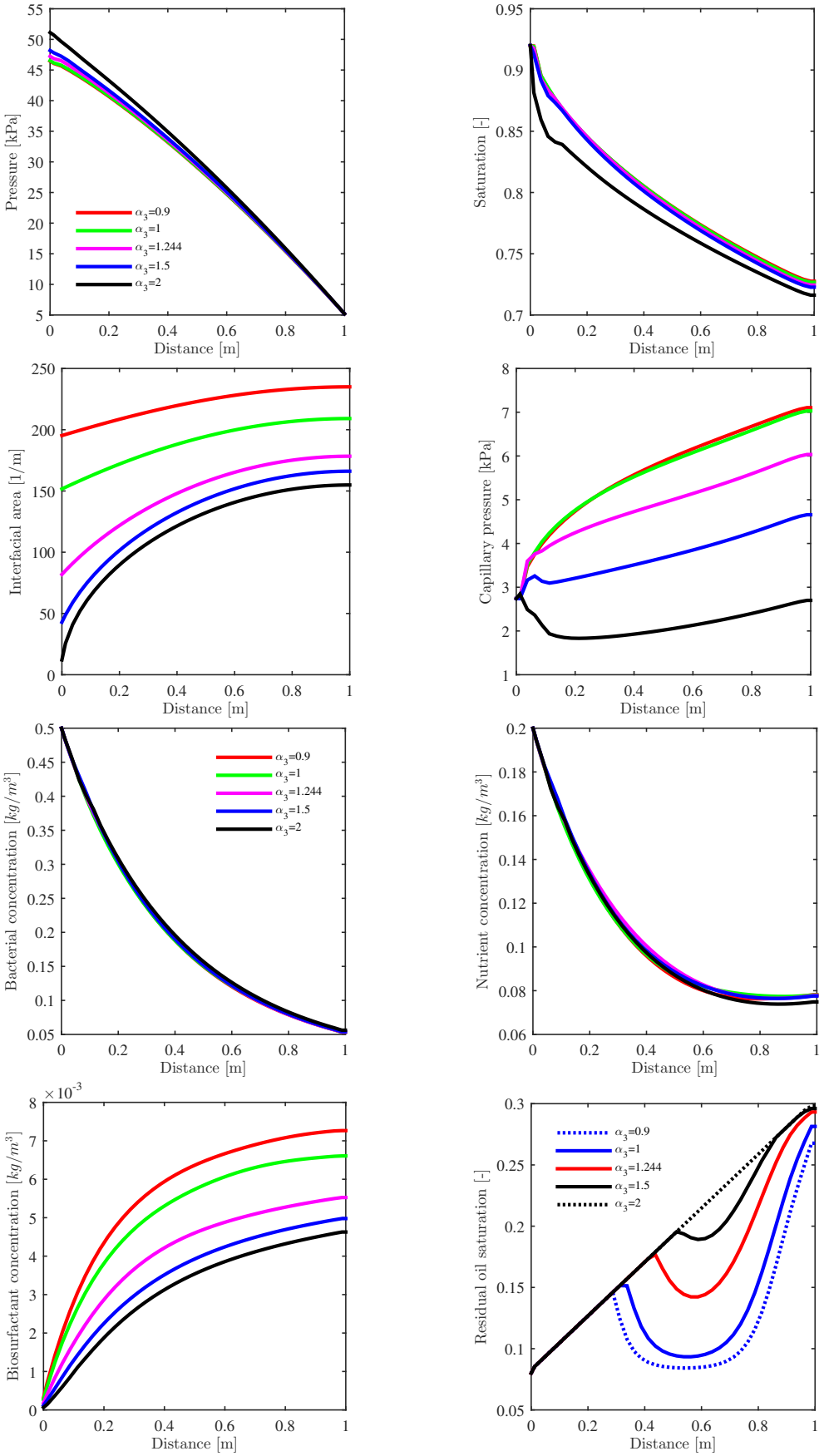

Figure 5.1.13 Profiles in the parametric study of α_3, T=10 hr. For s_{or}, T=4 hr.

5.1.6 Case V: influence of the interfacial area parameter α_4 in the oil recovery

In this case we do a sensitivity analysis for α_4, displaying the results of oil recovery and the different variables in Figs. 5.1.14 and 5.1.15 respectively.

Fig. 5.1.15 shows the different profiles after 10 hours for the average pressure, water saturation, interfacial area, capillary pressure, residual oil saturation, bacterial, nutrient and biosurfactant concentration, while changing the values of the parameter α_4 in the interfacial area parameterization. We observe a faster displacement of oil for $\alpha_4 = -1.3$. However, we notice in the interfacial area profiles that for $\alpha_4 = -1.3$ the interfacial area is practically constant even the water saturation is not, so in our numerical experiment this is not a physical value for the parameter α_4. From the same figure, we notice after 5 hours of injection we have not recovered residual oil for $\alpha_4 = -0.5$, but for -0.75 we start to recover it.

Fig. 5.1.14 shows the oil recovery for the different values of α_4. We notice that after four pore volumes injected to the reservoir, the oil extraction follows the same behavior.

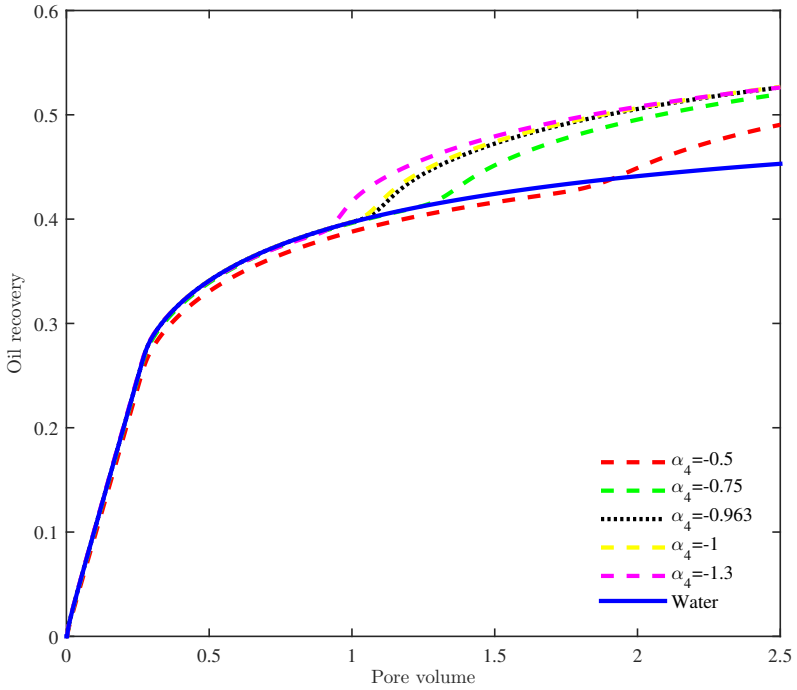

Figure 5.1.14 Comparison of the oil recovery after 10 hours in the parametric study of α_4.

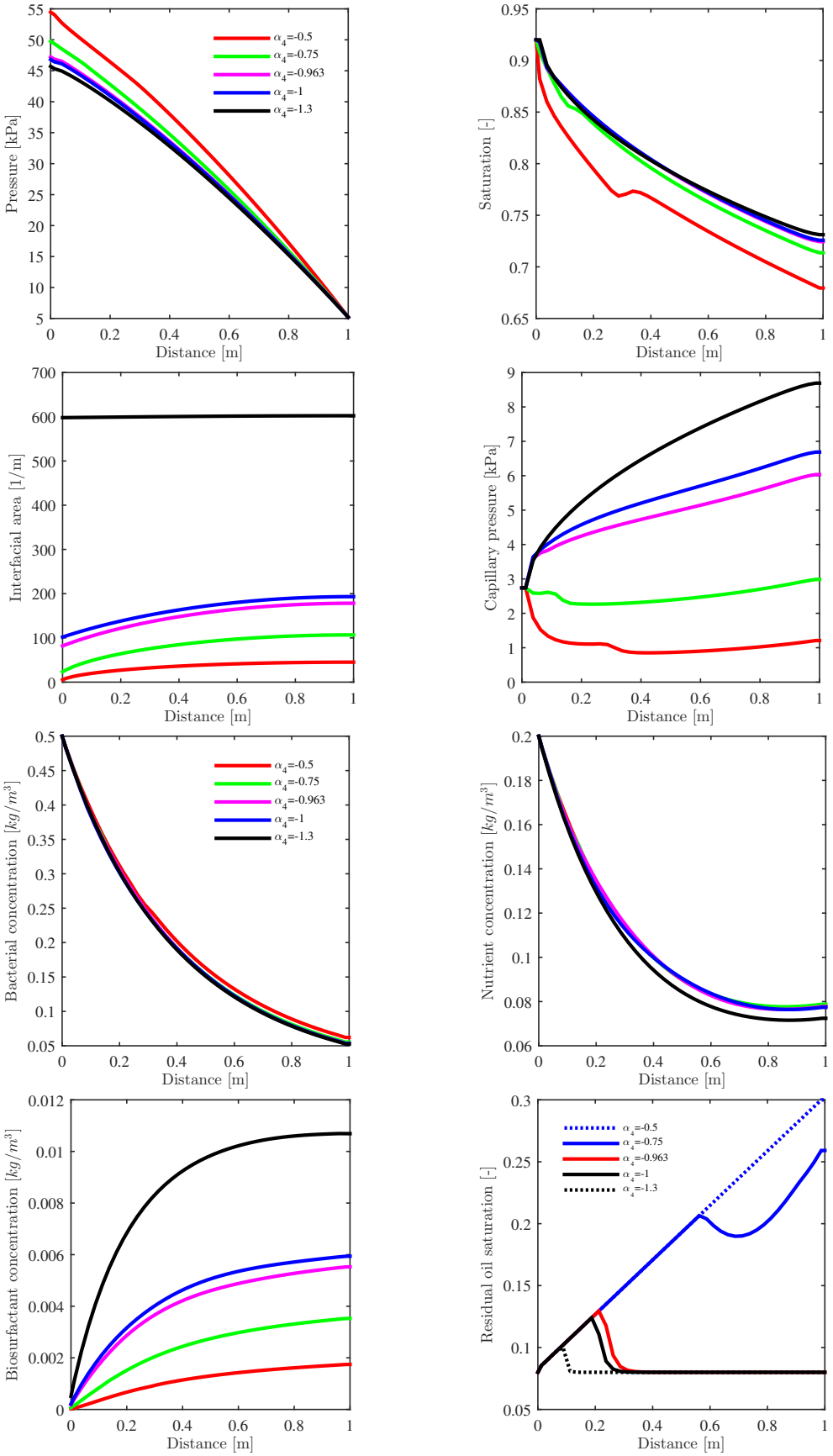

Figure 5.1.15 Profiles in the parametric study of α_4, T=10 hr. For s_{or}, T=5 hr.

5.2 Simulations in a porous medium with a thief zone

In the 2-D case, we study a porous medium with a thief zone. There are different definitions for the thief zones (Li et al. 2015); one of them given by Feng et al. 2010, who considers the thief zone as a high permeability layer with residual oil saturation. Similar studies has been done by Kou and Sun 2004 and Amundsen 2015, with a 2-D porous medium with same permeability values in the upper and lower parts but greater permeability value in the middle. However, due to the symmetry (gravity is not considered), we can just solve half of the domain. Fig. 5.2.1 shows this porous medium, coloring the different permeability zones.

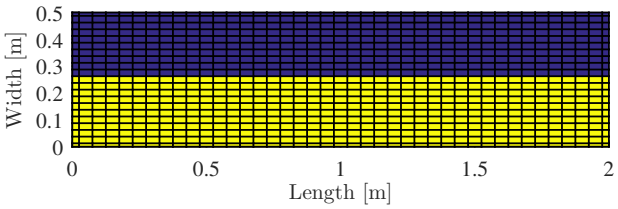

Figure 5.2.1 2-D porous medium with a thief zone. The upper half has a permeability of 2 mD, while the lower half has a permeability of 0.5 mD.

In the numerical experiments, we consider a porous medium with the same parameters, initial and boundary conditions to the 1-D case; the only difference are the values of the permeabilities. We inject water, bacteria and nutrients on the left side and we obtain oil, water, bacteria, nutrients and biosurfactants on the right side. We consider the top and bottom boundaries are closed, meaning that there is not flux through them. Table 5.2.1 shows the initial and boundary conditions used for this reservoir.

Table 5.2.1 Initial and boundary conditions for the 2-D numerical experiments.

Pressure	
$p(x,y,0) = 5199$ Pa	$p(L,y,t) = 5199$ Pa
$\mathbf{n}\cdot\mathbf{u}_\Sigma(x,W,t) = 0$	$\mathbf{n}\cdot\mathbf{u}_\Sigma(0,y,t) = -2.78\times10^{-5}$m/s
$\mathbf{n}\cdot\mathbf{u}_\Sigma(x,0,t) = 0$	
Saturation	
$s_w(x,y,0) = s_{wi} + (1-s_{or}-s_{wi})\frac{p_e}{p_c}^{\lambda}$	$\mathbf{n}\cdot\nabla s_w(L,y,t) = 0$
$\mathbf{n}\cdot\nabla s_w(x,W,t) = 0$	$s_w(0,y,t) = 0.92$
$\mathbf{n}\cdot\nabla s_w(x,0,t) = 0$	
Interfacial area	
$a_{wn}(x,y,0) = 452.07\ 1/m$	$\mathbf{n}\cdot\nabla a_{wn}(L,y,t) = 0$
$\mathbf{n}\cdot\nabla a_{wn}(x,W,t) = 0$	$a_{wn}(0,y,t) = 81.89\ 1/m$
$\mathbf{n}\cdot\nabla a_{wn}(x,0,t) = 0$	
Bacterial concentration	
$C_b(x,y,0) = 0$	$\mathbf{n}\cdot\nabla C_b(L,y,t) = 0$
$\mathbf{n}\cdot(-\phi s_w D_b\nabla C_b(x,W,t) + \mathbf{u}_w C_b(x,W,t)) = 0$	$C_b(0,y,t) = 0.5\ kg/m^3$
$\mathbf{n}\cdot(-\phi s_w D_b\nabla C_b(x,0,t) + \mathbf{u}_w C_b(x,0,t)) = 0$	
Nutrient concentration	
$C_n(x,y,0) = 0$	$\mathbf{n}\cdot\nabla C_n(L,y,t) = 0$
$\mathbf{n}\cdot(-\phi s_w D_n\nabla C_n(x,W,t) + \mathbf{u}_w C_n(x,W,t)) = 0$	$C_n(0,y,t) = 0.2\ kg/m^3$
$\mathbf{n}\cdot(-\phi s_w D_n\nabla C_n(x,0,t) + \mathbf{u}_w C_n(x,0,t)) = 0$	
Biosurfactant concentration	
$C_p(x,y,0) = 0$	$\mathbf{n}\cdot\nabla C_p(L,y,t) = 0$
$\mathbf{n}\cdot(-\phi s_w D_p\nabla C_p(x,W,t) + \mathbf{u}_w C_p(x,W,t)) = 0$	$\mathbf{n}\cdot(-\phi s_w D_p\nabla C_p(x,0,t) + \mathbf{u}_w C_p(x,0,t)) = 0$
$\mathbf{n}\cdot(-\phi s_w D_p\nabla C_p(0,y,t) + \mathbf{u}_w C_p(0,y,t)) = 0$	

5.2.1 Pressure, saturation, interfacial area and concentration distributions

We ran the numerical simulations until a final time of 10 hours. Intuitively, the results we expect is faster water flux in the zone with greater permeability value, leading to faster oil recovery in this zone. In this numerical experiment the upper permeability is 4 times bigger than the lower permeability, thus we expect a flux four times faster in the zone with large permeability. On the other hand, regarding the capillary pressure and interfacial area profiles, we expect to have greater values in the zones with lower water saturation.

Fig. 5.2.2 shows the pressure and saturation profiles after 5 and 10 hours. As we mentioned before, more oil has been displaced in the more permeable zone. In respect to the pressure profiles, we notice a slight difference on the left pressure values in order to keep the same flux in both zones.

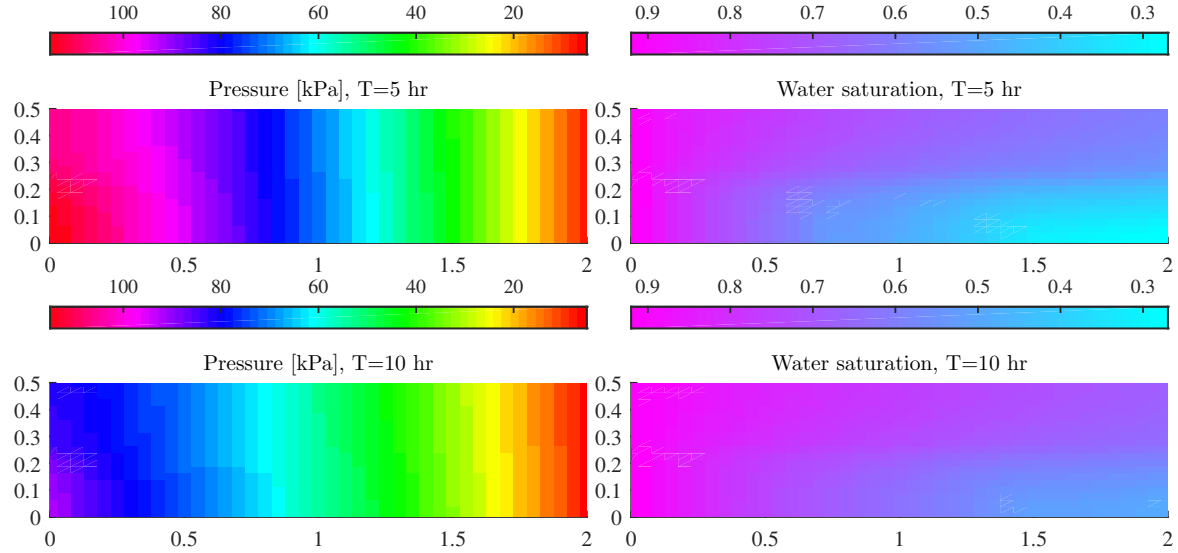

Figure 5.2.2 Pressure and saturation profiles in the reservoir with a thief zone.

Fig. 5.2.3 shows the capillary pressure and interfacial area profiles. After 10 hours we observe lower capillary pressure in the less permeable zone, in accordance with the standard behavior of greater interfacial area in zones with lower water saturation. Despite the interfacial area increases from left to right, we do not notice differences between both permeable zones. Therefore, we attribute this behavior to the rate of production of specific interfacial area expression E_{wn}.

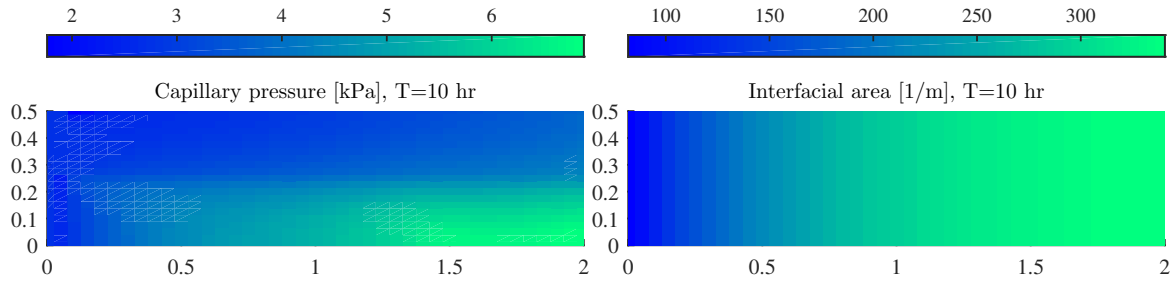

Figure 5.2.3 Capillary pressure and interfacial area profiles in the reservoir with a thief zone.

Fig. 5.2.4 shows the evolution in time for the bacteria and nutrients after 0.5, 1.5 and 2.5 hours. We notice that the bacteria is transported faster in the more permeable zone, but there is also a loss due to some bacteria attaching to the rock, dying or producing biosurfactants. For the nutrients, we observe that most of them are transported without being consumed by the bacteria. This behavior is due to the election of the coefficients Y_n and $Y_{p/n}$.

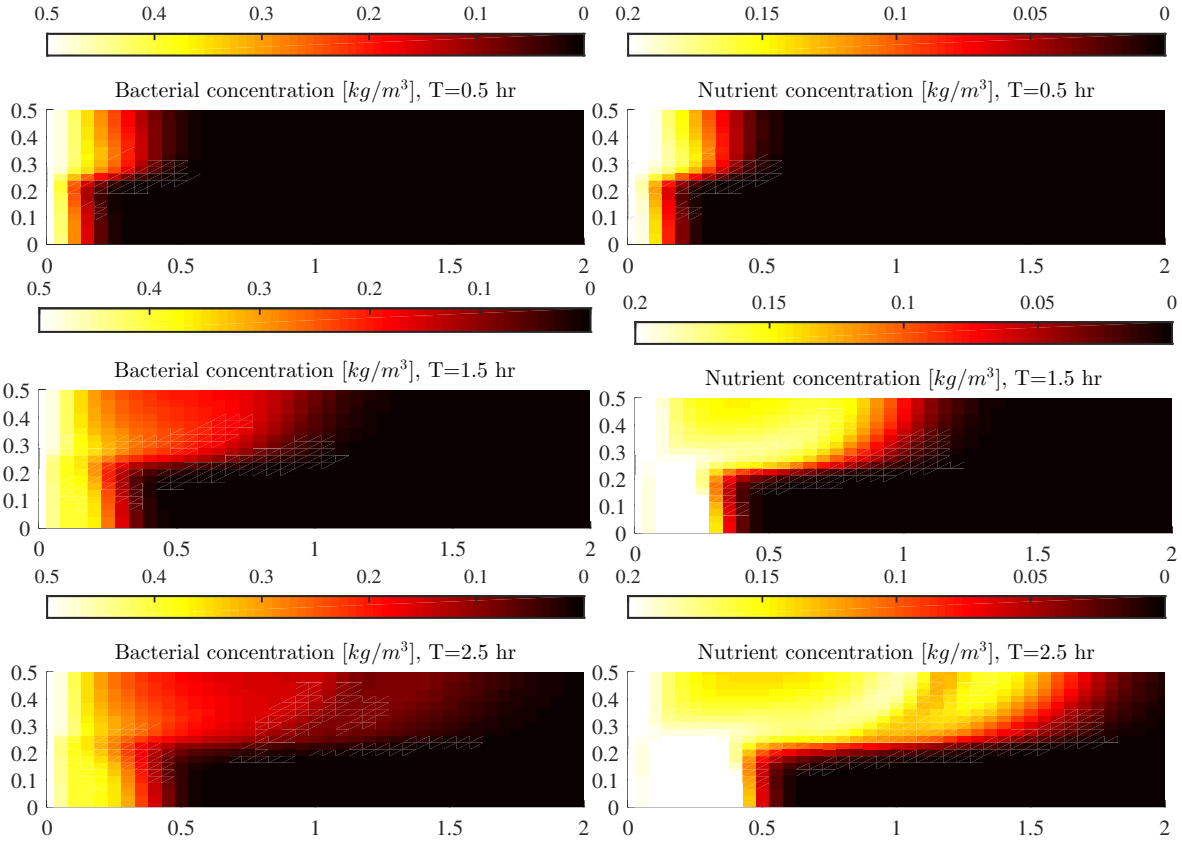

Figure 5.2.4 Bacterial and nutrient profiles in the reservoir with a thief zone.

Fig. 5.2.5 shows the biosurfactant and residual oil saturation profiles after 2, 4 and 6 hours of injection. In the first two hours, we observe that some residual oil has been already removed in both parts. After 6 hours, the oil in the thief region has already been removed. However, in the region with permeability 0.5 mD, the biosurfactants has not reached a sufficient concentration to lower the interfacial tension.

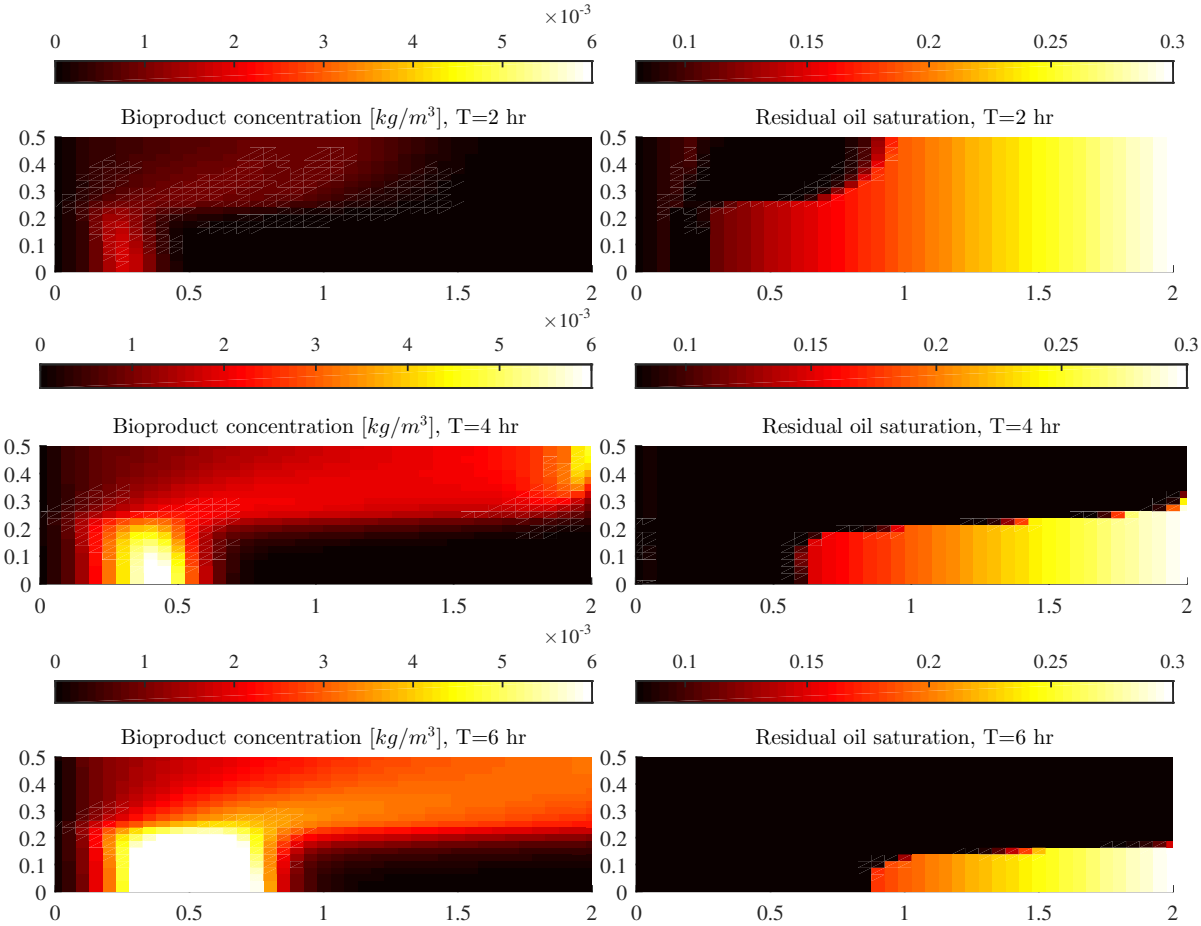

Figure 5.2.5 Biosurfactant and residual oil saturation profiles in the reservoir with a thief zone.

5.2.2 Bioclogging

In Chapter 2 we mentioned that MEOR has different applications in order to improve the oil recovery, one of them being to lock the paths where the water flows easily in order to reach another zone with oil.

Fig. 5.2.6 shows the porosity after 10 hours of injection. We notice in the thief zone a greater decrease of porosity than in the lower part. However, both porosity reductions are small, as a result of the parameters k_1, k_2, k_3, $g_{1,\max}$ and d_1.

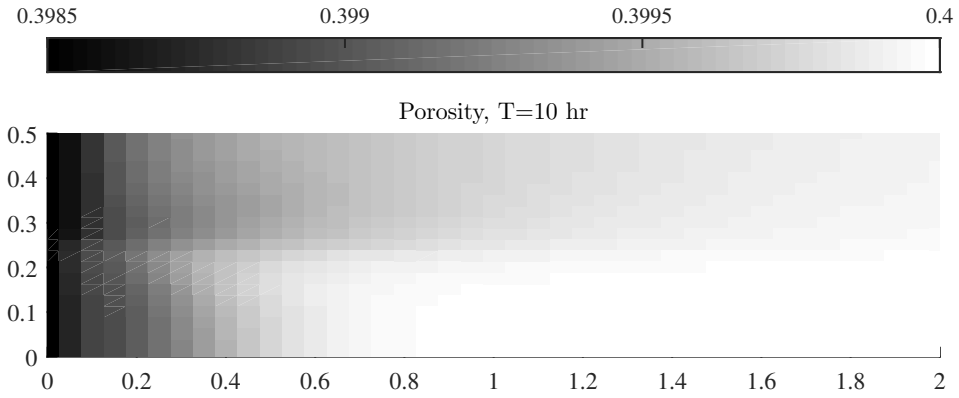

Figure 5.2.6 Porosity profile in the reservoir with a thief zone.

Fig. 5.2.7 shows the permeability ratio k/k_0 after 10 hours of injection. Because we use a model where the relation between permeability ratio and biomass-modified porosity ratio is given by the parameter C, we have similar results for the permeability ratio in the porous medium. We notice greater decrease of permeability in the thief zone.

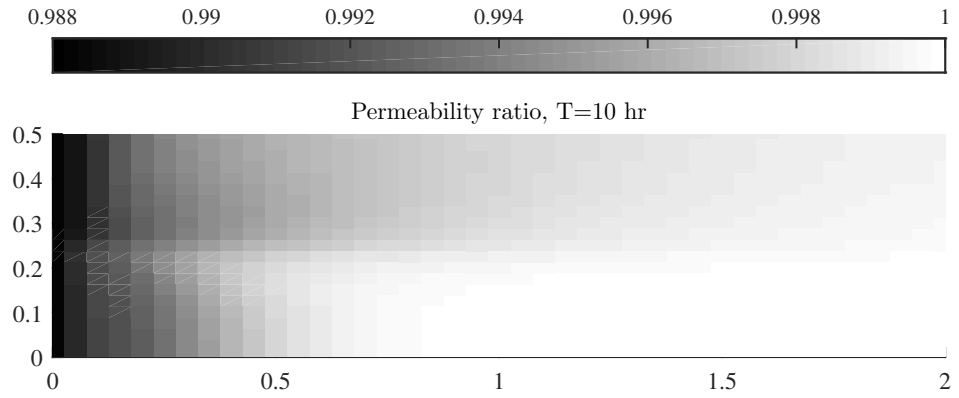

Figure 5.2.7 Permeability ratio profile in the reservoir with a thief zone.

5.2.3 Oil recovery

The main goal of MEOR it is to enhance the oil recovery using bacteria. In order to have a measure of the improvements in the oil extraction, we compute the oil recovery.

Fig. 5.2.8 shows the oil recovery as a function of the pore volume injected in the reservoir with a thief zone. We notice that 10 hours of water injection equals to 2.5 pore volumes. We observe that after injecting 0.8 pore volumes of water, the biosurfactant starts to lower the interfacial tension and we raise the oil production. In comparison with the oil extraction in the 1-D case in Fig. 5.1.5, the effects of the biosurfactants start after 1 pore volume unit of water injection. This difference in the oil extraction is due to the different permeability values.

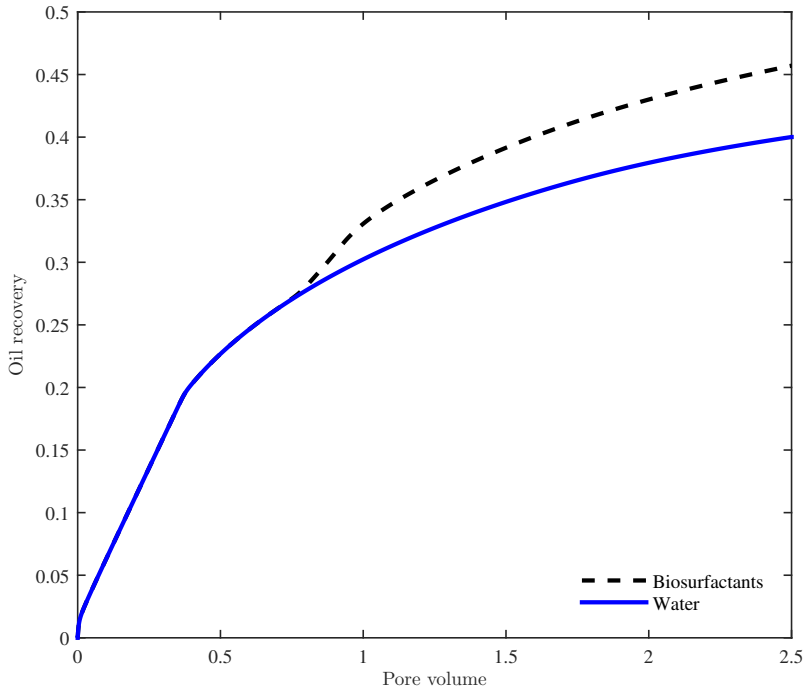

Figure 5.2.8 Comparison of the oil recovery due to biosurfactants in the reservoir with a thief zone.

All these results show that the program is adequate for modeling water flooding, transport of products, bioclogging and biosurfactant effects including the oil-water interfacial area.

Chapter 6

Conclusion

A new model for MEOR, which includes two-phase flow, bacteria, nutrient and biosurfactant transport and considers the role of the oil-water interfacial area, bioclogging and reduction of residual oil saturation due to the action of biosurfactants has been developed. The model was implemented in 1D and 2D in MATLAB and tested against analytic examples and benchmark problems. The developed model is currently one of the most complete models of MEOR. The model particularly includes the oil-water interfacial area in order to eliminate the hysteresis in the capillary pressure relationship and takes in account that biosurfactants are mainly living at the oil-water interface. To our knowledge, these are the first studies of the effects of MEOR including the oil-water interfacial area.

The MEOR model consists on a system of nonlinear coupled PDEs and ODEs, whose solution represents a challenge by itself. In order to have an efficient and stable scheme, we used an implicit stepping that considers a linear approximation of the capillary pressure gradient. The time discretization of the equations was obtained using BE and the spatial discretization using FD and TPFA. The details of the implementation are presented in Chapter 4, including the treatment of the boundary conditions. Although the implementation of the algorithm was challenging, we wrote in MATLAB the full code without using any commercial petroleum software.

We tested our numerical solver against analytic solutions, obtaining a reduction in the error when we lowered the value of the spatial and temporal steps, which corroborates the correctness of the implementation. We also tested our numerical solver against benchmark simulations, obtaining a good match with the results showed in Hendry et al. 1997, Amaziane et al. 2009 and Li et al. 2011.

In order to model that biosurfactants are mainly living at the oil-water interface, we considered the maximum specific biomass production rate as a function of the interfacial area a_{wn} in the form of the Monod-type model $\mu_{\mathrm{p,max}} = \mu_{\mathrm{pa,max}} a_{wn}/(K_a + a_{wn})$. In the 1-D case, we investigated the impact of the relevant parameters. We ascertained that the interfacial area distribution is very sensitive to the interfacial permeability k_{wn}. In the 2-D case, we considered a porous medium with a thief zone, which is a problem we cannot simulate in 1D. Although the capillary pressure distribution was different in both permeable regions, the interfacial area profile had the same values along the y direction, even though we had different water saturation values along this direction. We attribute this result to the production/destruction rate of interfacial area E_{wn} (currently there is just one model for E_{wn}).

In regard to our main goal, notwithstanding that we put together models with parameters from different experiments, we succeed in finding new parameters and making the full implementation of the two-phase flow model with transport equations including bioclogging and interfacial area. We obtained different water flux profiles and oil recovery predictions when we considered the interfacial area in the model. In the numerical experiments, we observed an improvement in the oil recovery when the biosurfactants were presented in the reservoir. Even though real reservoirs are more complex than the model presented, this work is useful for understanding the main phenomena involved in the recovery of petroleum. Moreover, for better testing of our model, it is necessary to do more experiments in the laboratory in order to compare with the numerical simulations and validate all the model assumptions.

Finally, we propose further work inspired in this thesis. Following the procedure showed in Chapter 3 for the discretization of the model in 1-D and 2-D cores, one can easily extend the discretization to the three-dimensional scenario; however, the implementation is more challenging. Also, in this work we solved the equations for the pressure, saturation and interfacial area iteratively, verifying the convergence rate numerically. Nevertheless, it is necessary to do a theoretical analysis of the convergence of the scheme in order to determinate the maximum time step size for having convergence. In order to have a more complete model, we should extend it considering more phenomena, for example chemotaxis (Lapidus and Schiller 1974), fractures (Shapiro 1987, Fumagalli and Scotti 2013), biosurfactant transportation in the oil phase (Nielsen et al. 2010), compresibility (Klöfkorn 2012) and changes in the viscosities (Sugai et al. 2007). It is necessary to investigate new relations for the production/destruction rate of interfacial area E_{wn} because currently there is just one model. Following the fact that the more interfacial area, the more residual oil recovered, new relations for the interfacial tension reduction and residual oil saturation should be investigated including the interfacial area.

Appendices

A. List of Symbols and Abbreviations

Symbol	Unit	Description
A	m^2	Cross sectional area
a_{wn}	$1/m$	Interfacial area
C	$-$	Parameter for the permeability modification
C_b, C_n, C_p, C_p	kg/m^3	Bacterial, nutrient and biosurfactant concentration
C_s^*	kg/m^3	Critical nutrient concentration for metabolism
d_1	$1/s$	Bacterial decay rate coefficient
$D_b^{\text{eff}}, D_n^{\text{eff}}, D_p^{\text{eff}}$	m^2/s	Effective diffusion coefficients
E_{wn}	m^3/s	Rate of production of specific interfacial area
e_{wn}	$1/m$	Production rate of specific interfacial area
$\mathbf{g}$	m/s^2	Gravity
$g_{1,\max}$	$1/s$	Maximum bacterial growth rate coefficient
h	m	Hydraulic head
$\mathbf{j}, \mathbf{j}_{\text{adv}}, \mathbf{j}_{\text{dif}}$	$kg/m^2 \cdot s$	Total, advective and diffusive flux
k_1, k_2, k_3	$1/s$	Reversible attachment, detachment and irreversible attachment
$\mathbf{k}, \mathbf{k}_w, \mathbf{k}_n$	m^2	Absolute, wetting and non-wetting effective permeabilities
$k_{r,w}, k_{r,n}$	$-$	Wetting and non-wetting relative permeabilities
$\mathbf{k}_{wn}$	m^3/s	Interfacial permeability
$K_{b/n}, K_{p/n}$	kg/m^3	Half saturation constants for producing bacteria and biosurfactants
$l_1,\ l_2,\ l_3$	$-, -, kg/s^2$	Fitting parameters for modeling the interfacial area
L	m	Length of porous medium
M	kg	Mass
N_{Ca}	$-$	Capillary number
p, p_e, p_w, p_n	$kg/m \cdot s^2$	Average, entry, wetting and non-wetting pressure
pv	$-$	Number of pore volume injected
Q_T	m^3/s	Water injection rate
r	m	Tube radius
s_w, s_n	$-$	Wetting and non-wetting saturation
$s_{or}, s_{or}^{\min}, s_{or}^{\max}$	$-$	Residual oil saturation, minimum and maximum
s_{wi}	$-$	Irreducible water saturation
s_w^*	$-$	Effective water saturation
T_1, T_2	$-$	Fitting parameters for modeling the residual oil saturation
$\mathbf{u}, \mathbf{u}_\Sigma$	m/s	Volumetric and total flow rate per area
v_g	m/s	Settling velocity of bacteria
v_{wn}	m/s	Interfacial velocity
V_p	m^3	Pore volume
W_i	m^3	Volume injected of water
$Y_{p/b}, Y_{p/n}$	$-$	Biosurfactant yield coefficients per unit bacteria and nutrient
z	m	Distance to the datum for the hydraulic head

Greek symbols

Symbol	Unit	Description
α_0	$^\circ$	Angle of flow relative to the horizontal
$\alpha_1, \alpha_2, \alpha_3, \alpha_4$	$-$	Parameters for the interfacial area relation
$\alpha_{b,L}, \alpha_{n,L}, \alpha_{p,L}$	m	Longitudinal dispersivities
$\alpha_{b,T}, \alpha_{n,T}, \alpha_{p,T}$	m	Tranverse dispersivities
$\Delta\rho$	kg/m^3	Density difference between wetting and non-wetting phases
Δt	s	Time step
Δx	m	Space step
η	$-$	Parameter for the Van Genuchten parameterizations
$\boldsymbol{\kappa}$	m/s	Hydraulic conductivity
λ	$-$	Parameter for the Brooks-Corey parameterizations
λ_w, λ_n	$m \cdot s/kg$	Wetting and non-wetting mobilities
μ	$kg/m \cdot s$	Viscosity
$\mu_{p,\max}$	$1/s$	Maximum specific biomass production rate
$\mu_{pa,\max}$	$1/s$	Maximum specific biomass production rate including interfacial area
ϕ	$-$	Porosity
ρ	kg/m^3	Density
$\sigma, \sigma_1, \sigma_2$	$-$	Volumetric fraction attached totally, reversibly and irreversibly
$\sigma_{\text{Int}}, \sigma_{\text{Int,min}}, \sigma_{\text{Int,max}}$	kg/s^2	Interfacial tension, minimum and maximum
θ	$^\circ$	Contact angle
ϱ	$-$	Exponent parameter for modeling the interfacial tension
ς	$-$	Exponent parameter for the Van Genuchten parameterizations

Abbreviations

Abbreviation	Name
BE	Backward Euler
EOR	Enhanced oil recovery
EEOR	Enzyme-enhanced oil recovery
FD	Finite differences
GEMEOR	Genetically-engineered microorganism for MEOR
IMPES	Implicit pressure explicit saturation
MEOR	Microbial enhanced oil recovery
MIOR	Microbial improved oil recovery
MPFA	Multi-point flux approximation
ODE(s)	Ordinary differential equation(s)
PDE(s)	Partial differential equation(s)
REV	Representative elementary volume
TPFA	Two-point flux approximation

Bibliography

I. Aavatsmark. An introduction to multipoint flux approximations for quadrilateral grids. *Computational Geosciences*, 6:405–432, 2002.

B. Amaziane, M. Jurak, and A.Z. Keko. Modeling and numerical simulations of water-gas flow in porous media using the concept of global pressure. *Transp. in Porous Media*, 84:133–152, 2009. doi: 10.1007/s11242-009-9489-8.

A. Amundsen. Microbial enhanced oil recovery: Modeling and numerical simulations. Master's thesis, Morwegian University of Science and Technology, Norway, 2015.

K. Aziz and A. Settari. *Petroleum Reservoir Simulation*. Elsevier, 1979.

S.O. Babatunde. Modeling of oil reservoirs with focus on microbial induced effects. Master's thesis, University of Bergen, Norway, 2014.

A. Bahadori, C. Nwaoha, and M.W. Clark. *Dictionary of Oil, Gas and Petrochemical Processing*. CRC Press, 2014.

T.D Bennett. *Transport by Advection and Difusion*. Wiley, 2012.

R. T. Brooks and A.T. Corey. *Hydraulic properties of porous media*. in Tech, Colorado State University, Fort Collins, Colo., 1964.

R.S. Bryant. MEOR screening criteria fit 27% of U.S. oil reservoirs. *Oil Gas*, 15:56–59, 1991.

C. Canuto and A. Tabacco. *Mathematical Analysis I*. Springer Milan, Italy, 2008.

G. Castorena-Cortés, I. Zapata-Peñasco, T. Roldán-Carrillo, J. Reyes-Avila, M. Mayol-Castillo, S. Román-Vargas, and P. Olguín-Lora. Evaluation of indigenous anaerobic microorganisms from mexican carbonate reservoirs with potential MEOR application. *Journal of Petroleum Science and Engineering*, 81:86–93, 2012.

D. Chen, L.J. Pyrak-Nolte, J. Griffin, and N.J. Giordano. Measurement of interfacial area per volume for drainage and imbibition. *Water Resour. Res.*, 43, 2007.

Z. Chen, G. Huan, and Y. Ma. *Computational Methods for Multiphase Flow in Porous Media*. Society for Industrial and Applied Mathematics, USA, 2006.

T.P. Clement, B.S. Hooker, and R.S. Skeen. Macroscopic models for predicting changes in saturated porous media properties caused by microbial growth. *Ground Water*, 34(5):934–942, 1996.

G. Dalquist and A. Bjorck. *Numerical Methods in Scientific Computing*. Society for Industrial and Applied Mathematics, 2008.

E.C. Donaldson, G.V. Chilingarian, and T.F. Yen. *Enhanced Oil Recovery, II: Processes and Operations*. ELSEVIER, 1989.

M.F. El-Amin, R. Meftah, A. Salama, and S. Sun. Numerical treatment of two-phase flow in porous media including specific interfacial area. *Procedia Computer Science*, 51:1249–1258, 2015.

T. W. Engler. *Fluid Flow in Porous Media*. NEW MEXICO TECH, 2010.

Q.H. Feng, S. Wang, G.Q. Gao, and C.Y. Li. A new approach to thief zone identification based on interference test. *J Petrol Sci Eng*, 75:13–18, 2010.

A. Fumagalli and A Scotti. A numerical method for two-phase flow in fractured porous media with non-matching grids. *Advances in Water Resources*, 62:454–464, 2013.

S.M. Hassanizadeh and W.G. Gray. Mechanics and thermodynamics of multiphase flow in porous media including interphase boundaries. *Water Resources Research*, 13:169–186, 1990.

S.M. Hassanizadeh and W.G. Gray. Thermodynamic basis of capillary pressure in porous media. *Water Resources Research*, 29:3389–3405, 1993.

M.J. Hendry, J.R. Lawrence, and P. Maloszewski. The role of sorption in the transport of *Klebsiella oxytoca* through saturated silica sand. *Ground Water*, 35:574–584, 1997.

A. Iserles. *A first course in the numerical analysis of differential equations*. Cambridge University Press, 2009.

V. Joekar-Niasar and S.M. Hassanizadeh. Uniqueness of specific interfacial area-capillary pressure-saturation relationship under non-equilibrium conditions in two-phase porous media flow. *Transport in Porous Media*, 94(2):465–486, 2012.

E.A. Jorg, T. Gimse, and K.A. Lie. *An introduction to the Numerics of Flow in Porous Media using Matlab*. SINTEF ICT, Dept. of Applied Mathematics, Oslo, 2009.

S.B. Kim. Numerical analysis of bacteria transport in saturated porous media. *Hydrol. Process*, 20: 1177–1186, 2006.

R.A. Klausen, F.A. Radu, and G.T. Eigestad. Convergence of MPFA on triangulations and for Richard's equation. *Int. J. Numer. Meth. Fluids*, 58:1327–1351, 2008.

R. Klöfkorn. Efficient Matrix-Free Implementation of Discontinuous Galerkin Methods for Compressible Flow Problems. In A. Handlovicova et al., editor, *Proceedings of the ALGORITMY 2012*, pages 11–21, 2012.

N. Kosaric and F Varder-Sukan. *BIOSURFACTANTS: Production and Utilization-Processes, Technologies, and Economics*. CRC Press, 2015.

J. Kou and S. Sun. On iterative IMPES formulation for two-phase flow with capillarity in heterogeneous porois media. *International Journal of Numerical Analysis and Modeling*, 1(1):20–40, 2004.

K. Kumar, I.S. Pop, and F.A. Radu. Convergence analysis of mixed numerical schemes for reactive flow in a porous medium. *SIAM J. Num. Anal.*, 51:2283–2308, 2013.

K. Kumar, I.S. Pop, and F.A. Radu. Convergence analysis for a conformal discretization of a model for precipitation and dissolution in porous media. *Numerische Mathematik*, 127:715–749, 2014.

A. Kvashchuk. A robust implicit scheme for two-phase flow in porous media. Master's thesis, University of Bergen, Norway, 2015.

E. Lacerda, C.M. Da Silva, V.I. Priimenko, and A.P. Pires. Microbial EOR: a quantitative prediction of recovery factor. *Society of Petroleum Engineers*, 2012.

I.R Lapidus and R. Schiller. A mathematical model for bacterial chemotaxis. *Biophysical Journal*, 14 (11):825–834, 1974.

I. Lazar, I.G. Petrisor, and T.F. Yen. Microbial enhanced oil recovery (MEOR). *Petroleum Science and Technology*, 25:1353–1366, 2007.

D. Li, J. Yang, and D. Lu. Thief zone identification based on transient pressure analysis: a field case study. *Journal of Petroleum Exploration and Production Technology*, 6(1):63–72, 2015.

J. Li, J. Liu, M.G. Trefry, J. Park, K. Liu, B. Haq, C.D. Johnston, and H. Volk. Interactions of microbial-enhanced oil recovery processes. *Transport in porous media*, 87(1):77–104, 2011.

Y. Li, L.M. Abriola, T.J. Phelan, C.A. Ramsburg, and K.D. Pennell. Experimental and numerical validation of the total trapping number for prediction of DNAPL mobilization. *Environ. Sci. Technol.*, 41(23):8135–8141, 2007.

F. List and F.A. Radu. A study on iterative methods for solving Richards' equation. *Computational Geosciences*, 20(2):341–353, 2016.

T. Lunde. Comparison between mimetic and two-point flux-approximation schemes on PEBI-grids. Master's thesis, University of Oslo, Norway, 2006.

S. Maneerat. Production of biosurfactants using substrates from renewable-resources. *Songklanakarin J. Sci. Technol*, 27, 2005.

P.C. Matthews. *Vector Calculus*. Springer, 1998.

S.M. Nielsen, A. Shapiro, E.H. Stenby, and M.L. Michelsen. *Microbial Enhanced Oil Recovery - Advanced Reservoir Simulation*. PhD thesis, Technical University of Denmark (DTU), Denmark, 2010.

S.M. Nielsen, I. Nesterov, and A.A. Shapiro. Microbial enhanced oil recovery—a modeling study of the potential of spore- forming bacteria. *Computational Geosciences*, 20(3):567–580, 2015.

J. Niessner and S.M. Hassanizadeh. A model for two-phase flow in porous media including fluid-fluid interfacial area. *Water Resources Research*, 44(8), 2008a.

J. Niessner and S.M. Hassanizadeh. Two-phase flow and transport in porous media including fluid-fluid interfacial area. 2008b. URL http://www.nupus.uni-stuttgart.de/07_Preprints_Publications/Preprints/Preprints-PDFs/NUPUS_2008-08_online.pdf.

J.M. Nordbotten and M.A. Celia. *Geological storage of CO2: modeling approaches for large-scale simulation*. John Wiley And Sons, 2011.

L. Olsen-Kettle. *Numerical solution of partial differential equations*. The University of Queensland, 2011.

I. Patel, S. Borgohain, M. Kumar, V. Rangarajan, P. Somasundaran, and R. Sen. Recent developments in microbial enhanced oil recovery. *Renewable and Sustainable Energy Reviews*, 52:1539–1558, 2015.

I.S. Pop, F. Radu, and P. Knabner. Mixed finite elements for the Richards'equation: linearization procedure. *J. Comput. and Appl. Math.*, 168:365–373, 2004.

M.L. Porter, D. Wildenschild, G. Grant, and J.I. Gerhard. Measurement and prediction of the relationship between capillary pressure, saturation, and interfacial area in a NAPL-water-glass bead system. *Water Resources Research*, 46, 2010.

F.A. Radu, I.S. Pop, and S. Attinger. Analysis of an Euler implicit - mixed finite element scheme for reactive solute transport in porous media. *Numerical Methods for Partial Differential Equations*, 26 (2):320–344, 2010.

F.A. Radu, K. Kumar, I.S. Pop, and J.M. Nordbotten. A convergent mass conservative numerical scheme based on mixed finite elements for two-phase flow in porous media. 2015a.

F.A. Radu, J.M. Nordbotten, I.S. Pop, and K. Kumar. A robust linearization scheme for finite volume based discretizations for simulation of two-phase flow in porous media. *J. Comput. and Appl. Math.*, 289(1):134–141, 2015b.

R. Sen. Biotechnology in petroleum recovery: The microbial EOR. *Progress in Energy and Combustion Science*, 34:714–724, 2008.

Allen M. Shapiro. *Advances in Transport Phenomena in Porous Media*, chapter Transport Equations for Fractured Porous Media, pages 405–471. Springer Netherlands, Dordrecht, 1987.

K. Skiftestad. Numerical modelling of microbial enhanced oil recovery with focus on dynamic effects: An iterative approach. Master's thesis, University of Bergen, Norway, 2015.

I. Skjaelaaen. *Mathematical Modeling of Microbial Induced Processes in Oil Reservoirs.* PhD thesis, University of Bergen, Norway, 2010.

W.A. Strauss. *Partial Differential Equations: An Introduction.* Wiley, Brown University, 2008.

Y. Sugai, C. Hong, T. Chida, and H. Enomoto. Simulation studies on the mechanisms and performances of MEOR using a polymer producing microorganism clostridium sp. TU-15A. *Society of Petroleum Engineers*, 34:714–724, 2007.

J.W. Thomas. *Numerical Partial Differential Equations: Finite Difference Methods.* Springer-Verlag, City of New York, State of New York, 1995.

D. Tiab and E.C. Donaldson. *Petrophysics: Theory and Practice of Measuring Reservoir Rock and Fluid Transport Properties.* Elsevier/Gulf Publishing Co., Houston, TX, 2003.

L.N. Trefethen and D. Bau. *Numerical Linear Algebra.* siam, Philadelphia, 1997.

M.T. Van Genuchten. A closed-form equation for predicting the hydraulic conductivity of unsaturated soils. *Soil Sc. Soc. of America*, 44(5):892–898, 1980.

Q. D. Weihong, D. Liangjun, Z. Zhongkui, Y. Jie, L. Huamin, and Zongshi. Microbial processes in oil fields: Culprits, problems, and opportunities. *Advances in applied microbiology*, 66:141–251, 2009.

Z. Wu, X. Yue, T. Cheng, J. Yu, and H. Yang. Effect of viscosity and interfacial tension of surfactant-polymer flooding on oil recovery in high-temperature and high-salinity reservoirs. *Journal of Petroleum Exploration and Production Technology*, 4:9–16, 2013.

N. Youssef, M.S. Elshahed, and M.J. McInerney. Interfacial behavior of pure surfactants for enhanced oil recovery-part 1: A study on the adsorption and distribution of cetylbenzene sulfonate. *Tenside, Surfactants, Detergents*, 40:87–89, 2003.

N. Youssef, D. R. Simpson, K. E. Duncan, M. J. McInerney, M. Folmsbee, T. Fincher, and R. M. Knapp. *In situ* biosurfactant production by *Bacillus* strains injected into a limestone petroleum reservoir. *Appl. Environ. Microbiol*, 73:1239–1247, 2007.

C.D. Yuan, W. F. Pu, X. C. Wang, L. Sun, Y.C. Zhang, and S. Cheng. Effects of interfacial tension, emulsification, and surfactant concentration on oil recovery in surfactant flooding process for high temperature and high salinity reservoirs. *Energy Fuels*, 29:6165–6176, 2015.